DESIGN OF A TENSEGRITY CONTROL MOMENT GYROSCOPE

A Thesis

by

TYLER ARYN BRYANT

Submitted to the Graduate and Professional School of
Texas A&M University
in partial fulfillment of the requirements for the degree of

MASTER OF SCIENCE

Chair of Committee,	Manoranjan Majji
Committee Members,	Raktim Bhattacharya
	Dileep Manisseri Kalathil
	Srinivas Rao Vadali
Head of Department,	Ivett Leyva

December 2022

Major Subject: Aerospace Engineering

ABSTRACT

The focus of this thesis will be the development of a tensegrity flywheel with the goal of minimizing the mass while achieving the desired amount of angular momentum for attitude control of a spacecraft. Currently, flywheels are designed using a continuum of material to achieve the desired amount of angular momentum due to the large gyroscopic forces and torques that the flywheel has to withstand, but this thesis will show that a continuum flywheel is not necessary to withstand these large gyroscopic forces and torques and still have the capability of meeting angular momentum and torque requirements. With a discrete approach, a large percentage of mass can be saved when compared to the current designs because the mass near the continuum wheel's spin axis does not contribute significantly to the angular momentum output. If a percentage of the mass near the center could be moved to the edge and replaced with a high strength to weight ratio structure, the mass of the flywheel could be reduced and the stored energy could be increased. This would save a significant amount of money when sending attitude control systems into space that utilize flywheels such as reaction wheels and control moment gyroscopes. The design proposed for this thesis will implement tensegrity to reduce the mass of the flywheel when compared to the current continuum designs. Two separate topologies will be analyzed in both two-dimensional and three-dimensional space and the results will show that utilizing a tensegrity design can significantly reduce mass of a flywheel.

DEDICATION

To my parents, for their love and guidance.

ACKNOWLEDGMENTS

I would like to thank my advisers Dr. Manoranjan Majji, Dr. Raktim Bhattacharya, Dr. Dileep Manisseri Kalathil, and Dr. Srinivas Rao Vadali for their guidance during my time at Texas A&M University. I would also like to thank Dr. Robert Skelton for his mentorship.

CONTRIBUTORS AND FUNDING SOURCES

Contributors

This work was supported by a thesis committee consisting of Professor Manoranjan Majji, Raktim Bhattacharya, and Srinivas Rao Vadali of the Department of Aerospace Engineering and Professor Dileep Manisseri Kalathil of the Department of Electrical Engineering.

All work conducted for the thesis was completed by the student independently.

Funding Sources

This work was funded by NASA NIAC Phase II Grant on Tensegrity Approaches for Construction of a 1g Growable Space Habitat.

NOMENCLATURE

m	Mass
ρ	Density / Aspect Ratio
σ	Yield Stress
Δ	Thickness
I	Inertia
h	Angular Momentum
ω	Angular Rate
r/R	Radius
C	Connectivity Matrix
N	Nodal Matrix
W	External Force Matrix
q, p, b	Complexity Parameters
ϕ, β, α	Topology Angles
c	Centrifugal Force Coefficient
τ	Torque
t	Torque Coefficient
B	Bar Matrix
S	String Matrix
γ	String Force Density
λ	Bar Force Density
s	String Vector Magnitude
b	Bar Vector Magnitude

TABLE OF CONTENTS

LIST OF FIGURES

FIGURE Page

LIST OF TABLES

TABLE Page

1. INTRODUCTION AND LITERATURE REVIEW

Current flywheels used for control moment gyroscopes (CMGs) or reaction wheels currently utilize solid designs. The mass near the center of the spin axis of the flywheel does not contribute much to the angular momentum of the CMG. If this mass could be moved to the edge of the wheel and be replaced by a high strength to weight ratio structure, the overall mass of the flywheel could be reduced. This could save money on shipping the CMG systems to space for attitude control. For example, each flywheel for the CMG system on the ISS weigh 220 lbs [11]. Currently, it costs about $10,000 to send a pound of mass into space. If even a small percentage of the mass of the wheel could be reduced, the savings would be significant from shipping costs alone.

The proposed solution to this problem would be to use a tensegrity structure to replace the removed material since all the members of the structure are only axially loaded. Two different tensegrity topologies will be analyzed in this thesis. First, the spiral wheel will be analyzed and is of interest due to its torsional properties. The foundation of the spiral wheel is the Michell truss which is the optimal structure for cantilevered loads for minimal mass under yielding constraints [3]. If that structure is taken and rotated around the center it would create a disk. This disk will be referred to as the spiral wheel. The spiral wheel should be good for torsional loads. The CMG wheel will experience large centrifugal loads and the spiral wheel has not been analyzed for these type of loads before. The second configuration to be analyzed will be the bicycle wheel. Different numbers of spokes and spoke angles will be analyzed to determine which is optimal for minimal mass subject to the large centrifugal forces and torques.

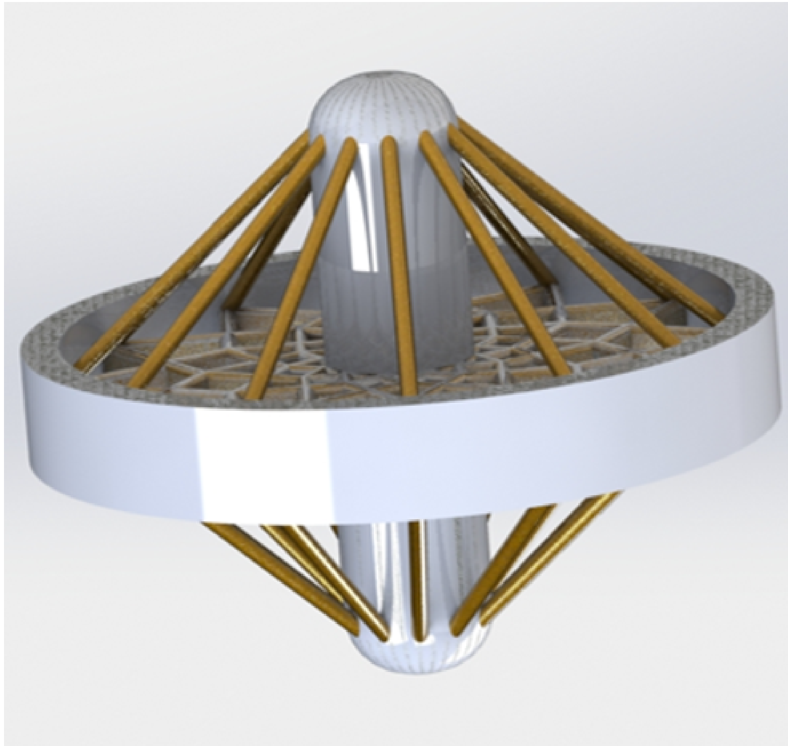

Figure 1.1: Conceptual design of the tensegrity CMG

1.1 State of the Art

The optimal flywheel problem was first presented in the late 19th century by Stodola [8]. This problem was looked at by various people over the next 60 to 70 years. The problem was revitalized in the 1970s by the energy crises and interest in the optimal flywheel and in rotating disks in general reached a new high. Energy efficiency was the main driving force in the optimization process. Today, the state of the art flywheels consist of multi-layer composite rims that are placed in a vacuum and use magnetic bearings instead of machanical bearings [9]. In these designs the main driving factor is energy storage and not minimizing the mass of the flywheel itself. Many computational methods of optimizing a flywheel have been developed such as dividing the flywheel into separate rings and the thickness of each ring is varied. An optomization process has been created for the modeling and optimization of heterogeneous flywheels [7]. All of this work has been done for continuum flywheels.

This thesis will use tensegrity structures to optimize a flywheel used for CMGs. The difference for this problem is that the optimization process will aim to minimize mass while maintaining a certain amount of angular momentum output for the flywheel. This new approach could lead to a bigger mass savings while maintaining the needed stiffness because the structure will be more efficient due to all the members being axially loaded only.

1.2 Michell Truss

Michell theory is based upon the fundamental work of Maxwell [2]. Michell built upon the work of Maxwell and showed the continuum configuration of material that minimized the volume of the structure under bending loads [3]. This structure is commonly known as the Michell truss. A discrete solution to this problem was given by Skelton [4]. Recently, work has been done to extend the two-dimensional theory to three-dimensions for continuum structures subjected to torsion [5]. The Michell truss and the Michell sphere have been shown to be the optimal structures, for minimal volume, for bending loads and torsional loads respectively with yielding constraints. CMGs experience very large centrifugal forces as well as torsional loads that are not accounted for in the current literature. This thesis will analyze how the spiral wheel responds to these different loading conditions.

1.3 Bicycle Wheel

Much work has been done on the design of a bicycle wheel. It is very well known how the bicycle wheel behaves for loading conditions during use on a bicycle. Such as the lateral loads, the radial loads, and the torsional loads [6]. The stiffness of a bicycle wheel and rim has been examined in detail [10]. The difference between things that have already been done and what will be proposed in this thesis is that the radial loads for the normal cases are much larger and point away from the hub instead of towards it. The stiffness required for such large loads along the radial direction and the torques that will be applied out of the plane of the wheel need to be examined. The optimal bicycle wheel when considering these different loading conditions for minimal mass has not been examined in the past literature and will be examined for this thesis.

1.4 Comparison Between a Solid Disk and a Hollow Cylinder

A comparison of a solid disk and a hollow cylinder will be done to determine the possible mass savings between the two when matching some of the design parameters such as radius, angular rate, and angular momentum. Figure 1.2 and Figure 1.3 depict a hollow cylinder and a solid disk respectively. The mass of a hollow cylinder is shown in (1.1) where ρ is the density, Δ is the thickness, R is the outer radius, and r is the inner radius.

$$m = \pi\rho\Delta(R^2 - r^2) \tag{1.1}$$

The moment of inertia about the z-axis, I, for the hollow cylinder is shown in (1.2) where the mass is replaced by (1.2).

$$I = \frac{1}{2}m(R^2 + r^2) = \frac{1}{2}\pi\rho\Delta(R^4 - r^4) \tag{1.2}$$

The angular momentum about the z-axis, h, for the hollow cylinder is shown in (1.3).

$$h = \frac{1}{2}\pi\rho\Delta\omega(R^4 - r^4) \tag{1.3}$$

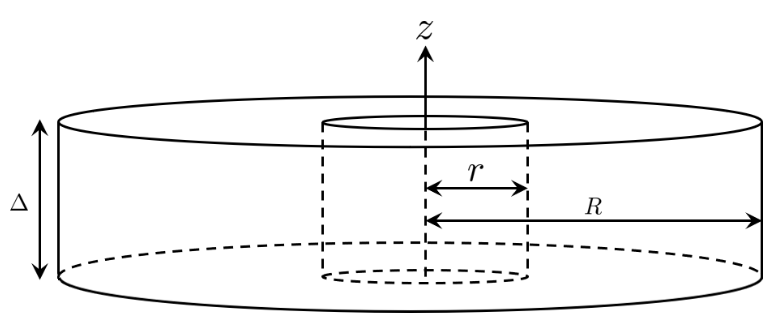

Figure 1.2: A hollow cylinder.

The mass of the solid disk is shown below in (1.4) where $\bar{\rho}$, $\bar{\Delta}$, and $\bar{R}$ are the density, thickness, and radius of the solid disk respectively.

$$\bar{m} = \pi\bar{\rho}\bar{\Delta}\bar{R}^2 \tag{1.4}$$

The moment of inertia about the z-axis of the solid disk, $\bar{I}$, is shown in (1.5) with the mass replaced by (1.4).

$$\bar{I} = \frac{1}{2}\bar{m}\bar{R}^2 = \frac{1}{2}\pi\bar{\rho}\bar{\Delta}\bar{R}^4 \tag{1.5}$$

The angular momentum about the z-axis of the solid disk, $\bar{h}$, is shown in (1.6).

$$\bar{h} = \frac{1}{2}\pi\bar{\rho}\bar{\Delta}\bar{\omega}\bar{R}^4 \tag{1.6}$$

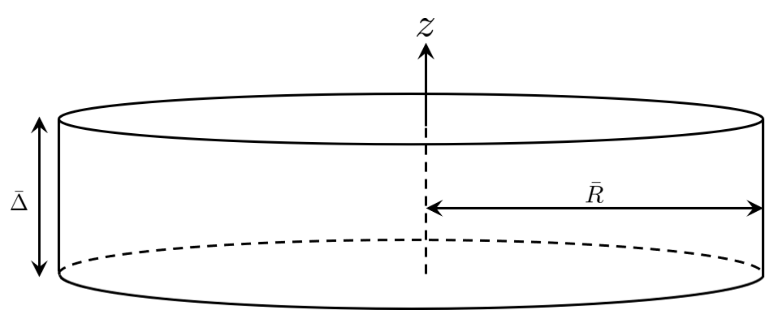

Figure 1.3: A solid disk.

The goal is to match the angular momentum of the solid disk while saving mass by using a hollow cylinder with the void replaced with a tensegrity structure. So, setting the angular momentum of both equal to each other, $h = \bar{h}$, the mass ratio will be solved for to determine what the limit of the possible mass savings is without the added structure there. After setting the angular momentum of each wheel equal to the other is shown in (1.7).

$$\frac{1}{2}\pi\rho\Delta\omega(R^4 - r^4) = \frac{1}{2}\pi\bar{\rho}\bar{\Delta}\bar{\omega}\bar{R}^4 \tag{1.7}$$

Solving for the density ratio using 1.7 results in 1.8.

$$\frac{\rho}{\bar{\rho}} = \frac{\bar{\Delta}\bar{\omega}\bar{R}^4}{\Delta\omega(R^4 - r^4)} \tag{1.8}$$

The mass ratio is found by dividing 1.1 by 1.4 and the result is shown below in 1.9.

$$\frac{m}{\bar{m}} = \frac{\pi\rho\Delta(R^2 - r^2)}{\pi\bar{\rho}\bar{\Delta}\bar{R}^2} = \frac{\rho\Delta(R^2 - r^2)}{\bar{\rho}\bar{\Delta}\bar{R}^2} \tag{1.9}$$

The result of substituting the density ratio into (1.9) is shown below in (1.10), where $d = R - r$. This is the mass ratio of the hollow cylinder to the solid disk when setting the angular momentum of each wheel equal to one another.

$$\frac{m}{\bar{m}}(h = \bar{h}) = \frac{\bar{\omega}\bar{R}^2}{\omega(R^2 + r^2)} = \frac{\bar{\omega}\bar{R}^2}{\omega(R^2 + (R - d)^2)} \tag{1.10}$$

Now if the outer radius of both wheels are set equal to each other, the mass ratio becomes (1.11).

$$\frac{m}{\bar{m}}(h = \bar{h}, R = \bar{R}) = \frac{\bar{\omega}\bar{R}^2}{\omega(2\bar{R}^2 - 2\bar{R}d + d^2)} \tag{1.11}$$

If instead the angular momentum and the angular rate of each wheel is set equal to each other, the mass ratio becomes (1.12).

$$\frac{m}{\bar{m}}(h = \bar{h}, \omega = \bar{\omega}) = \frac{\bar{R}^2}{R^2 + r^2} = \frac{\bar{R}^2}{R^2 + (R - d)^2} \tag{1.12}$$

If the angular rate of each wheel is also set equal to each other, the mass ratio becomes (1.13).

$$\frac{m}{\bar{m}}(h = \bar{h}, R = \bar{R}, \omega = \bar{\omega}) = \frac{\bar{R}^2}{2\bar{R}^2 - 2\bar{R}d + d^2} \tag{1.13}$$

If the outer radius of the wheel is fixed, than $0 < d < \bar{R}$. This fact and (1.11), (1.12), and (1.13) will be used in the following Lemmas.

Lemma 1. *If $h = \bar{h}$, $R = \bar{R}$, and $\omega = \bar{\omega}$ then*

$$\frac{1}{2} < \frac{m}{\bar{m}} < 1.$$

Lemma 2. *If $h = \bar{h}$ and $R = \bar{R}$ then*

$$\frac{\bar{\omega}}{2\omega} < \frac{m}{\bar{m}} < \frac{\bar{\omega}}{\omega}.$$

Lemma 3. *If $h = \bar{h}$ and $\omega = \bar{\omega}$ then*

$$\frac{1}{2}\left(\frac{\bar{R}}{R}\right)^2 < \frac{m}{\bar{m}} < \left(\frac{\bar{R}}{R}\right)^2.$$

2. TWO-DIMENSIONAL DESIGN

This chapter will characterize the nodal and connectivity matrices for both the spiral wheel and the bicycle wheel, describe the two static load cases that will be analyzed, introduce the algorithm to minimize the mass of both of the wheel designs subject to an angular momentum constraint, analyze the sensitivity of the mass and the angular momentum output of each design to the diameter of the axle, and show the minimum mass results for each design for each load case. The results show the spiral wheel is the optimal mass structure when compared to the bicycle wheel and a solid wheel when centrifugal forces or a combination of centrifugal forces and a torque are applied if there is an angular momentum requirement for the wheel. The results also show that both designs do not need any compression members and only use tensile members.

2.1 Topology

This section will describe two separate topologies that will be used to design a minimal mass flywheel in two-dimensions. The nodal matrix and the bar and string connectivity matrices will be defined for both the spiral wheel and the bicycle wheel, and a rim topology will be defined that will be augmented with the spiral wheel and the bicycle wheel utilizing the algorithm from Appendix B.

2.1.1 Spiral Wheel

The foundation of this topology will be the discretized Michell Spiral, which was first described in [4] and the definition of the Michell Spiral used in that resource will be the same one used here. The spirals will be described by the angles ϕ and β. These angles are shown below in Figure 2.1. The sequence of lines of length $p_l, p_{l+1}, ...$ are connected end to end. The geometry of these connections can be described as follows when relative to a common origin.

Definition 1. *Let r_l define a set of radii from a common origin, **0**, for $l = 0, 1, 2, ..., q-1$. Let p_l, $l = 0, 1, 2, ..., q-1$, define the lengths of lines beginning at points with radius r_l and terminating at points with radius r_{l+1}. Then a Michell Spiral of order q is defined by the end-to-end connections*

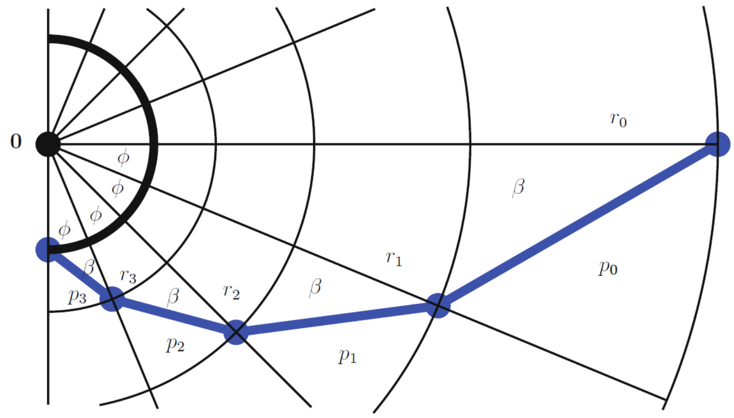

Figure 2.1: A Michell Spiral (q = 4) - "Reprinted from [4]"

of lines of length p_l*, satisfying,*

$$r_{l+1} = ar_l, \qquad p_l = cr_l, \qquad l = 0, 1, 2, ..., q, \tag{2.1}$$

where $a > 0$ *and* $c > 0$*.*

If

$$a = \frac{\sin\beta}{\sin(\beta+\phi)}, \qquad c = \frac{\sin\phi}{\sin(\beta+\phi)} \tag{2.2}$$

then the sequence generates a Michell Spiral as in Figure 2.1. The relations between (a,c) and (ϕ,β) given above follow from Figure 2.1 by observing that

$$r_{l+1}\cos\phi + p_l\cos\beta = r_l \tag{2.3}$$

$$r_{l+1}\sin\phi = p_l\sin\beta. \tag{2.4}$$

To create the spiral wheel topology, the Michell Spiral is rotated about the origin by the angle 2ϕ a total of p times. All the spirals are then mirrored about their radial line from the origin to the outermost point of the spiral and the resulting topology is shown in Figure 2.2. Figure 2.2 depicts how the nodes are numbered and how they are connected by the bars and strings for the spiral wheel topology. The numbering of the nodes starts on the outermost ring. The numbering on the first ring goes form 1 to p. The number of times the truss touches the outer rim is p and will be referred to as the circumferential complexity. The nodes on the next ring starts at $p+1$ and goes to $2p$. This happens until the final $q+1$ ring is reached. The final node would be number $p(q+1)$, where q is the radial complexity of the wheel.

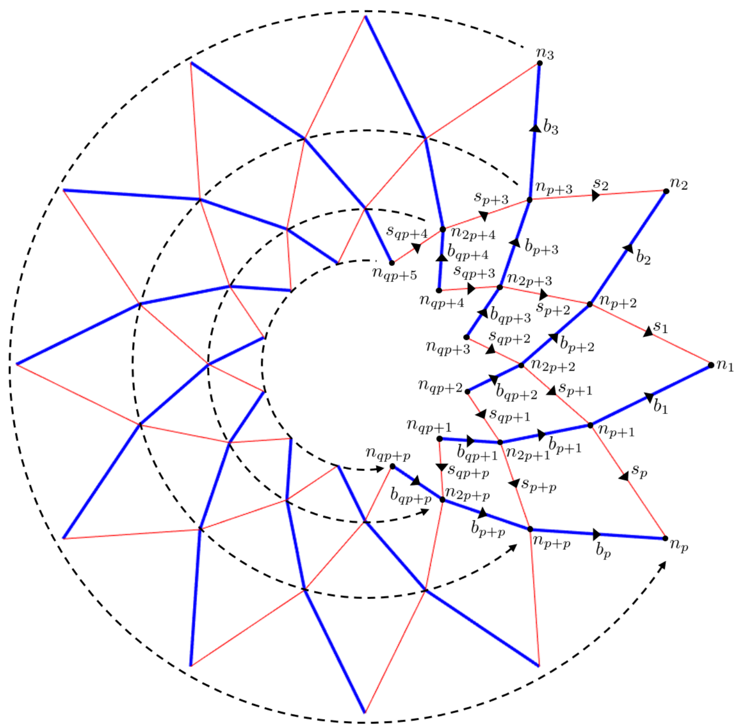

Figure 2.2: A spiral wheel showing how the nodes, bars, and strings are numbered and how they are connected

2.1.1.1 *Nodal Matrix*

The nodes will be defined using the angles ϕ, β, and their radius from the center of the wheel. Using (2.1) and (2.2) the angles β and ϕ will be solved for in terms of the complexities p and q. The angle between each outer node is equal to 2ϕ. The total number of angles between nodes is

$2\phi p$. This total angle needs to be equal to 2π so that there is an integer value for the number of times the spirals touch the outer most ring and so there are not any overlapping spirals. Using (2.5), p is solved for in terms of ϕ and shown in (2.6).

$$2p\phi = 2\pi \tag{2.5}$$

$$\phi = \frac{\pi}{p} \tag{2.6}$$

Using (2.1) and (2.2), the ratio of the outer radius and the inner radius, ρ, of the spiral tensegrity wheel can be written in terms of the angle β, the angle ϕ, and radial complexity q and is shown in (2.7).

$$\rho = \frac{r_q}{r_0} = a^q = \left(\frac{\sin\beta}{\sin(\beta+\phi)}\right)^q \tag{2.7}$$

After using an angle-sum triginometry identity and replacing ϕ with (2.6), the aspect ratio of the wheel, ρ, can be written as shown in (2.8).

$$\rho = \left(\frac{\sin\beta}{\sin(\beta)\cos(\phi)+\sin(\phi)\cos(\beta)}\right)^q = \left(\frac{\sin\beta}{\sin(\beta)\cos(\frac{\pi}{p})+\sin(\frac{\pi}{p})\cos(\beta)}\right)^q \tag{2.8}$$

Solving (2.8) for β results in (2.9) shown below.

$$\beta = \arctan\left(\frac{\sin(\frac{\pi}{p})}{\rho^{-\frac{1}{q}}-\cos(\frac{\pi}{p})}\right) \tag{2.9}$$

Now the two parameters describing the spiral tensegrity wheel topology β and ϕ are solved for in terms of the circumferintial complexity and the radial complexity respectively. Since both complexities can only be integers, this removes a considerable amount of points to check during the optimization process for minimal mass in the next section.

The numbering of the nodes starts with the outermost ring. The radius of this ring is r_0. The angle between each node on each ring is 2ϕ. So, the first node starts at the angle 0 from the horizontal axis and the second will be at the angle 2ϕ and so on until the p^{th} node is at an angle of $2(p-1)\phi$. The nodal matrix representing nodes one to node p on the first ring is shown below in (2.10).

$$\mathbf{R}_0 = \begin{bmatrix} r_0\cos(0) & r_0\cos(2\phi) & \cdots & r_0\cos(2(p-1)\phi) \\ r_0\sin(0) & r_0\sin(2\phi) & \cdots & r_0\sin(2(p-1)\phi) \\ 0 & 0 & \cdots & 0 \end{bmatrix} \tag{2.10}$$

The next set of nodes for the second ring is shown in matrix form below in (2.11). This time the first node on this ring starts at an angle of $-\phi$. The next node is at ϕ and so on until the final node on this ring is at an angle of $2(p-1)\phi$. This matrix describes the location of the nodes from number $p+1$ to $2p$.

$$\mathbf{R}_1 = \begin{bmatrix} r_1\cos(-\phi) & r_1\cos(\phi) & \cdots & r_1\cos(2(p-1)\phi-\phi) \\ r_1\sin(-\phi) & r_1\sin(\phi) & \cdots & r_1\sin(2(p-1)\phi-\phi) \\ 0 & 0 & \cdots & 0 \end{bmatrix} \tag{2.11}$$

This same pattern continues until the final ring in the structure. The matrix for the final ring is shown below in (2.12).

$$\mathbf{R}_q = \begin{bmatrix} r_q\cos(-q\phi) & r_q\cos(2\phi-q\phi) & \cdots & r_q\cos(2(p-1)\phi-q\phi) \\ r_q\sin(-q\phi) & r_q\sin(2\phi-q\phi) & \cdots & r_q\sin(2(p-1)\phi-q\phi) \\ 0 & 0 & \cdots & 0 \end{bmatrix} \tag{2.12}$$

The final nodal matrix for the entire spiral wheel topology is shown below in (2.13). The total number of nodes of this structure is equal to $(q+1)p$ which leads to the size of the nodal matrix shown in (2.14).

$$\mathbf{N} = \begin{bmatrix} \mathbf{R}_0 & \vdots & \mathbf{R}_1 & \vdots & \cdots & \vdots & \mathbf{R}_q \end{bmatrix} \tag{2.13}$$

$$\mathbf{N} \in \Re^{3\times(q+1)p} \tag{2.14}$$

2.1.1.2 Connectivity Matrices

Using the numbering system shown in Figure 2.2, the bar connectivity matrix can be written as shown in (2.15). The size of each identity matrix is $p \times p$. The size of the bar connectivity matrix is shown in (2.16).

$$\mathbf{C}_B^T = \begin{bmatrix} I_p & 0 & 0 & 0 \\ -I_p & I_p & 0 & 0 \\ 0 & -I_p & \ddots & 0 \\ 0 & 0 & \ddots & I_p \\ 0 & 0 & 0 & -I_p \end{bmatrix} \tag{2.15}$$

$$\mathbf{C}_B^T \in \Re^{(q+1)p\times qp} \tag{2.16}$$

The string connectivity can be written as shown below in (2.17). The off diagonal identity matrices are now the matrix J which is shown in (2.18). The size of the string connectivity matrix is shown in (2.19).

$$\mathbf{C}_S^T = \begin{bmatrix} I_p & 0 & 0 & 0 \\ -J_p & I_p & 0 & 0 \\ 0 & -J_p & \ddots & 0 \\ 0 & 0 & \ddots & I_p \\ 0 & 0 & 0 & -J_p \end{bmatrix} \tag{2.17}$$

$$J_p = \begin{bmatrix} 0 & \cdots & 0 & 1 \\ 1 & 0 & 0 & 0 \\ 0 & \ddots & 0 & 0 \\ 0 & 0 & 1 & 0 \end{bmatrix} \tag{2.18}$$

$$\mathbf{C}_S^T \in \Re^{(q+1)p \times qp} \tag{2.19}$$

2.1.2 Bicycle Wheel

Figure 2.3 shows the numbering system for the nodes and strings for the bicycle wheel topology. This image depicts a spoke arrangement with complexity three ($b = 3$) and a non-zero spoke angle, α, coming off the inner circle. The spokes can have several unique spoke angles where the value depends on the radius of the inner circle, the radius of the outer circle, and the complexity of the topology. The inner ring of nodes are numbered so that the first half of those nodes would be on the top half of the axle in three-dimensions. The second half of the inner ring of nodes would be on the bottom half of the axle in three-dimensions. The outer ring of nodes are numbered so that the first node will connect to the first node on the inner ring, the second node would be connected to the second inner ring node, and so on until the last outer ring node. The strings are numbered by starting at the first node and the string vectors always start at the higher number node and point towards the lower numbered node.

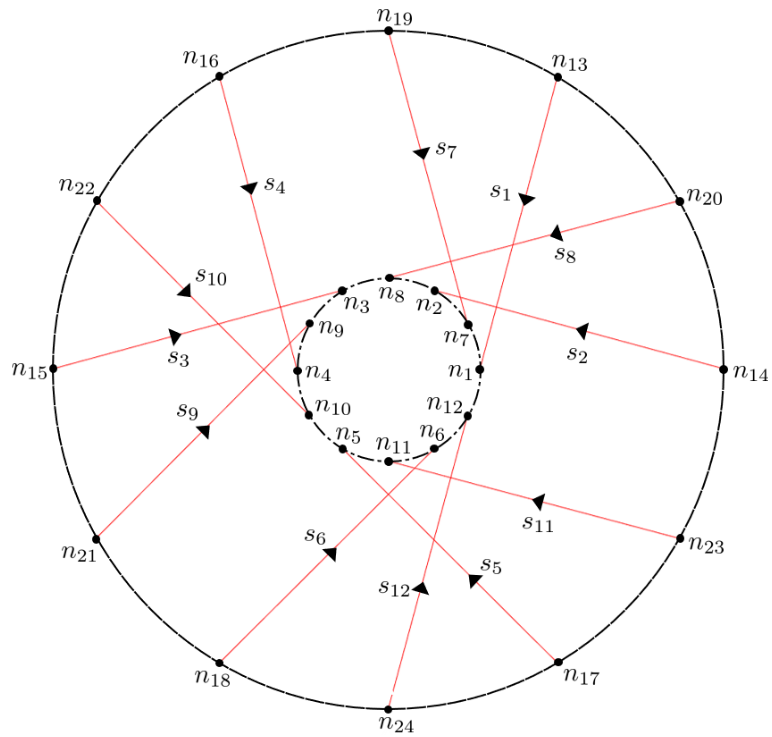

Figure 2.3: Bicycle wheel of complexity three with a non-zero spoke angle

2.1.2.1 Nodal Matrix

The total number of inner nodes is equal to $4b$. Dividing 2π by $4b$ results in the angle between the inner ring nodes and outer ring nodes for the bicycle spokes shown in 2.20.

$$\phi = \frac{\pi}{2b} \tag{2.20}$$

The matrix describing the first set of inner nodes of the bicycle spokes is given below by (2.21), where r is the radius of the inner ring. The fist node starts at an angle of 0, the second node has an angle of 2ϕ, and so on until the final node of this set is at an angle of $2(b-1)\phi$, where ϕ is defined positive in the counter-clockwise direction.

$$\mathbf{N}_{I_1} = \begin{bmatrix} r\cos(0) & r\cos(2\phi) & \cdots & r\cos(2(b-1)\phi) \\ r\sin(0) & r\sin(2\phi) & \cdots & r\sin(2(b-1)\phi) \\ 0 & 0 & \cdots & 0 \end{bmatrix} \tag{2.21}$$

The matrix describing the second set of inner nodes of the bicycle spokes is given below by (2.22). The radius to the second set of inner nodes is also r. The fist node starts at an angle of ϕ, the second node has an angle of 3ϕ, and so on until the final node of this set is at an angle of $(4b-1)\phi$.

$$\mathbf{N}_{I_2} = \begin{bmatrix} r\cos(\phi) & r\cos(3\phi) & \cdots & r\cos((4b-1)\phi) \\ r\sin(\phi) & r\sin(3\phi) & \cdots & r\sin((4b-1)\phi) \\ 0 & 0 & \cdots & 0 \end{bmatrix} \tag{2.22}$$

The angle the spokes make with respect to the tangential line from the inner ring will be called the spoke angle, α. This angle must be between 0 and $\frac{\pi}{2}$. This is shown below in Figure 2.4.

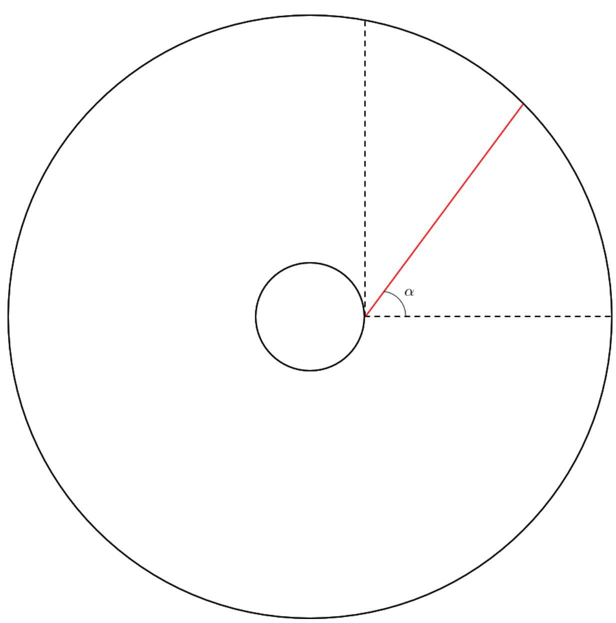

Figure 2.4: The angle of the spoke relative to the hub and the limits of its magnitude

The matrices describing the outer nodes along the rim of the bicycle wheel are shown below in (2.23) and (2.24), where R is the radius of the outer ring or the rim of the wheel.

$$\mathbf{N}_{O_1} = \begin{bmatrix} R\cos(0+2i\phi) & R\cos(2\phi-2i\phi) & \cdots & R\cos(2(b-1)\phi+2i\phi) \\ R\sin(0+2i\phi) & R\sin(2\phi-2i\phi) & \cdots & R\sin(2(b-1)\phi+2i\phi) \\ 0 & 0 & \cdots & 0 \end{bmatrix} \tag{2.23}$$

$$\mathbf{N}_{O_2} = \begin{bmatrix} R\cos(\phi+2i\phi) & R\cos(3\phi-2i\phi) & \cdots & R\cos((4b-1)\phi+2i\phi) \\ R\sin(\phi+2i\phi) & R\sin(3\phi-2i\phi) & \cdots & R\sin((4b-1)\phi+2i\phi) \\ 0 & 0 & \cdots & 0 \end{bmatrix} \tag{2.24}$$

The angle index, i, can be any positive integer including zero as long as (2.25) is less than or equal to $\frac{\pi}{2}$.

$$\alpha = \arctan\left(\frac{R\sin(2i\phi)}{R\cos(2i\phi)-r}\right) \tag{2.25}$$

The final nodal matrix describing all the nodes for the bicycle wheel topology is given below in (2.26) and the size of this matrix is shown in (2.27).

$$\mathbf{N} = \begin{bmatrix} \mathbf{N}_{I_1} & \mathbf{N}_{I_2} & \mathbf{N}_{O_1} & \mathbf{N}_{O_2} \end{bmatrix} \tag{2.26}$$

$$\mathbf{N} \in \Re^{3\times 8b} \tag{2.27}$$

2.1.2.2 Connectivity Matrices

Using the numbering system shown in Figure 2.3, the string connectivity matrix can be written as follows. The columns of the matrix shown below in (2.28) represent the vectors of each string and the rows represent the nodes of the structure. For this specific topology, the matrix is made of an identity matrix of size $4b$ and a negative identity matrix of the same size placed below it. The size of this matrix is a $8b \times 4b$ matrix where b is the complexity of the topology and is shown below in (2.29).

$$\mathbf{C}_S^T = \begin{bmatrix} I_{4b} \\ -I_{4b} \end{bmatrix} \tag{2.28}$$

$$\mathbf{C}_S^T \in \Re^{8b \times 4b} \tag{2.29}$$

2.1.3 Rim Type 1

Figure 2.5 shows the numbering system for the nodes and bars for the bicycle rim topology. This image shows a complexity of two ($q = 6$). The angle between each node is ϕ and that angle is shown in the same figure. The numbering system for the bars starts from the second node and points towards the first node for bar one. The numbering continues counter clock-wise around the polygon in the same fashion by starting from the higher numbered node and pointing to the lower number node until the last bar in the polygon. This last bar starts at the first node and points towards the last node and this is done to keep the direction of the bar vectors consistent.

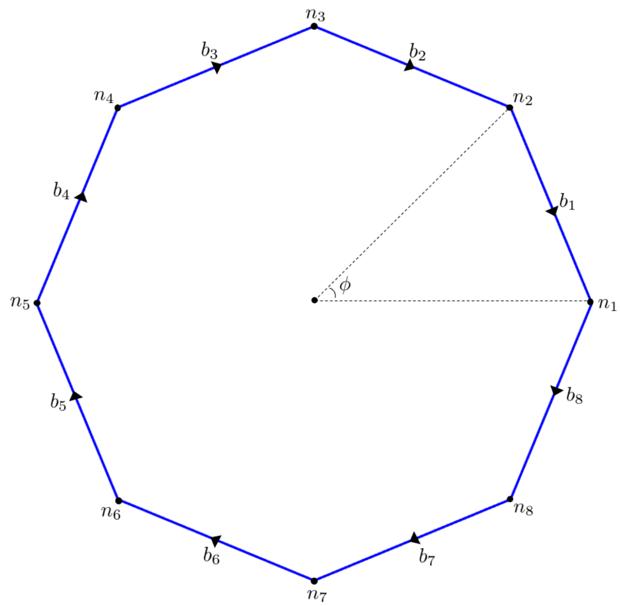

Figure 2.5: Bicycle rim topology of complexity 6

2.1.3.1 Rim Type 1 Nodal Matrix

The matrix describing all the nodes for the bicycle rim topology is given by (2.34) and the size of the matrix is shown in (2.31). The radius of the circle that the nodes are attached to is R. The fist node starts at an angle of 0, the second node has an angle of ϕ, and so on until the final node of this set is at an angle of $(q+1)\phi$, where ϕ is defined to be positive in the counter-clockwise direction.

$$\mathbf{N} = \begin{bmatrix} R\cos(0) & R\cos(\phi) & \cdots & R\cos((q+1)\phi) \\ R\sin(0) & R\sin(\phi) & \cdots & R\sin((q+1)\phi) \\ 0 & 0 & \cdots & 0 \end{bmatrix} \tag{2.30}$$

$$\mathbf{N} \in \Re^{3\times(q+2)} \tag{2.31}$$

2.1.3.2 Rim Type 1 Connectivity Matrix

The numbering system shown in Figure 2.5 is used to write the connectivity matrix for the bars of the bicycle rim topology. Using that numbering system leads to (2.32). A diagonal of ones are placed on the main diagonal of the matrix and negative ones are placed on the off diagonal as shown. For the last bar, a negative one is placed in the top right corner of the matrix. The size of this matrix is shown below in (2.33).

$$\mathbf{C}_B^T = \begin{bmatrix} 1 & 0 & 0 & -1 \\ -1 & 1 & 0 & 0 \\ 0 & \ddots & \ddots & 0 \\ 0 & 0 & -1 & 1 \end{bmatrix} \tag{2.32}$$

$$\mathbf{C}_B^T \in \Re^{(q+2)\times(q+2)} \tag{2.33}$$

2.1.4 Rim Type 2

Figure 2.6 shows the numbering system for the nodes and bars for the second bicycle rim topology. This image shows a complexity of two ($q = 2$). The angle between each node is ϕ and that angle is shown in the same figure. This rim is created by taking an n-sided polygon and duplicating it and rotating the duplication such that the nodes split the angles between nodes of the first polygon in two. The nodes are then connected along the circumference by more bars. This rim type is only used for the centrifugal force and tangential force due to torque load case for the bicycle wheel. The bicycle wheel is not stable for that load case when using rim type 1.

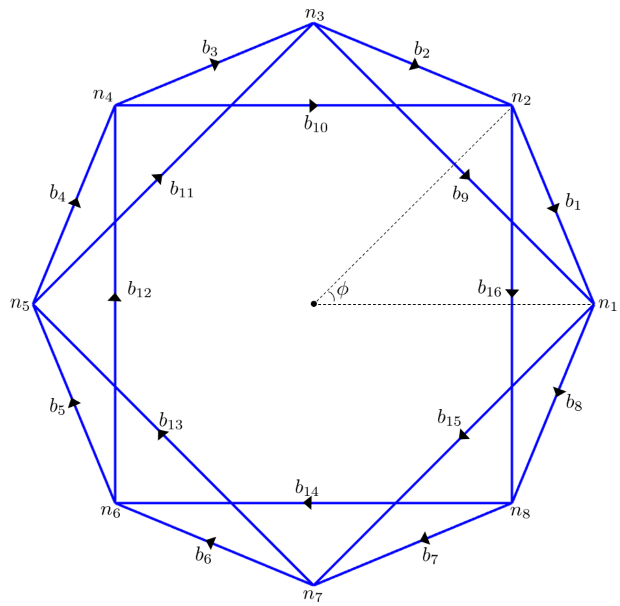

Figure 2.6: Bicycle rim type 2 topology of complexity 2

2.1.4.1 Rim Type 2 Nodal Matrix

The matrix describing all the nodes for the bicycle rim topology is given by (2.34) and the size of the matrix is shown in (2.31). The radius of the circle that the nodes are attached to is R. The fist node starts at an angle of 0, the second node has an angle of ϕ, and so on until the final node of this set is at an angle of $(4q-1)\phi$, where ϕ is defined to be positive in the counter-clockwise direction.

$$\mathbf{N} = \begin{bmatrix} R\cos(0) & R\cos(\phi) & \cdots & R\cos((4q-1)\phi) \\ R\sin(0) & R\sin(\phi) & \cdots & R\sin((4q-1)\phi) \\ 0 & 0 & \cdots & 0 \end{bmatrix} \tag{2.34}$$

2.1.4.2 Rim Type 1 Connectivity Matrix

The numbering system shown in Figure 2.6 is used to write the connectivity matrix for the bars of the bicycle rim type 2 topology. Using that numbering system leads to (2.35). The size of this matrix is shown below in (2.36).

$$\mathbf{C}_B^T = \begin{bmatrix} 1 & 0 & 0 & 0 & -1 & 1 & 0 & 0 & -1 & 0 \\ -1 & 1 & 0 & 0 & 0 & 0 & 1 & 0 & 0 & -1 \\ 0 & \ddots & \ddots & 0 & 0 & -1 & 0 & \ddots & 0 & 0 \\ 0 & 0 & \ddots & \ddots & 0 & 0 & \ddots & 0 & \ddots & 0 \\ 0 & 0 & 0 & -1 & 1 & 0 & 0 & -1 & 0 & 1 \end{bmatrix} \tag{2.35}$$

$$\mathbf{C}_B^T \in \Re^{4q \times 8q} \tag{2.36}$$

2.2 Static Load Cases

This section will discuss the two static load cases that will be applied to each of the wheels discussed in the previous section. The forces that will be discussed are really dynamic forces, but they will be applied at a snapshot in time. The first load case will be the centrifugal forces applied to each node of the structure due to the wheel spinning about its own axle. The second load case will be the centrifugal forces and the tangential forces due to the change in rotational velocity from the torque applied to the axle of the wheel. For each wheel, the mass of the rim (shown in blue in the images below) is evenly divided by the number of nodes that are coincident with the rim. For each wheel, each of the string masses are divided by two and placed at each of the two nodes that defines each string. The external force matrix, **W**, will be shown below for each of the load cases for each of the wheels.

2.2.1 Spiral Wheel

2.2.1.1 Centrifugal Force

The mass of the rim will be split evenly between the p number of nodes that lie on the circle with radius equal to r_0. The mass of each string is divided by two and the mass is distributed to the two nodes the string is connected to. For the first set of nodes, this is done by taking the total mass of the strings that lie between r_0 and r_1, which will be referred to as $m_{s_{total_1}}$, and dividing by the total number of strings that lie between those radii which is equal to $2p$. The centrifugal force on each node that lies on that circle is shown below in (2.37), where ω is the angular rate about the axle of the wheel.

$$c_0 = \frac{r_0\omega^2}{p}\left(m_r + \frac{m_{s_{total_1}}}{2}\right) \tag{2.37}$$

For the nodes that lie on the circle with radius equal to r_1, the total mass of the strings between r_1 and r_2 and the total mass of the strings between r_0 and r_1 are both divided by $2p$. These total masses will be referred to as $m_{s_{total_2}}$ and $m_{s_{total_1}}$ respectively. The centrifugal force on each node that lies on that circle is shown below in (2.38).

$$c_1 = \frac{r_1\omega^2}{2p}\left(m_{s_{total_1}} + m_{s_{total_2}}\right) \tag{2.38}$$

Following the procedure for (2.38), a general equation for the centrifugal force can be written for the nodes that are within the outer radius of the wheel. The radius r_q is not considered since those nodes are fixed to the axle of the wheel. Shown below in (2.39), is the general equation.

$$c_{q-1} = \frac{r_{q-1}\omega^2}{2p}\left(m_{s_{total_{q-2}}} + m_{s_{total_{q-1}}}\right) \tag{2.39}$$

The external force matrix for this load case is shown below in (2.40). This is compiled by taking the scalar equations derived in this section and multiplying by the corresponding segmentation of **N** where each column of **N** is now a unit vector. The final segmentation of the external force matrix is equal to zero due to the nodes on the axle being fixed.

$$\mathbf{W}_C = \begin{bmatrix} c_0\hat{\mathbf{R}}_0 & \vdots & c_1\hat{\mathbf{R}}_1 & \vdots & \cdots & \vdots & c_{q-1}\hat{\mathbf{R}}_{q-1} & \vdots & \mathbf{0} \end{bmatrix} \tag{2.40}$$

An example of the unit vector segmentation is shown below in (2.41). This example uses (2.10) where each column is now a unit vector. This is done for all other segmentations of (2.13) as well.

$$\hat{\mathbf{R}}_0 = \begin{bmatrix} \cos(0) & \cos(2\phi) & \cdots & \cos(2(p-1)\phi) \\ \sin(0) & \sin(2\phi) & \cdots & \sin(2(p-1)\phi) \\ 0 & 0 & \cdots & 0 \end{bmatrix} \tag{2.41}$$

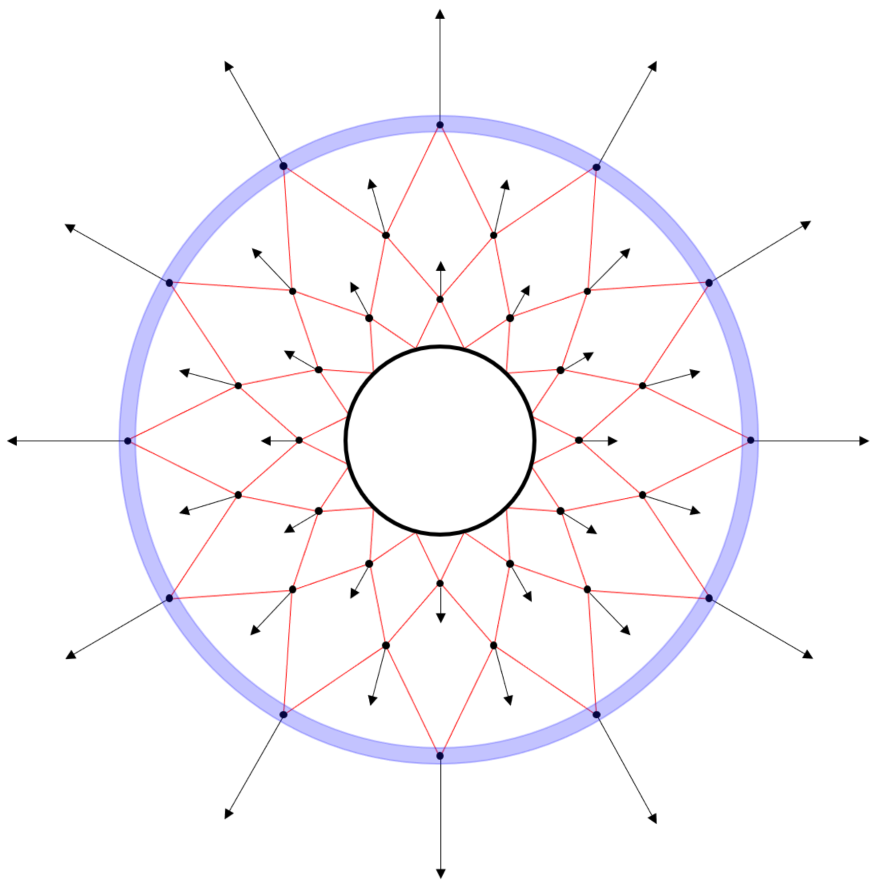

Figure 2.7: Spiral wheel with the centrifugal forces applied statically

2.2.1.2 Centrifugal Force And Tangential Force Due To Torque

The mass of the rim and the strings is distributed to the nodes of the wheel in the same manner as for the centrifugal forces. The tangential force, due to applied torque on the axle of the wheel, for the nodes that lie on that circle that has a radius equal to r_0 is shown below in (2.42), where τ

is the torque applied about the axle of the wheel and I is the sum of the inertia of the rim and the strings.

$$t_0 = \frac{r_0 \tau}{pI} \left(m_r + \frac{m_{s_{total_1}}}{2} \right) \tag{2.42}$$

The tangential force on each node that lies on the circle with a radius equal to r_1 is shown below in (2.43).

$$t_1 = \frac{r_1 \tau}{2pI} \left(m_{s_{total_1}} + m_{s_{total_2}} \right) \tag{2.43}$$

The general equation for the tangential force can be written for the nodes that are within the outer radius of the wheel. The radius r_q is not considered since those nodes are fixed to the axle of the wheel similar to the centrifugal force. Shown below in (2.44), is the general equation.

$$t_{q-1} = \frac{r_{q-1} \tau}{2pI} \left(m_{s_{total_{q-2}}} + m_{s_{total_{q-1}}} \right) \tag{2.44}$$

The external force matrix for the tangential force is shown below in (2.45). This is compiled by taking the scalar equations derived in this section and multiplying by the corresponding segmentation of **N** where each column of **N** is now a unit vector. The final segmentation of the external force matrix is equal to zero due to the nodes on the axle being fixed. The unit vectors are rotated ninety degrees so that the tangential force is perpendicular to the centrifugal force. This is done by pre-multiplying the unit vectors by the direction cosine matrix for a ninety degree rotation, **D**, for either a positive or negative rotation depending on the direction of the applied torque about the axle of the wheel.

$$\mathbf{W}_T = \left[t_0 \mathbf{D} \hat{\mathbf{R}}_0 \;\vdots\; t_1 \mathbf{D} \hat{\mathbf{R}}_1 \;\vdots\; \cdots \;\vdots\; t_{q-1} \mathbf{D} \hat{\mathbf{R}}_{q-1} \;\vdots\; \mathbf{0} \right] \tag{2.45}$$

The total external force matrix for this load case is given by adding (2.40) to (2.45) and is shown below in (2.46).

$$\mathbf{W} = \mathbf{W}_C + \mathbf{W}_T \tag{2.46}$$

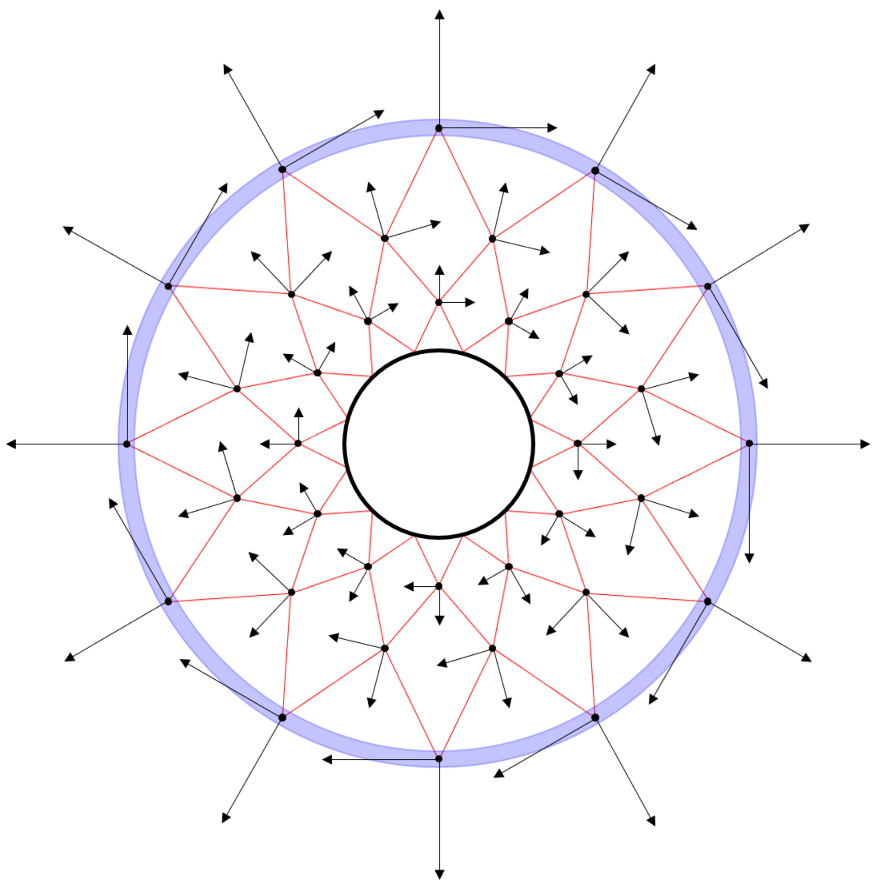

Figure 2.8: Spiral wheel with the centrifugal forces and tangential force due to torque applied statically

2.2.2 Bicycle Wheel

2.2.2.1 Centrifugal Force

The mass of the rim will be split evenly between the $4b$ number of nodes that lie on the circle with radius equal to R. The mass of each string is divided by two and the mass is distributed to the two nodes the string is connected to. This is done by taking the total mass of the strings, $m_{s_{total}}$, and dividing by the total number of strings which is equal to $4b$. The centrifugal force on each node that lies on that circle is shown below in (2.47), where ω is the angular rate about the axle of the wheel.

$$c = \frac{R\omega^2}{4b}\left(m_r + m_{s_{total}}\right) \tag{2.47}$$

The external force matrix for this load case is shown below in (2.48). This is compiled by taking the scalar equations derived in this section and multiplying by the corresponding segmentation of **N** where each column of **N** is now a unit vector. The first two segmentations of the external force matrix are equal to zero due to the nodes on the axle being fixed.

$$\mathbf{W}_C = \begin{bmatrix} \mathbf{0} & \mathbf{0} & c\hat{\mathbf{N}}_{0_1} & c\hat{\mathbf{N}}_{0_2} \end{bmatrix} \tag{2.48}$$

An example of the unit vector segmentation is shown below in (2.49). This example uses (2.23) where each column is now a unit vector. This is done for the other segmentation of outer nodes as well.

$$\hat{\mathbf{N}}_{O_1} = \begin{bmatrix} \cos(0+2i\phi) & \cos(2\phi-2i\phi) & \cdots & \cos(2(b-1)\phi+2i\phi) \\ \sin(0+2i\phi) & \sin(2\phi-2i\phi) & \cdots & \sin(2(b-1)\phi+2i\phi) \\ 0 & 0 & \cdots & 0 \end{bmatrix} \tag{2.49}$$

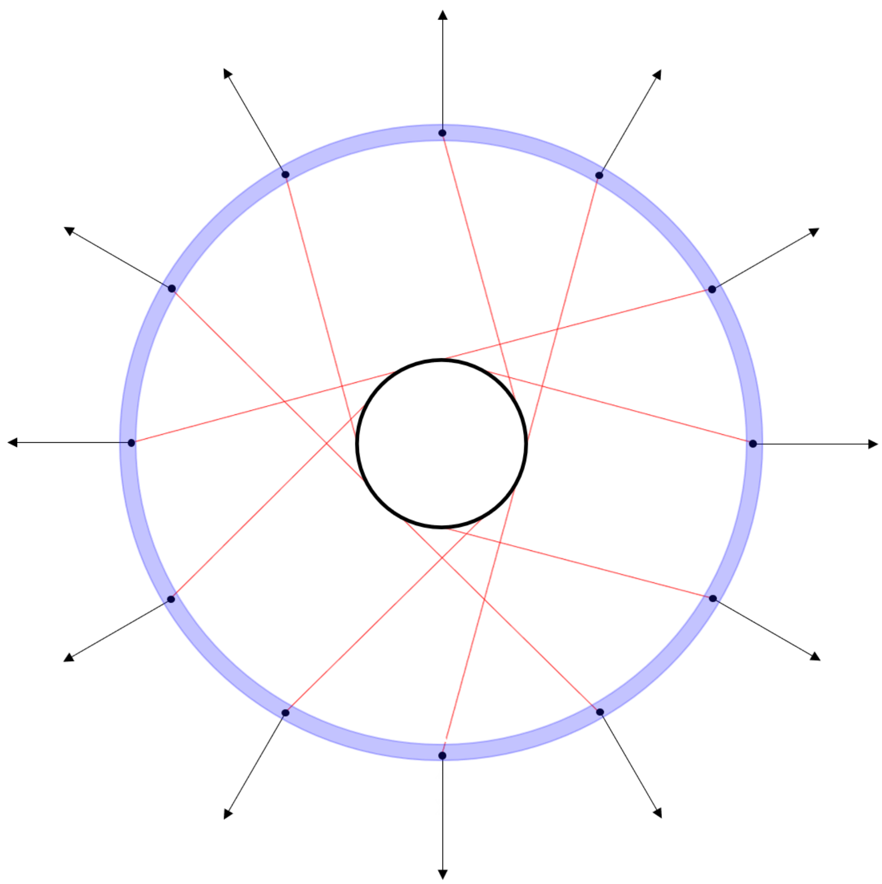

Figure 2.9: Bicycle wheel with the centrifugal forces applied statically

2.2.2.2 *Centrifugal Force And Tangential Force Due To Torque*

The mass of the rim and the strings is distributed to the nodes of the wheel in the same manner as for the centrifugal forces. The tangential force, due to applied torque on the axle of the wheel, for the nodes that lie on that circle that has a radius equal to R is shown below in (2.50), where τ is the torque applied about the axle of the wheel and I is the sum of the inertia of the rim and the strings.

$$t = \frac{R\tau}{4bI}\left(m_r + m_{s_{total}}\right) \tag{2.50}$$

The external force matrix for the tangential force is shown below in (2.51). This is compiled by taking the scalar equation derived in this section and multiplying by the corresponding segmentation of **N** where each column of **N** is now a unit vector. The first two segmentations of the external force matrix are equal to zero due to the nodes on the axle being fixed. The unit vectors are rotated ninety degrees so that the tangential force is perpendicular to the centrifugal force. This is done by pre-multiplying the unit vectors by the direction cosine matrix for a ninety degree rotation, **D**, for either a positive or negative rotation depending on the direction of the applied torque about the axle of the wheel.

$$\mathbf{W}_T = \begin{bmatrix} \mathbf{0} & \mathbf{0} & t\mathbf{D}\hat{\mathbf{N}}_{0_1} & t\mathbf{D}\hat{\mathbf{N}}_{0_2} \end{bmatrix} \tag{2.51}$$

The total external force matrix for this load case is given by adding (2.48) to (2.51) and is shown below in (2.52).

$$\mathbf{W} = \mathbf{W}_C + \mathbf{W}_T \tag{2.52}$$

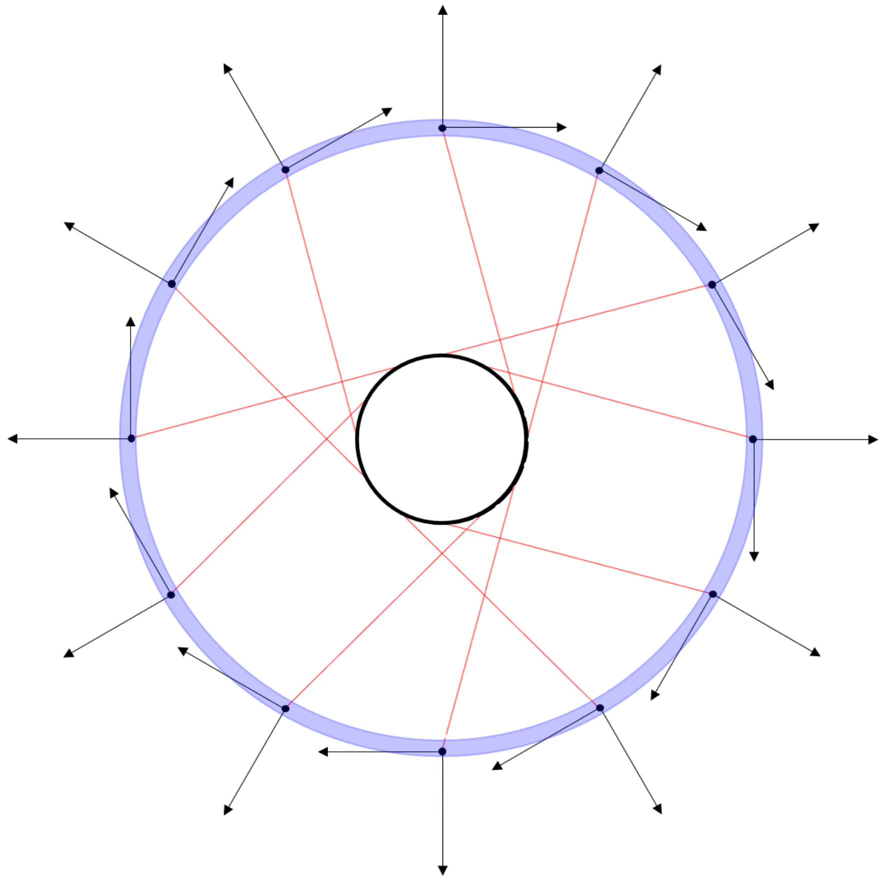

Figure 2.10: Bicycle wheel with the centrifugal forces and tangential force due to torque applied statically

2.3 Algorithm To Minimize Mass Subject To An Angular Momentum Constraint

An algorithm to minimize the mass of a tensegrity wheel subject to the static equilibrium equation and an angular momentum constraint will be presented in this section. A flowchart of the algorithm is shown in Figure 2.11. The next sections will describe each box of this flowchart in detail.

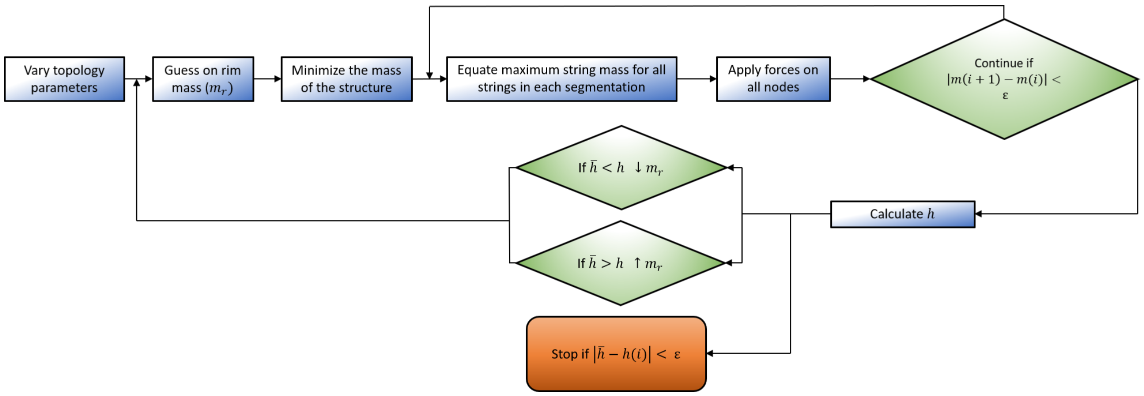

Figure 2.11: Flowchart describing the algorithm to minimize the mass of a tensegrity wheel

2.3.1 Varying The Topology Parameters

The algorithm begins by picking the topology parameters. For the spiral wheel, the parameters p and q are chosen. The radial complexity must be equal to or greater than one. The circumferential complexity p must be greater than or equal to three for stability. For the bicycle wheel, the complexity b and the spoke angle index can be varied and a pair is chosen at the beginning of the algorithm. Both the complexity of the bicycle wheel and the spoke angle index must be greater than or equal to one. For each of the topologies, the rim topology discussed in 2.1.3 is augmented utilizing the algorithm presented in Appendix B. After the algorithm finishes for the chosen pair, other pairs can be chosen to compare the minimum mass to find the overall minimum mass to find the optimal topology configuration for both the spiral wheel and the bicycle wheel.

2.3.2 Guessing On The Rim Mass

After a topology has been defined, a guess for the rim mass is needed to determine the forces that will be applied on the nodes along the circumference of the structure from the centrifugal forces. An angular momentum output is chosen based upon the control needs for the spacecraft. This angular momentum requirement will be referred to as $\bar{h}$. The angular momentum of the rim is equal to the inertia of the rim multiplied by the angular rate. For a thin hoop, the inertia is equal to the mass of the rim multiplied by the outer radius squared and is shown below in (2.53).

$$\bar{h} = I\omega = m_r r_0^2 \omega \tag{2.53}$$

The angular rate is chosen by the control needs of the spacecraft and restrictions on the dimensions of the flywheel itself. Solving for the mass of the rim results in (2.54). This will serve as the initial guess for the rim mass for the algorithm and will change on each iteration of the algorithm until convergence.

$$m_r = \frac{\bar{h}}{\omega r_0^2} \tag{2.54}$$

2.3.3 Minimizing The Mass Of The Structure

The mass minimimization process will be taken form Theorem 6.1 from [1] and will be summarized here. First consider a tensegrity system described by (2.55) - (2.57).

$$\boldsymbol{B} = \boldsymbol{N}\boldsymbol{C}_B^T \tag{2.55}$$

$$\boldsymbol{S} = \boldsymbol{N}\boldsymbol{C}_S^T \tag{2.56}$$

$$\boldsymbol{S}\hat{\gamma}\boldsymbol{C}_S - \boldsymbol{B}\hat{\lambda}\boldsymbol{C}_B = \boldsymbol{W} \tag{2.57}$$

Suppose the system is at an equilibrium in the given configuration $\boldsymbol{N}$ with an external force $\boldsymbol{W}$. The minimal mass structure under a yield stress constraint is given by the solution of the linear problem shown below

$$\underset{\boldsymbol{x}}{minimize} \;\; \bar{m} = \boldsymbol{c}^T\boldsymbol{x}, \;\; subject \;\; to \;\; \boldsymbol{A}\boldsymbol{x} = \boldsymbol{w} \;\; and \;\; \boldsymbol{x} \geq \boldsymbol{x}_0, \tag{2.58}$$

where

$$\boldsymbol{x} = [\lambda_1 \cdots \lambda_{n_b} | \gamma_1 \cdots \gamma_{n_s}]^T \tag{2.59}$$

$$\boldsymbol{c}^T = [c_{b_1} \cdots c_{b_{n_b}} | c_{s_1} \cdots c_{s_{n_s}}] \tag{2.60}$$

$$\boldsymbol{A} = [-(\boldsymbol{C}_B^T \otimes \boldsymbol{I}_3)\hat{\boldsymbol{B}} \ \ (\boldsymbol{C}_S^T \otimes \boldsymbol{I}_3)\hat{\boldsymbol{S}}] \tag{2.61}$$

where $c_{b_i} = \rho_{b_i} b_i^2 / \sigma_{b_i}$, $c_{s_i} = \rho_{s_i} s_i^2 / \sigma_{s_i}$, $\hat{\boldsymbol{B}} =$ b.d.$(\boldsymbol{b}_1, \cdots, \boldsymbol{b}_{n_b})$, $\hat{\boldsymbol{S}} =$ b.d.$(\boldsymbol{s}_1, \cdots, \boldsymbol{s}_{n_s})$, and $\boldsymbol{x}_0 \geq \mathbf{0}$ is a constant vector. Cross-section area of each member is given by (2.61), and the total mass m is given by the sum of the mass of the bars and the strings shown below in (2.62).

$$m = m_b + m_s = \sum_{i=1}^{n_b} \rho_{b_i} A_{b_i} b_i + \sum_{i=1}^{n_s} \rho_{s_i} A_{s_i} s_i \tag{2.62}$$

where $b_i = ||\boldsymbol{b}_i||$, $s_i = ||\boldsymbol{s}_i||$ are the lengths of the members of the bars and strings respectively and ρ_{b_i} and ρ_{s_i} are the mass densities. The initial force matrix $\boldsymbol{W}$ only has forces on the outer nodes of the structure for both the spiral wheel and bicycle wheel topologies. For the bicycle wheel, the force matrices that were derived will remain the same, but for the spiral wheel the force matrices will be reduced to (2.63) and (2.64) shown below.

$$\mathbf{W}_C = \left[c_0 \hat{\mathbf{R}}_0 \ \vdots \ \mathbf{0} \ \vdots \ \cdots \ \vdots \ \mathbf{0} \right] \tag{2.63}$$

$$\mathbf{W}_T = \left[t_0 \mathbf{D} \hat{\mathbf{R}}_0 \ \vdots \ \mathbf{0} \ \vdots \ \cdots \ \vdots \ \mathbf{0} \right] \tag{2.64}$$

Now the linear programming problem can be solved and the minimum mass for the chosen loading condition is found. Now that the mass of the strings are known, the mass of the structure can be taken into account in the force matrix.

2.3.4 Equate Maximum String Mass For All Strings In Each Segmentation

Depending on the load case, the mass of the strings after the minimization process could be unsymmetrical. For example, for the centrifugal plus torque load case the strings that take the tangential force load will have a higher mass than the strings that would take the load if the torque was applied in the opposite direction. To rectify this, the max mass of all the strings for each segmentation is taken and the mass of all the strings in that segmentation are set equal to that maximum value.

2.3.5 Applying Forces On All Nodes

After the mass of each string is found from the mass minimization process in the previous section, forces can be applied to every node of the structure using the mass of the structure itself. After these forces are added, the mass minimization problem is solved again. This will result in a different mass for the strings and the new added mass will need to be accounted for again. This process is performed iteratively until the mass of the structure changes within some specified tolerance. Once the difference between successive iterations is within that tolerance, the algorithm continues to the next block in the diagram.

2.3.6 Total Angular Momentum

The total angular momentum of the wheel will now be calculated to be compared to the angular momentum constraint. To do this, the total moment of inertia of the wheel must be derived including the rim, strings, and axle. The total angular momentum is shown below in (2.65) for both the spiral wheel and the bicycle wheel.

$$h = (I_s + I_r + I_a)\omega \tag{2.65}$$

2.3.6.1 Moment Of Inertia Of The Spiral Wheel

The total moment of inertia of the strings of the spiral wheel is shown below in (2.66).

$$I_s = \sum_{i=1}^{n_s} \frac{1}{12} m_{s_i} \|s_i\|^2 + \sum_{j=1}^{q} \frac{1}{4} m_{s_{total_j}} (r_{j-1} + r_j)^2 \tag{2.66}$$

The moment of inertia of the rim of the spiral wheel is shown below in (2.67).

$$I_r = m_r r_0^2 \tag{2.67}$$

The moment of inertia of the axle of the spiral wheel is shown below in (2.68).

$$I_a = \frac{1}{2} m_r r_q^2 \tag{2.68}$$

2.3.6.2 Moment Of Inertia Of The Bicycle Wheel

The total moment of inertia of the strings of the bicycle wheel is shown below in (2.69).

$$I_s = \sum_{i=1}^{n_s} \frac{1}{12} m_{s_i} \|s_i\|^2 + \frac{1}{2} m_{s_i} (r + R)^2 \tag{2.69}$$

The moment of inertia of the rim of the bicycle wheel is shown below in (2.70).

$$I_r = m_r R^2 \tag{2.70}$$

The moment of inertia of the axle of the bicycle wheel is shown below in (2.71).

$$I_a = \frac{1}{2} m_r r^2 \tag{2.71}$$

2.3.7 Loop Exit Criteria

Once the absolute value of the difference between the angular momentum constraint and the total angular momentum of the wheel is within a specified tolerance, the loop exits and the final design of the wheel for the specified topology configuration is completed. The criteria is shown below in (2.72). If the criteria is not met, the algorithm caries on to the next step.

$$\left|\bar{h} - h\right| < \epsilon \tag{2.72}$$

2.3.8 New Rim Mass Guess

If the total angular momentum is greater than the angular momentum constraint, then the initial rim mass guess is decreased. If the total angular momentum is less than the angular momentum constraint, then the initial rim mass guess is increased. The initial rim mass guess is multiplied by the ratio of the angular momentum constraint divided by the total angular momentum of the wheel shown below in (2.73)

$$m_{r_{i+1}} = \frac{\bar{h}}{h} m_{r_i} \tag{2.73}$$

2.4 Results

Using the algorithm developed in the previous section, the spiral tensegrity wheel and the bicycle wheel were optimized. The inputs into the algorithm were chosen to match the flywheel from the CMGs on the ISS from the introduction chapter as closely as possible. The table shown below lists the input parameters for the dimensions of the wheel, the angular momentum requirement, the angular rate of the wheel, and the torque that is applied to the wheel. The inner radius of the wheel was chosen to be as small as possible due to the mass optimal wheel having the smallest possible axis.

Table 2.1: Input parameters for the topology optimization

Parameters	**Values**
$\bar{\omega}$ (RPM)	6600
$\bar{h}$ (N*m*s)	4760
R (m)	0.37
r_q/r (m)	0.01
τ (N*m)	258

Two different material combinations between the rim and the strings were used. The first combination (Selection #1) uses Type 321 Stainless Steel for the rim and Spectra Fiber for the strings. The material properties for this selection is shown below in Table 2.2. The second combination (Selection #2) uses tungsten alloy K1850 for the rim and Ti-6Al-4V (Grade 5) titanium for the strings shown below in Table 2.3. The material selection not only results in a difference of mass for both topologies and both load cases, but also results in a difference in complexity for the optimal structure.

Table 2.2: Material combination selection #1

Parameters	**Values**
ρ_s	0.97e3 $\frac{kg}{m^3}$
σ_s	3000e6 Pa
ρ_b	8.00e3 $\frac{kg}{m^3}$
σ_b	415e6 Pa

Table 2.3: Material combination selection #2

Parameters	**Values**
ρ_s	4.43e3 $\frac{kg}{m^3}$
σ_s	880e6 Pa
ρ_b	18.50e3 $\frac{kg}{m^3}$
σ_b	655e6 Pa

For the centrifugal force load case, the spiral wheel is more mass optimal compared to the bicycle wheel. This result seems counter intuitive at first. One would think the mass optimal structure for forces radially outwards would be a structure where the tensile members are also oriented radially outwards from the spin axis. This would be true if not for the angular momentum constraint on the optimization process. The reasons for this is the center of mass of the strings of the spiral wheel are further from the spin axis than the bicycle wheel strings.

The spiral wheel is also the mass optimal structure compared to the bicycle wheel for the centrifugal force and torque load case. This result was expected due to the ideal torque properties from the Michell Truss. The increase in mass is small in comparison to the centrifugal force load case. The centrifugal forces are significantly more important than the torque.

The tables shown in the following subsections show the optimal complexity highlighted in green. For some cases, multiple cells are highlighted. For these cases, there are multiple complexity combinations that have the same minimal mass. The lowest complexity was chosen since that would be the cheapest wheel to manufacture. In future work, other reasons could determine which of the optimal complexity pairs would be chosen such as dynamic properties or restrictions needed for deployability of the wheels. The blank cells in the table correspond to complexity pairs that violate any of the geometric constraints presented earlier in the chapter. The cells filled with 'NS' or no solution are complexity pairs where the structure does not have a static equilibrium for that particular load case. The only table that has 'NS' in some cells is for the bicycle wheel when a torque is applied and the complexity pair is one in which the strings are oriented radially outwards from the spin axis. Gradient tables are shown below to demonstrate how the mass of the wheel changes with respect to the topology parameters.

2.4.1 Spiral Wheel

2.4.1.1 Centrifugal Force (Material Property Selection #1)

Table 2.4: Final mass of the rim for the spiral wheel (centrifugal force load case / selection #1)

	Spiral Wheel - Rim Mass (kg)																			
	q																			
p	1	2	3	4	5	6	7	8	9	10	11	12	13	14	15	16	17	18	19	20
3	50.2306	50.2213	50.2059																	
4	50.2309	50.2261	50.2164	50.2046																
5	50.2310	50.2285	50.2220	50.2136	50.2042															
6	50.2309	50.2298	50.2252	50.2191	50.2119	50.2040														
7	50.2307	50.2306	50.2273	50.2226	50.2170	50.2107	50.2040													
8	50.2304	50.2312	50.2286	50.2250	50.2206	50.2154	50.2098	50.2039												
9	50.2302	50.2315	50.2296	50.2267	50.2231	50.2189	50.2142	50.2092	50.2039											
10	50.2299	50.2317	50.2303	50.2279	50.2249	50.2214	50.2175	50.2132	50.2086	50.2039										
11	50.2296	50.2319	50.2308	50.2288	50.2264	50.2234	50.2200	50.2163	50.2124	50.2082	50.2039									
12	50.2293	50.2320	50.2311	50.2295	50.2274	50.2249	50.2220	50.2188	50.2154	50.2117	50.2079	50.2039								
13	50.2290	50.2321	50.2314	50.2301	50.2283	50.2261	50.2236	50.2208	50.2178	50.2145	50.2111	50.2075	50.2039							
14	50.2287	50.2322	50.2316	50.2305	50.2290	50.2271	50.2249	50.2224	50.2198	50.2169	50.2138	50.2106	50.2073	50.2039						
15	50.2284	50.2322	50.2318	50.2309	50.2295	50.2279	50.2260	50.2238	50.2214	50.2188	50.2161	50.2132	50.2102	50.2071	50.2039					
16	50.2281	50.2322	50.2320	50.2312	50.2300	50.2285	50.2268	50.2249	50.2228	50.2204	50.2180	50.2153	50.2126	50.2098	50.2069	50.2039				
17	50.2278	50.2322	50.2321	50.2314	50.2304	50.2291	50.2276	50.2258	50.2239	50.2218	50.2196	50.2172	50.2147	50.2121	50.2094	50.2067	50.2039			
18	50.2274	50.2322	50.2322	50.2316	50.2307	50.2295	50.2282	50.2266	50.2249	50.2230	50.2210	50.2188	50.2165	50.2141	50.2117	50.2091	50.2065	50.2039		
19	50.2271	50.2322	50.2323	50.2318	50.2310	50.2299	50.2287	50.2273	50.2257	50.2240	50.2222	50.2202	50.2181	50.2159	50.2136	50.2113	50.2089	50.2064	50.2039	
20	50.2268	50.2322	50.2323	50.2319	50.2312	50.2303	50.2292	50.2279	50.2265	50.2249	50.2232	50.2214	50.2195	50.2174	50.2153	50.2132	50.2109	50.2086	50.2063	50.2039

Table 2.5: Gradient table for the rim mass of the spiral wheel (centrifugal force load case / selection #1)

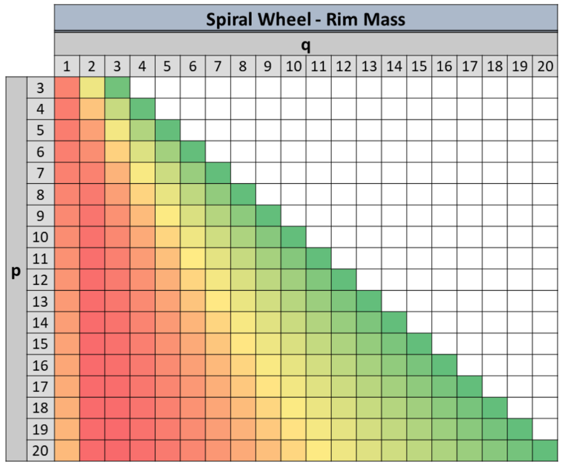

Table 2.6: Final mass of the strings for the spiral wheel (centrifugal force load case / selection #1)

Spiral Wheel - String Mass (kg)																				
p \ q	1	2	3	4	5	6	7	8	9	10	11	12	13	14	15	16	17	18	19	20
3	0.2225	0.2220	0.2226																	
4	0.2220	0.2206	0.2217	0.2223																
5	0.2222	0.2197	0.2207	0.2216	0.2222															
6	0.2227	0.2192	0.2198	0.2208	0.2216	0.2221														
7	0.2234	0.2189	0.2192	0.2201	0.2210	0.2216	0.2220													
8	0.2241	0.2188	0.2188	0.2195	0.2204	0.2211	0.2216	0.2220												
9	0.2249	0.2187	0.2185	0.2191	0.2198	0.2205	0.2212	0.2216	0.2220											
10	0.2258	0.2188	0.2184	0.2187	0.2194	0.2201	0.2207	0.2212	0.2216	0.2220										
11	0.2267	0.2189	0.2182	0.2185	0.2190	0.2197	0.2203	0.2208	0.2213	0.2217	0.2219									
12	0.2275	0.2190	0.2182	0.2183	0.2187	0.2193	0.2199	0.2205	0.2209	0.2213	0.2217	0.2219								
13	0.2284	0.2191	0.2182	0.2182	0.2185	0.2190	0.2196	0.2201	0.2206	0.2210	0.2214	0.2217	0.2219							
14	0.2293	0.2193	0.2182	0.2181	0.2183	0.2187	0.2193	0.2198	0.2203	0.2207	0.2211	0.2214	0.2217	0.2219						
15	0.2303	0.2195	0.2182	0.2180	0.2182	0.2185	0.2190	0.2195	0.2200	0.2204	0.2208	0.2212	0.2215	0.2217	0.2219					
16	0.2312	0.2196	0.2182	0.2179	0.2181	0.2184	0.2188	0.2192	0.2197	0.2201	0.2205	0.2209	0.2212	0.2215	0.2217	0.2219				
17	0.2321	0.2198	0.2183	0.2179	0.2180	0.2182	0.2186	0.2190	0.2194	0.2198	0.2203	0.2206	0.2210	0.2213	0.2215	0.2217	0.2219			
18	0.2330	0.2200	0.2184	0.2179	0.2179	0.2181	0.2184	0.2188	0.2192	0.2196	0.2200	0.2204	0.2207	0.2210	0.2213	0.2215	0.2217	0.2219		
19	0.2339	0.2202	0.2184	0.2179	0.2179	0.2180	0.2183	0.2186	0.2190	0.2194	0.2198	0.2201	0.2205	0.2208	0.2211	0.2213	0.2216	0.2217	0.2219	
20	0.2349	0.2204	0.2185	0.2179	0.2178	0.2179	0.2182	0.2185	0.2188	0.2192	0.2195	0.2199	0.2203	0.2206	0.2209	0.2211	0.2214	0.2216	0.2217	0.2219

Table 2.7: Gradient table for the string mass of the spiral wheel (centrifugal force load case / selection #1)

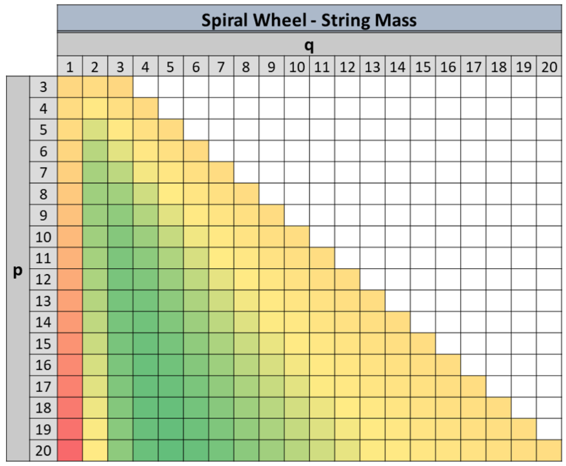

Table 2.8: Final total mass of the spiral wheel (centrifugal force load case / selection #1)

Spiral Wheel - Total Mass (kg)																				
p \ q	1	2	3	4	5	6	7	8	9	10	11	12	13	14	15	16	17	18	19	20
3	50.4531	50.4433	50.4284																	
4	50.4529	50.4467	50.4381	50.4269																
5	50.4532	50.4482	50.4427	50.4352	50.4264															
6	50.4536	50.4490	50.4451	50.4399	50.4335	50.4261														
7	50.4540	50.4495	50.4465	50.4428	50.4380	50.4323	50.4260													
8	50.4546	50.4499	50.4475	50.4446	50.4409	50.4365	50.4315	50.4259												
9	50.4551	50.4502	50.4481	50.4458	50.4429	50.4394	50.4354	50.4308	50.4259											
10	50.4557	50.4505	50.4486	50.4467	50.4443	50.4415	50.4382	50.4344	50.4303	50.4259										
11	50.4563	50.4508	50.4490	50.4473	50.4454	50.4431	50.4403	50.4372	50.4337	50.4299	50.4258									
12	50.4568	50.4510	50.4493	50.4478	50.4462	50.4442	50.4419	50.4393	50.4363	50.4330	50.4295	50.4258								
13	50.4574	50.4512	50.4496	50.4482	50.4468	50.4451	50.4432	50.4409	50.4384	50.4355	50.4325	50.4292	50.4258							
14	50.4580	50.4514	50.4498	50.4486	50.4473	50.4458	50.4442	50.4422	50.4400	50.4376	50.4349	50.4320	50.4290	50.4258						
15	50.4586	50.4516	50.4500	50.4489	50.4477	50.4464	50.4450	50.4433	50.4413	50.4392	50.4369	50.4343	50.4316	50.4288	50.4258					
16	50.4592	50.4518	50.4502	50.4491	50.4481	50.4469	50.4456	50.4441	50.4424	50.4406	50.4385	50.4362	50.4338	50.4313	50.4286	50.4258				
17	50.4599	50.4520	50.4504	50.4493	50.4483	50.4473	50.4461	50.4448	50.4433	50.4417	50.4398	50.4378	50.4357	50.4334	50.4309	50.4284	50.4258			
18	50.4605	50.4522	50.4505	50.4495	50.4486	50.4476	50.4466	50.4454	50.4441	50.4426	50.4410	50.4392	50.4372	50.4352	50.4330	50.4307	50.4283	50.4258		
19	50.4611	50.4524	50.4507	50.4497	50.4488	50.4479	50.4470	50.4459	50.4447	50.4434	50.4419	50.4403	50.4386	50.4367	50.4347	50.4326	50.4304	50.4281	50.4258	
20	50.4617	50.4526	50.4508	50.4498	50.4490	50.4482	50.4473	50.4464	50.4453	50.4441	50.4428	50.4413	50.4397	50.4380	50.4362	50.4343	50.4323	50.4302	50.4280	50.4258

Table 2.9: Gradient table for the total mass of the spiral wheel (centrifugal force load case / selection #1)

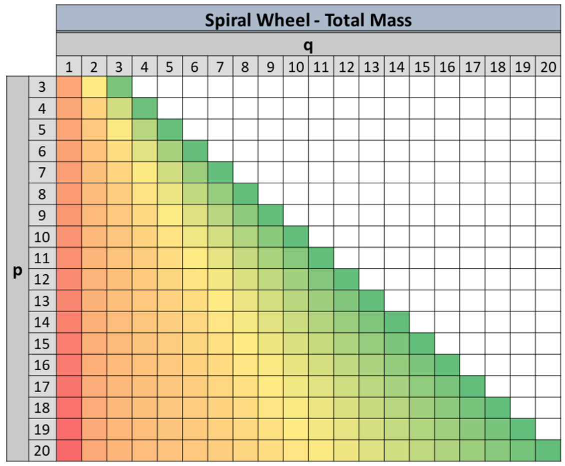

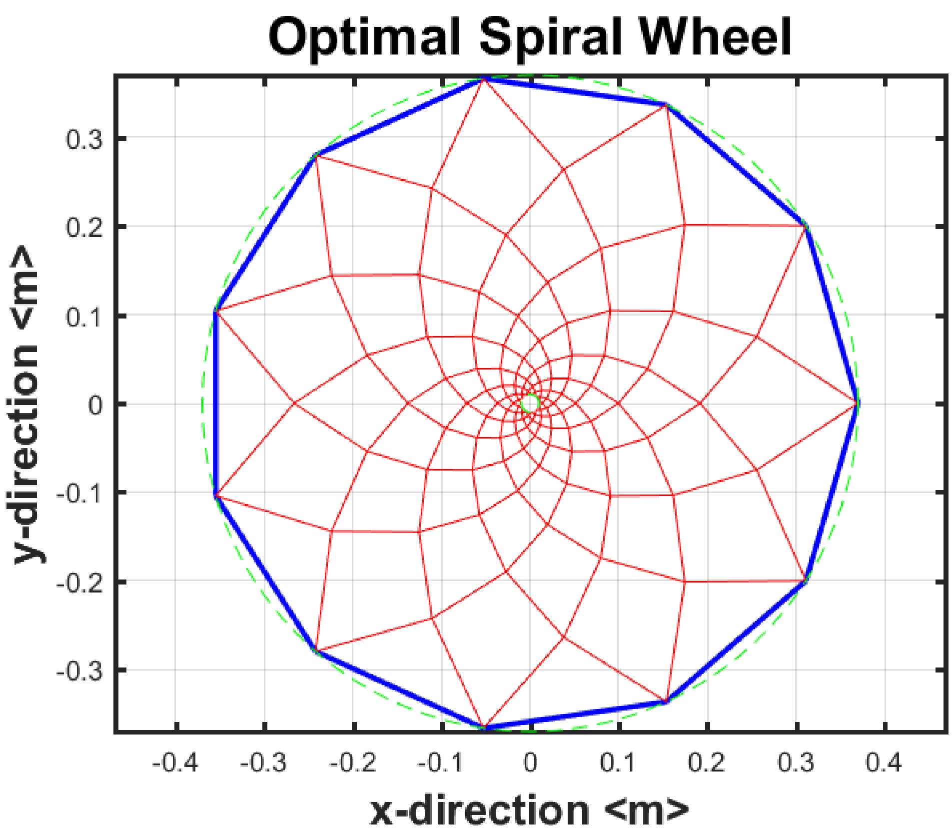

Figure 2.12: Optimal topology of the spiral wheel (centrifugal force load case / selection #1)

2.4.1.2 Centrifugal Force (Material Property Selection #2)

Table 2.10: Final mass of the rim for the spiral wheel (centrifugal force load case / selection #2)

Spiral Wheel - Rim Mass (kg)																									
p \ q	1	2	3	4	5	6	7	8	9	10	11	12	13	14	15	16	17	18	19	20	21	22	23	24	25
3	47.3992	47.0563	46.5147																						
4	47.4257	47.2489	46.9315	46.5248																					
5	47.4388	47.3462	47.1517	46.8769	46.5498																				
6	47.4461	47.4014	47.2799	47.0890	46.8471	46.5718																			
7	47.4506	47.4356	47.3604	47.2251	47.0430	46.8272	46.5889																		
8	47.4535	47.4580	47.4140	47.3171	47.1777	47.0065	46.8121	46.6018																	
9	47.4556	47.4736	47.4513	47.3819	47.2740	47.1364	46.9764	46.7999	46.6116																
10	47.4570	47.4848	47.4784	47.4291	47.3448	47.2331	47.1002	46.9510	46.7895	46.6190															
11	47.4581	47.4932	47.4986	47.4646	47.3983	47.3068	47.1955	47.0685	46.9292	46.7805	46.6248														
12	47.4589	47.4996	47.5140	47.4919	47.4397	47.3641	47.2701	47.1613	47.0406	46.9104	46.7727	46.6294													
13	47.4596	47.5045	47.5261	47.5133	47.4723	47.4095	47.3296	47.2357	47.1305	47.0159	46.8938	46.7658	46.6331												
14	47.4601	47.5085	47.5358	47.5304	47.4984	47.4460	47.3776	47.2962	47.2039	47.1027	46.9941	46.8793	46.7596	46.6361											
15	47.4605	47.5117	47.5436	47.5443	47.5197	47.4759	47.4170	47.3459	47.2647	47.1748	47.0777	46.9746	46.8664	46.7540	46.6385										
16	47.4609	47.5143	47.5500	47.5556	47.5372	47.5005	47.4496	47.3873	47.3153	47.2352	47.1482	47.0552	46.9571	46.8548	46.7491	46.6405									
17	47.4611	47.5165	47.5553	47.5651	47.5518	47.5210	47.4769	47.4220	47.3580	47.2863	47.2080	47.1239	47.0347	46.9414	46.8444	46.7445	46.6422								
18	47.4614	47.5183	47.5597	47.5731	47.5640	47.5384	47.5000	47.4514	47.3943	47.3299	47.2591	47.1828	47.1016	47.0162	46.9272	46.8351	46.7404	46.6437							
19	47.4616	47.5199	47.5635	47.5798	47.5745	47.5531	47.5197	47.4766	47.4254	47.3673	47.3031	47.2337	47.1595	47.0812	46.9993	46.9143	46.8266	46.7367	46.6449						
20	47.4618	47.5212	47.5667	47.5856	47.5834	47.5658	47.5366	47.4982	47.4522	47.3996	47.3413	47.2779	47.2099	47.1380	47.0625	46.9839	46.9025	46.8189	46.7332	46.6460					
21	47.4619	47.5223	47.5695	47.5906	47.5911	47.5767	47.5513	47.5170	47.4755	47.4277	47.3745	47.3165	47.2541	47.1878	47.1181	47.0452	46.9697	46.8918	46.8118	46.7301	46.6469				
22	47.4620	47.5233	47.5719	47.5949	47.5978	47.5863	47.5640	47.5334	47.4958	47.4523	47.4037	47.3504	47.2929	47.2317	47.1672	47.0996	47.0294	46.9567	46.8819	46.8053	46.7271	46.6477			
23	47.4621	47.5242	47.5741	47.5987	47.6037	47.5946	47.5752	47.5477	47.5136	47.4739	47.4293	47.3803	47.3273	47.2707	47.2108	47.1480	47.0825	47.0147	46.9447	46.8728	46.7993	46.7244	46.6484		
24	47.4622	47.5249	47.5759	47.6020	47.6088	47.6019	47.5850	47.5603	47.5294	47.4931	47.4520	47.4068	47.3578	47.3053	47.2497	47.1912	47.1301	47.0666	47.0010	46.9336	46.8644	46.7938	46.7219	46.6490	
25	47.4623	47.5256	47.5775	47.6050	47.6134	47.6084	47.5937	47.5716	47.5434	47.5100	47.4722	47.4304	47.3850	47.3362	47.2844	47.2298	47.1727	47.1133	47.0518	46.9884	46.9233	46.8566	46.7887	46.7196	46.6495

Table 2.11: Gradient table for the rim mass of the spiral wheel (centrifugal force load case / selection #2)

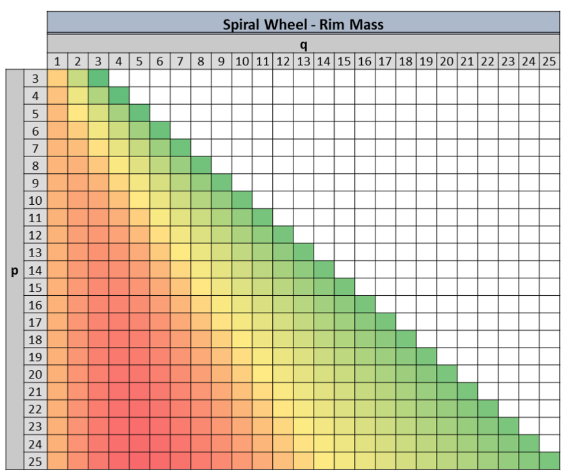

Table 2.12: Final mass of the strings for the spiral wheel (centrifugal force load case / selection #2)

Spiral Wheel - String Mass (kg)																									
	q																								
p	1	2	3	4	5	6	7	8	9	10	11	12	13	14	15	16	17	18	19	20	21	22	23	24	25
3	8.4333	8.4092	8.4121																						
4	8.3791	8.3202	8.3186	8.3505																					
5	8.3522	8.2626	8.2433	8.2712	8.3138																				
6	8.3371	8.2259	8.1880	8.2068	8.2463	8.2909																			
7	8.3278	8.2018	8.1482	8.1561	8.1903	8.2327	8.2760																		
8	8.3217	8.1852	8.1193	8.1169	8.1443	8.1832	8.2249	8.2658																	
9	8.3175	8.1735	8.0980	8.0865	8.1069	8.1414	8.1806	8.2202	8.2586																
10	8.3145	8.1648	8.0820	8.0628	8.0767	8.1064	8.1426	8.1804	8.2175	8.2532															
11	8.3122	8.1583	8.0696	8.0441	8.0521	8.0771	8.1099	8.1455	8.1812	8.2160	8.2492														
12	8.3105	8.1533	8.0599	8.0292	8.0321	8.0526	8.0818	8.1149	8.1490	8.1826	8.2151	8.2461													
13	8.3092	8.1494	8.0522	8.0170	8.0156	8.0319	8.0577	8.0882	8.1204	8.1527	8.1843	8.2146	8.2437												
14	8.3081	8.1463	8.0460	8.0071	8.0019	8.0146	8.0371	8.0648	8.0950	8.1259	8.1564	8.1860	8.2145	8.2418											
15	8.3073	8.1437	8.0409	7.9990	7.9904	7.9998	8.0193	8.0445	8.0725	8.1018	8.1312	8.1599	8.1878	8.2145	8.2402										
16	8.3066	8.1416	8.0367	7.9922	7.9808	7.9872	8.0040	8.0266	8.0526	8.0802	8.1083	8.1361	8.1632	8.1894	8.2147	8.2389									
17	8.3060	8.1398	8.0332	7.9865	7.9726	7.9765	7.9907	8.0110	8.0349	8.0608	8.0876	8.1143	8.1407	8.1663	8.1911	8.2149	8.2378								
18	8.3055	8.1384	8.0302	7.9816	7.9655	7.9672	7.9791	7.9973	8.0193	8.0435	8.0688	8.0945	8.1200	8.1449	8.1692	8.1926	8.2152	8.2369							
19	8.3051	8.1371	8.0277	7.9775	7.9595	7.9591	7.9690	7.9852	8.0053	8.0279	8.0518	8.0763	8.1009	8.1252	8.1488	8.1718	8.1940	8.2154	8.2361						
20	8.3047	8.1360	8.0255	7.9739	7.9543	7.9521	7.9601	7.9745	7.9929	8.0139	8.0364	8.0598	8.0834	8.1069	8.1300	8.1524	8.1743	8.1954	8.2158	8.2355					
21	8.3044	8.1351	8.0237	7.9708	7.9497	7.9459	7.9523	7.9650	7.9818	8.0013	8.0225	8.0447	8.0673	8.0900	8.1124	8.1344	8.1558	8.1765	8.1966	8.2161	8.2349				
22	8.3042	8.1343	8.0220	7.9681	7.9457	7.9405	7.9453	7.9565	7.9719	7.9900	8.0099	8.0309	8.0525	8.0744	8.0961	8.1175	8.1384	8.1588	8.1786	8.1978	8.2164	8.2344			
23	8.3039	8.1336	8.0206	7.9657	7.9422	7.9357	7.9392	7.9490	7.9629	7.9797	7.9984	8.0183	8.0389	8.0599	8.0809	8.1017	8.1222	8.1422	8.1617	8.1806	8.1989	8.2167	8.2340		
24	8.3037	8.1330	8.0193	7.9636	7.9391	7.9315	7.9337	7.9422	7.9549	7.9704	7.9879	8.0068	8.0264	8.0466	8.0668	8.0870	8.1070	8.1266	8.1457	8.1643	8.1824	8.2000	8.2170	8.2336	
25	8.3035	8.1325	8.0182	7.9617	7.9363	7.9277	7.9288	7.9362	7.9477	7.9620	7.9784	7.9962	8.0149	8.0342	8.0537	8.0733	8.0927	8.1118	8.1306	8.1489	8.1668	8.1841	8.2010	8.2173	8.2333

Table 2.13: Gradient table for the string mass of the spiral wheel (centrifugal force load case / selection #2)

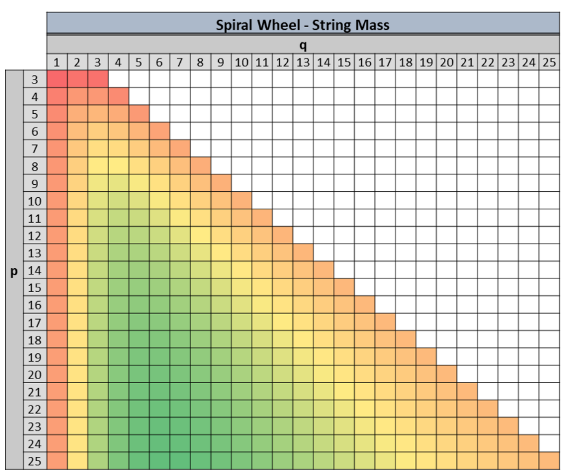

Table 2.14: Final total mass of the spiral wheel (centrifugal force load case / selection #2)

	Spiral Wheel - Total Mass (kg)																								
	q																								
p	1	2	3	4	5	6	7	8	9	10	11	12	13	14	15	16	17	18	19	20	21	22	23	24	25
3	55.8325	55.4655	54.9268																						
4	55.8048	55.5691	55.2501	54.8753																					
5	55.7910	55.6088	55.3950	55.1481	54.8635																				
6	55.7832	55.6273	55.4679	55.2957	55.0934	54.8628																			
7	55.7784	55.6373	55.5086	55.3812	55.2333	55.0599	54.8649																		
8	55.7753	55.6433	55.5333	55.4339	55.3221	55.1898	55.0370	54.8676																	
9	55.7731	55.6471	55.5493	55.4683	55.3809	55.2779	55.1571	55.0201	54.8702																
10	55.7715	55.6497	55.5603	55.4919	55.4215	55.3395	55.2428	55.1314	55.0070	54.8723															
11	55.7704	55.6515	55.5682	55.5087	55.4505	55.3839	55.3053	55.2140	55.1105	54.9965	54.8741														
12	55.7695	55.6529	55.5740	55.5210	55.4718	55.4167	55.3519	55.2762	55.1896	55.0930	54.9878	54.8756													
13	55.7688	55.6539	55.5784	55.5303	55.4879	55.4415	55.3873	55.3239	55.2509	55.1687	55.0781	54.9804	54.8768												
14	55.7682	55.6548	55.5818	55.5375	55.5003	55.4606	55.4147	55.3610	55.2990	55.2286	55.1505	55.0653	54.9741	54.8778											
15	55.7678	55.6554	55.5845	55.5432	55.5101	55.4757	55.4363	55.3904	55.3372	55.2766	55.2089	55.1345	55.0541	54.9686	54.8787										
16	55.7674	55.6559	55.5867	55.5478	55.5179	55.4877	55.4536	55.4139	55.3679	55.3155	55.2565	55.1913	55.1203	55.0443	54.9637	54.8794									
17	55.7671	55.6563	55.5885	55.5516	55.5243	55.4975	55.4676	55.4330	55.3930	55.3472	55.2955	55.2382	55.1754	55.1077	55.0355	54.9594	54.8801								
18	55.7669	55.6567	55.5900	55.5547	55.5296	55.5055	55.4791	55.4487	55.4136	55.3734	55.3279	55.2773	55.2216	55.1611	55.0964	55.0277	54.9556	54.8806							
19	55.7667	55.6570	55.5912	55.5573	55.5340	55.5122	55.4887	55.4618	55.4307	55.3952	55.3550	55.3100	55.2604	55.2064	55.1481	55.0861	55.0206	54.9521	54.8810						
20	55.7665	55.6572	55.5923	55.5595	55.5377	55.5179	55.4967	55.4727	55.4451	55.4135	55.3777	55.3377	55.2933	55.2449	55.1924	55.1363	55.0768	55.0142	54.9490	54.8814					
21	55.7663	55.6574	55.5932	55.5614	55.5408	55.5227	55.5035	55.4820	55.4573	55.4290	55.3970	55.3612	55.3214	55.2778	55.2305	55.1796	55.1255	55.0683	55.0084	54.9461	54.8818				
22	55.7662	55.6576	55.5940	55.5630	55.5435	55.5268	55.5093	55.4899	55.4676	55.4423	55.4135	55.3813	55.3455	55.3061	55.2633	55.2171	55.1678	55.1155	55.0605	55.0031	54.9435	54.8821			
23	55.7661	55.6578	55.5946	55.5644	55.5459	55.5303	55.5144	55.4967	55.4766	55.4537	55.4277	55.3986	55.3662	55.3306	55.2917	55.2497	55.2047	55.1569	55.1063	55.0534	54.9983	54.9412	54.8824		
24	55.7660	55.6579	55.5952	55.5656	55.5479	55.5334	55.5187	55.5026	55.4843	55.4635	55.4400	55.4136	55.3842	55.3518	55.3165	55.2782	55.2370	55.1932	55.1467	55.0979	55.0468	54.9938	54.9390	54.8826	
25	55.7659	55.6581	55.5958	55.5667	55.5497	55.5360	55.5225	55.5077	55.4910	55.4721	55.4507	55.4266	55.3999	55.3704	55.3381	55.3031	55.2654	55.2251	55.1824	55.1373	55.0900	55.0407	54.9896	54.9369	54.8828

Table 2.15: Gradient table for the total mass of the spiral wheel (centrifugal force load case / selection #2)

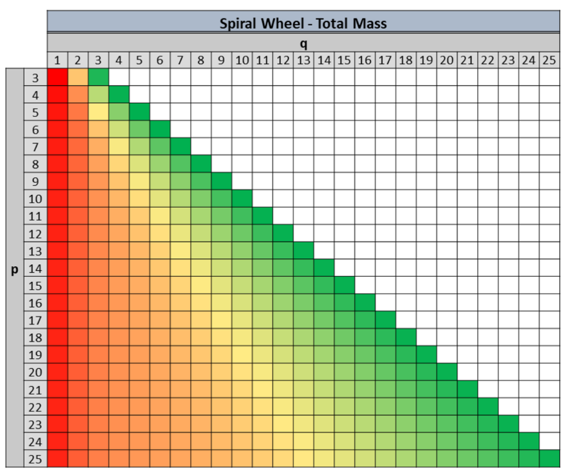

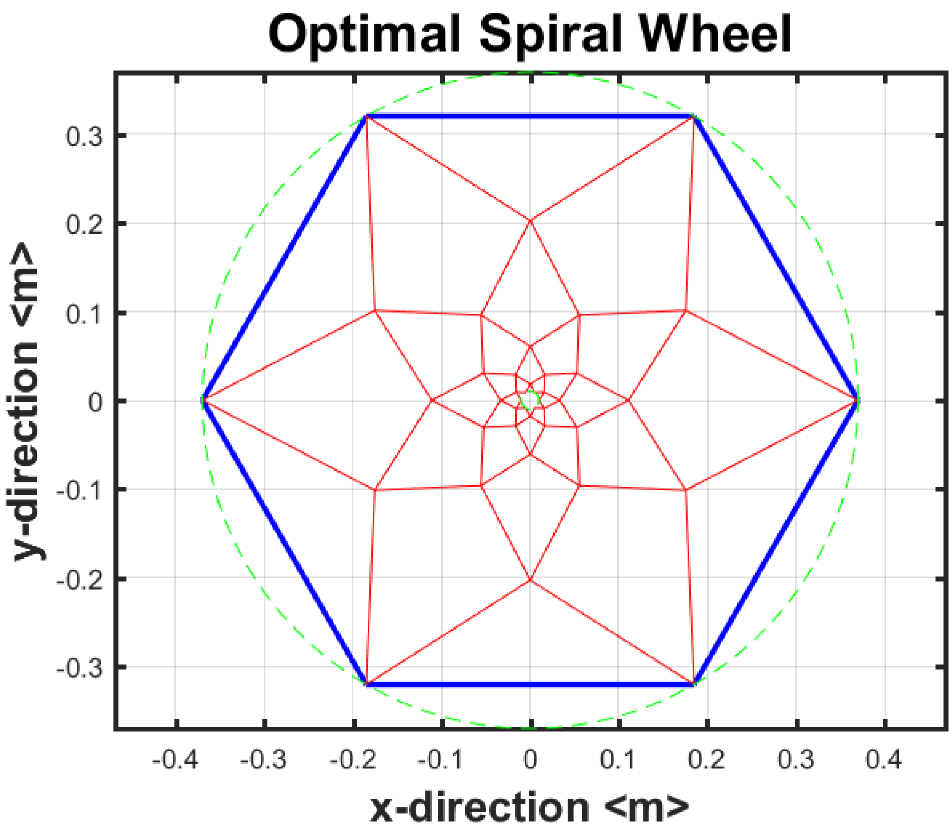

Figure 2.13: Optimal topology of the spiral wheel (centrifugal force load case / selection #2)

2.4.1.3 Centrifugal Force And Torque (Material Property Selection #1)

Table 2.16: Final mass of the rim for the spiral wheel (torque and centrifugal load case / selection #1)

	Spiral Wheel - Rim Mass (kg)																			
	q																			
p	1	2	3	4	5	6	7	8	9	10	11	12	13	14	15	16	17	18	19	20
3	50.2306	50.2213	50.2059																	
4	50.2309	50.2261	50.2164	50.2046																
5	50.2310	50.2285	50.2220	50.2136	50.2042															
6	50.2309	50.2298	50.2252	50.2191	50.2119	50.2040														
7	50.2307	50.2306	50.2273	50.2226	50.2170	50.2107	50.2040													
8	50.2304	50.2312	50.2286	50.2250	50.2206	50.2154	50.2098	50.2039												
9	50.2302	50.2315	50.2296	50.2267	50.2231	50.2189	50.2142	50.2092	50.2039											
10	50.2299	50.2317	50.2303	50.2279	50.2249	50.2214	50.2175	50.2132	50.2086	50.2039										
11	50.2296	50.2319	50.2308	50.2288	50.2264	50.2234	50.2200	50.2163	50.2124	50.2082	50.2039									
12	50.2293	50.2320	50.2311	50.2295	50.2274	50.2249	50.2220	50.2188	50.2154	50.2117	50.2079	50.2039								
13	50.2290	50.2321	50.2314	50.2301	50.2283	50.2261	50.2236	50.2208	50.2178	50.2145	50.2111	50.2075	50.2039							
14	50.2287	50.2322	50.2316	50.2305	50.2290	50.2271	50.2249	50.2224	50.2198	50.2169	50.2138	50.2106	50.2073	50.2039						
15	50.2284	50.2322	50.2318	50.2309	50.2295	50.2279	50.2260	50.2238	50.2214	50.2188	50.2161	50.2132	50.2102	50.2071	50.2039					
16	50.2281	50.2322	50.2320	50.2312	50.2300	50.2285	50.2268	50.2249	50.2228	50.2204	50.2180	50.2153	50.2126	50.2098	50.2069	50.2039				
17	50.2278	50.2322	50.2321	50.2314	50.2304	50.2291	50.2276	50.2258	50.2239	50.2218	50.2196	50.2172	50.2147	50.2121	50.2094	50.2067	50.2039			
18	50.2274	50.2322	50.2322	50.2316	50.2307	50.2295	50.2282	50.2266	50.2249	50.2230	50.2210	50.2188	50.2165	50.2141	50.2117	50.2091	50.2065	50.2039		
19	50.2271	50.2322	50.2323	50.2318	50.2310	50.2299	50.2287	50.2273	50.2257	50.2240	50.2222	50.2202	50.2181	50.2159	50.2136	50.2113	50.2089	50.2064	50.2039	
20	50.2268	50.2322	50.2323	50.2319	50.2312	50.2303	50.2292	50.2279	50.2265	50.2249	50.2232	50.2214	50.2195	50.2174	50.2153	50.2132	50.2109	50.2086	50.2063	50.2039

Table 2.17: Gradient table for the rim mass of the spiral wheel (torque and centrifugal load case / selection #1)

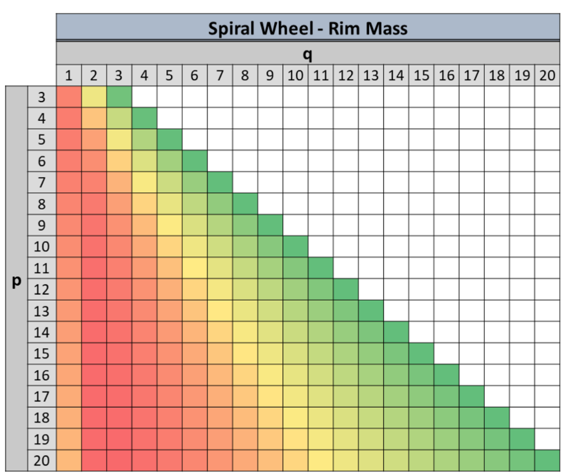

Table 2.18: Final mass of the strings for the spiral wheel (torque and centrifugal force load case / selection #1)

	Spiral Wheel - String Mass (kg)																			
	q																			
p	1	2	3	4	5	6	7	8	9	10	11	12	13	14	15	16	17	18	19	20
3	0.2225	0.2220	0.2226																	
4	0.2220	0.2206	0.2217	0.2223																
5	0.2222	0.2197	0.2207	0.2216	0.2222															
6	0.2227	0.2192	0.2198	0.2208	0.2216	0.2221														
7	0.2234	0.2189	0.2192	0.2201	0.2210	0.2216	0.2220													
8	0.2241	0.2188	0.2188	0.2195	0.2204	0.2211	0.2216	0.2220												
9	0.2249	0.2187	0.2185	0.2191	0.2198	0.2205	0.2212	0.2216	0.2220											
10	0.2258	0.2188	0.2184	0.2187	0.2194	0.2201	0.2207	0.2212	0.2216	0.2220										
11	0.2267	0.2189	0.2182	0.2185	0.2190	0.2197	0.2203	0.2208	0.2213	0.2217	0.2219									
12	0.2275	0.2190	0.2182	0.2183	0.2187	0.2193	0.2199	0.2205	0.2209	0.2213	0.2217	0.2219								
13	0.2284	0.2191	0.2182	0.2182	0.2185	0.2190	0.2196	0.2201	0.2206	0.2210	0.2214	0.2217	0.2219							
14	0.2293	0.2193	0.2182	0.2181	0.2183	0.2187	0.2193	0.2198	0.2203	0.2207	0.2211	0.2214	0.2217	0.2219						
15	0.2303	0.2195	0.2182	0.2180	0.2182	0.2185	0.2190	0.2195	0.2200	0.2204	0.2208	0.2212	0.2215	0.2217	0.2219					
16	0.2312	0.2196	0.2182	0.2179	0.2181	0.2184	0.2188	0.2192	0.2197	0.2201	0.2205	0.2209	0.2212	0.2215	0.2217	0.2219				
17	0.2321	0.2198	0.2183	0.2179	0.2180	0.2182	0.2186	0.2190	0.2194	0.2198	0.2203	0.2206	0.2210	0.2213	0.2215	0.2217	0.2219			
18	0.2330	0.2200	0.2184	0.2179	0.2179	0.2181	0.2184	0.2188	0.2192	0.2196	0.2200	0.2204	0.2207	0.2210	0.2213	0.2215	0.2217	0.2219		
19	0.2339	0.2202	0.2184	0.2179	0.2179	0.2180	0.2183	0.2186	0.2190	0.2194	0.2198	0.2201	0.2205	0.2208	0.2211	0.2213	0.2216	0.2217	0.2219	
20	0.2349	0.2204	0.2185	0.2179	0.2178	0.2179	0.2182	0.2185	0.2188	0.2192	0.2195	0.2199	0.2203	0.2206	0.2209	0.2211	0.2214	0.2216	0.2217	0.2219

Table 2.19: Gradient table for the string mass of the spiral wheel (torque and centrifugal force load case / selection #1)

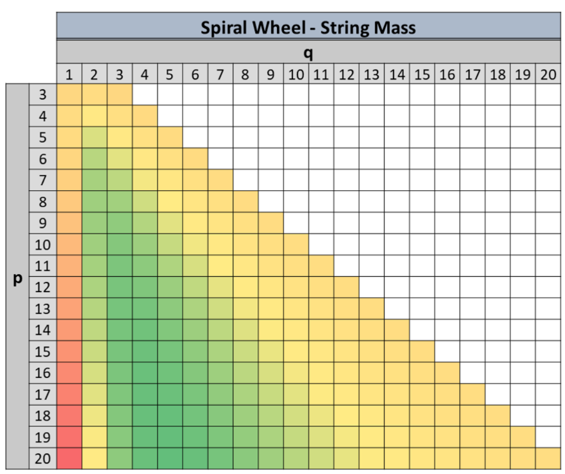

Table 2.20: Final total mass of the spiral wheel (torque centrifugal force load case / selection #1)

Spiral Wheel - Total Mass (kg)

p	q = 1	2	3	4	5	6	7	8	9	10	11	12	13	14	15	16	17	18	19	20
3	50.4531	50.4433	50.4284																	
4	50.4529	50.4467	50.4381	50.4269																
5	50.4532	50.4482	50.4427	50.4352	50.4264															
6	50.4536	50.4490	50.4451	50.4399	50.4335	50.4261														
7	50.4540	50.4495	50.4465	50.4428	50.4380	50.4323	50.4260													
8	50.4546	50.4499	50.4475	50.4446	50.4409	50.4365	50.4315	50.4259												
9	50.4551	50.4502	50.4481	50.4458	50.4429	50.4394	50.4354	50.4308	50.4259											
10	50.4557	50.4505	50.4486	50.4467	50.4443	50.4415	50.4382	50.4344	50.4303	50.4259										
11	50.4563	50.4508	50.4490	50.4473	50.4454	50.4431	50.4403	50.4372	50.4337	50.4299	50.4258									
12	50.4568	50.4510	50.4493	50.4478	50.4462	50.4442	50.4419	50.4393	50.4363	50.4330	50.4295	50.4258								
13	50.4574	50.4512	50.4496	50.4482	50.4468	50.4451	50.4432	50.4409	50.4384	50.4355	50.4325	50.4292	50.4258							
14	50.4580	50.4514	50.4498	50.4486	50.4473	50.4458	50.4442	50.4422	50.4400	50.4376	50.4349	50.4320	50.4290	50.4258						
15	50.4586	50.4516	50.4500	50.4489	50.4477	50.4464	50.4450	50.4433	50.4413	50.4392	50.4369	50.4343	50.4316	50.4288	50.4258					
16	50.4592	50.4518	50.4502	50.4491	50.4481	50.4469	50.4456	50.4441	50.4424	50.4406	50.4385	50.4362	50.4338	50.4313	50.4286	50.4258				
17	50.4599	50.4520	50.4504	50.4493	50.4483	50.4473	50.4461	50.4448	50.4433	50.4417	50.4398	50.4378	50.4357	50.4334	50.4309	50.4284	50.4258			
18	50.4605	50.4522	50.4505	50.4495	50.4486	50.4476	50.4466	50.4454	50.4441	50.4426	50.4410	50.4392	50.4372	50.4352	50.4330	50.4307	50.4283	50.4258		
19	50.4611	50.4524	50.4507	50.4497	50.4488	50.4479	50.4470	50.4459	50.4447	50.4434	50.4419	50.4403	50.4386	50.4367	50.4347	50.4326	50.4304	50.4281	50.4258	
20	50.4617	50.4526	50.4508	50.4498	50.4490	50.4482	50.4473	50.4464	50.4453	50.4441	50.4428	50.4413	50.4397	50.4380	50.4362	50.4343	50.4323	50.4302	50.4280	50.4258

Table 2.21: Gradient table for the total mass of the spiral wheel (torque centrifugal force load case / selection #1)

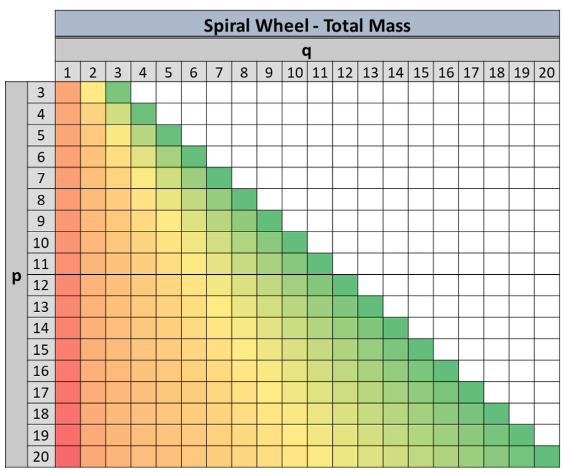

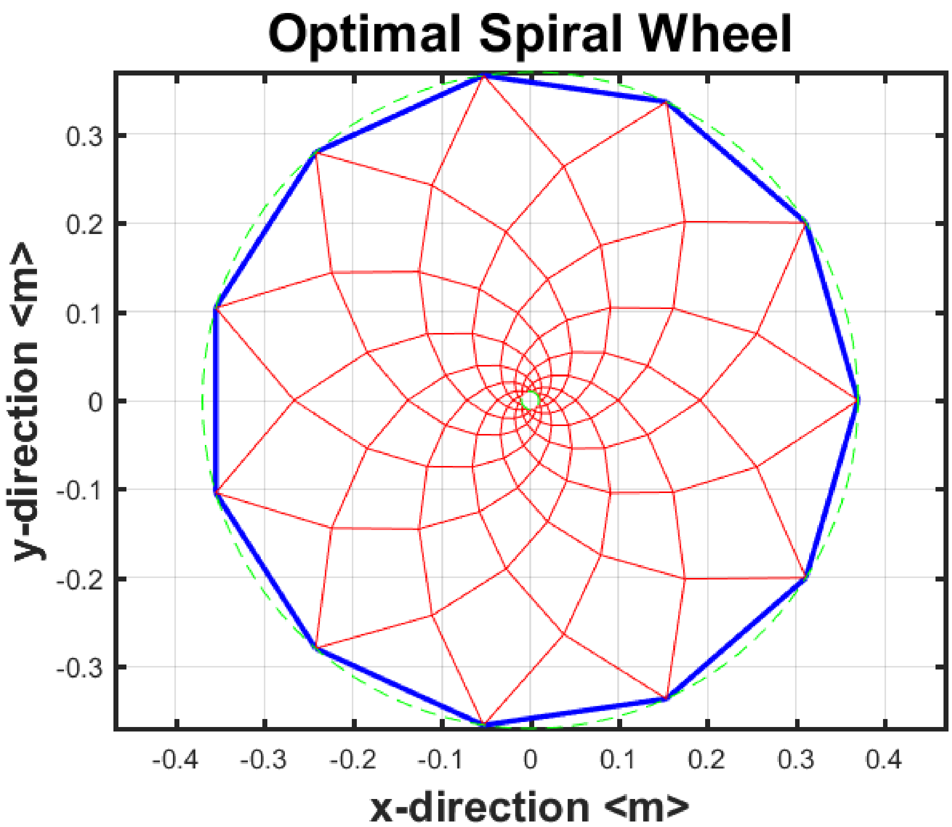

Figure 2.14: Optimal topology of the spiral wheel (torque and centrifugal force load case / selection #1)

2.4.1.4 Centrifugal Force And Torque (Material Property Selection #2)

Table 2.22: Final mass of the rim for the spiral wheel (torque and centrifugal load case / selection #2)

	Spiral Wheel - Rim Mass (kg)																			
	q																			
p	1	2	3	4	5	6	7	8	9	10	11	12	13	14	15	16	17	18	19	20
3	47.3764	47.0524	46.5123																	
4	47.3983	47.2446	46.9291	46.5229																
5	47.4060	47.3413	47.1491	46.8749	46.5480															
6	47.4078	47.3958	47.2770	47.0869	46.8453	46.5702														
7	47.4065	47.4291	47.3572	47.2228	47.0411	46.8255	46.5874													
8	47.4037	47.4509	47.4104	47.3146	47.1758	47.0048	46.8105	46.6003												
9	47.3998	47.4657	47.4475	47.3792	47.2719	47.1346	46.9748	46.7983	46.6101											
10	47.3954	47.4761	47.4742	47.4263	47.3426	47.2312	47.0985	46.9494	46.7880	46.6176										
11	47.3905	47.4836	47.4940	47.4616	47.3959	47.3048	47.1937	47.0669	46.9277	46.7791	46.6234									
12	47.3854	47.4892	47.5091	47.4886	47.4372	47.3620	47.2682	47.1596	47.0390	46.9088	46.7712	46.6280								
13	47.3801	47.4934	47.5208	47.5098	47.4696	47.4073	47.3276	47.2339	47.1288	47.0144	46.8923	46.7643	46.6317							
14	47.3746	47.4965	47.5301	47.5267	47.4956	47.4437	47.3756	47.2943	47.2022	47.1011	46.9925	46.8778	46.7581	46.6346						
15	47.3690	47.4989	47.5375	47.5403	47.5167	47.4734	47.4149	47.3440	47.2629	47.1732	47.0762	46.9731	46.8649	46.7526	46.6371					
16	47.3633	47.5007	47.5436	47.5515	47.5340	47.4979	47.4474	47.3853	47.3135	47.2336	47.1466	47.0536	46.9556	46.8534	46.7476	46.6391				
17	47.3576	47.5021	47.5485	47.5607	47.5484	47.5183	47.4746	47.4199	47.3562	47.2846	47.2063	47.1223	47.0332	46.9399	46.8430	46.7431	46.6408			
18	47.3518	47.5031	47.5526	47.5684	47.5605	47.5355	47.4976	47.4493	47.3924	47.3281	47.2574	47.1812	47.1000	47.0147	46.9257	46.8336	46.7390	46.6423		
19	47.3460	47.5038	47.5560	47.5750	47.5708	47.5502	47.5172	47.4743	47.4234	47.3654	47.3014	47.2320	47.1579	47.0797	46.9978	46.9128	46.8252	46.7353	46.6435	
20	47.3401	47.5043	47.5589	47.5805	47.5796	47.5627	47.5340	47.4959	47.4501	47.3977	47.3395	47.2761	47.2083	47.1364	47.0610	46.9824	46.9011	46.8174	46.7318	46.6446

Table 2.23: Gradient table for the rim mass of the spiral wheel (torque and centrifugal load case / selection #2)

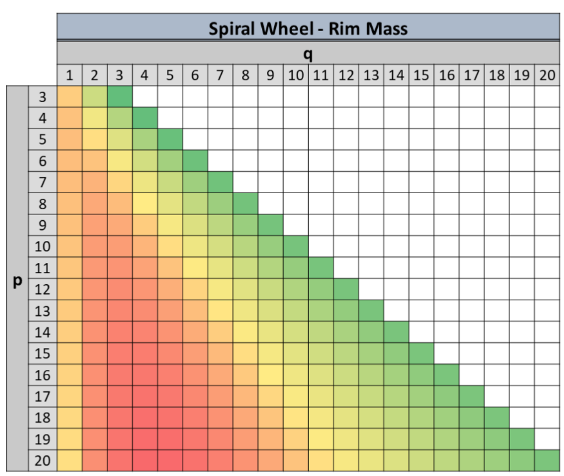

Table 2.24: Final mass of the strings for the spiral wheel (torque and centrifugal force load case / selection #2)

Spiral Wheel - String Mass (kg)	q																			
p	1	2	3	4	5	6	7	8	9	10	11	12	13	14	15	16	17	18	19	20
3	8.4992	8.4272	8.4254																	
4	8.4588	8.3404	8.3322	8.3624																
5	8.4475	8.2859	8.2581	8.2835	8.3251															
6	8.4488	8.2526	8.2044	8.2198	8.2580	8.3020														
7	8.4563	8.2320	8.1664	8.1702	8.2025	8.2439	8.2869													
8	8.4672	8.2191	8.1395	8.1321	8.1573	8.1949	8.2359	8.2766												
9	8.4801	8.2111	8.1201	8.1030	8.1207	8.1537	8.1920	8.2311	8.2692											
10	8.4944	8.2063	8.1061	8.0806	8.0914	8.1194	8.1545	8.1916	8.2283	8.2638										
11	8.5095	8.2036	8.0958	8.0633	8.0679	8.0908	8.1223	8.1570	8.1923	8.2267	8.2598									
12	8.5251	8.2025	8.0882	8.0498	8.0488	8.0670	8.0948	8.1269	8.1604	8.1936	8.2258	8.2567								
13	8.5413	8.2024	8.0827	8.0391	8.0334	8.0472	8.0714	8.1007	8.1321	8.1640	8.1952	8.2253	8.2542							
14	8.5577	8.2031	8.0786	8.0307	8.0207	8.0306	8.0514	8.0779	8.1072	8.1374	8.1675	8.1968	8.2251	8.2522						
15	8.5744	8.2045	8.0757	8.0240	8.0104	8.0168	8.0343	8.0580	8.0851	8.1137	8.1425	8.1709	8.1985	8.2251	8.2507					
16	8.5912	8.2063	8.0736	8.0187	8.0018	8.0051	8.0196	8.0408	8.0657	8.0925	8.1200	8.1474	8.1742	8.2001	8.2252	8.2493				
17	8.6082	8.2085	8.0723	8.0145	7.9948	7.9952	8.0070	8.0258	8.0485	8.0735	8.0996	8.1259	8.1518	8.1772	8.2017	8.2254	8.2483			
18	8.6253	8.2109	8.0715	8.0111	7.9889	7.9868	7.9962	8.0126	8.0334	8.0566	8.0812	8.1063	8.1314	8.1560	8.1800	8.2032	8.2257	8.2473		
19	8.6425	8.2136	8.0711	8.0085	7.9840	7.9796	7.9868	8.0012	8.0199	8.0415	8.0646	8.0885	8.1126	8.1365	8.1598	8.1826	8.2046	8.2259	8.2466	
20	8.6598	8.2165	8.0711	8.0064	7.9799	7.9735	7.9787	7.9911	8.0080	8.0279	8.0496	8.0723	8.0954	8.1184	8.1412	8.1634	8.1850	8.2060	8.2262	8.2459

Table 2.25: Gradient table for the string mass of the spiral wheel (torque and centrifugal force load case / selection #2)

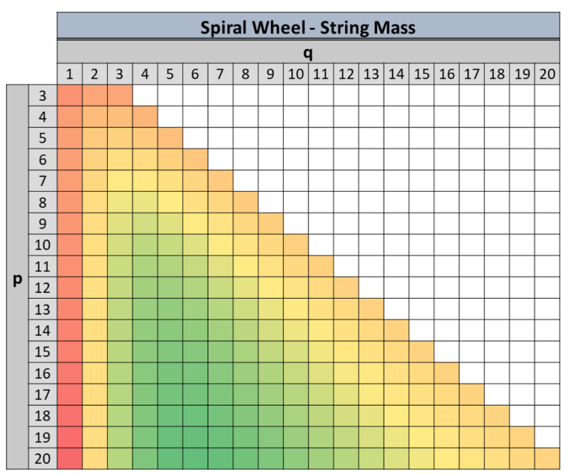

Table 2.26: Final total mass of the spiral wheel (torque centrifugal force load case / selection #2)

	Spiral Wheel - Total Mass (kg)																			
	q																			
p	1	2	3	4	5	6	7	8	9	10	11	12	13	14	15	16	17	18	19	20
3	55.8757	55.4796	54.9377																	
4	55.8571	55.5850	55.2613	54.8853																
5	55.8536	55.6271	55.4072	55.1584	54.8731															
6	55.8565	55.6483	55.4815	55.3067	55.1033	54.8722														
7	55.8628	55.6611	55.5236	55.3930	55.2436	55.0695	54.8742													
8	55.8708	55.6700	55.5499	55.4467	55.3331	55.1997	55.0464	54.8768												
9	55.8799	55.6768	55.5676	55.4822	55.3926	55.2883	55.1669	55.0294	54.8793											
10	55.8897	55.6824	55.5803	55.5069	55.4340	55.3506	55.2530	55.1410	55.0163	54.8814										
11	55.9000	55.6873	55.5898	55.5249	55.4638	55.3956	55.3160	55.2239	55.1200	55.0057	54.8832									
12	55.9105	55.6917	55.5973	55.5384	55.4860	55.4290	55.3630	55.2865	55.1994	55.1024	54.9970	54.8846								
13	55.9213	55.6958	55.6035	55.5489	55.5030	55.4545	55.3990	55.3346	55.2610	55.1783	55.0875	54.9896	54.8859							
14	55.9323	55.6997	55.6087	55.5573	55.5163	55.4743	55.4269	55.3722	55.3094	55.2386	55.1601	55.0746	54.9832	54.8869						
15	55.9434	55.7034	55.6132	55.5643	55.5271	55.4901	55.4491	55.4020	55.3480	55.2869	55.2187	55.1440	55.0634	54.9777	54.8877					
16	55.9545	55.7070	55.6172	55.5702	55.5359	55.5029	55.4670	55.4261	55.3792	55.3260	55.2666	55.2010	55.1298	55.0535	54.9728	54.8885				
17	55.9658	55.7105	55.6208	55.5752	55.5432	55.5135	55.4816	55.4457	55.4047	55.3581	55.3059	55.2482	55.1851	55.1171	55.0447	54.9685	54.8891			
18	55.9771	55.7140	55.6241	55.5795	55.5494	55.5223	55.4938	55.4619	55.4257	55.3847	55.3386	55.2875	55.2314	55.1707	55.1057	55.0369	54.9647	54.8896		
19	55.9885	55.7174	55.6271	55.5834	55.5548	55.5298	55.5040	55.4755	55.4433	55.4069	55.3660	55.3205	55.2705	55.2161	55.1577	55.0954	55.0298	54.9612	54.8901	
20	55.9999	55.7207	55.6300	55.5869	55.5595	55.5362	55.5127	55.4870	55.4581	55.4256	55.3891	55.3484	55.3037	55.2548	55.2021	55.1458	55.0861	55.0234	54.9581	54.8905

Table 2.27: Gradient table for the total mass of the spiral wheel (torque centrifugal force load case / selection #2)

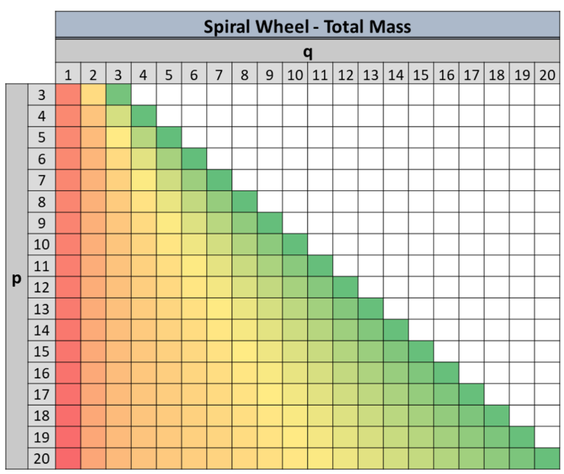

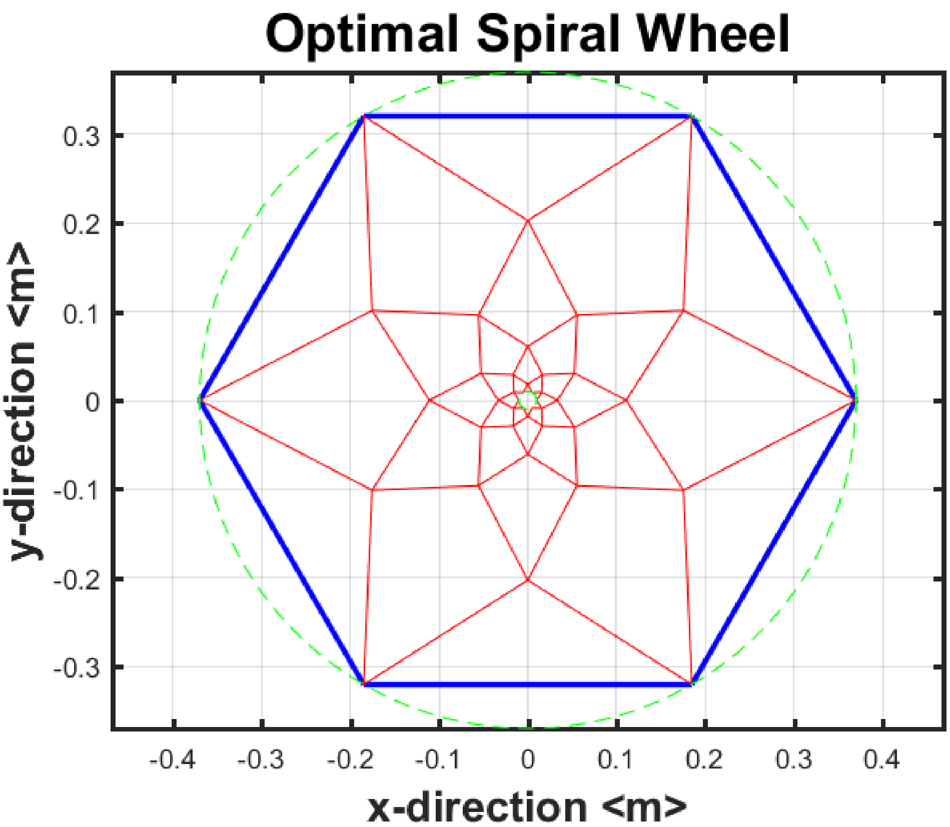

Figure 2.15: Optimal topology of the spiral wheel (torque and centrifugal force load case / selection #2)

2.4.2 Bicycle Wheel

2.4.2.1 Centrifugal Force (Material Property Selection #1)

Table 2.28: Final mass of the rim for the bicycle wheel (centrifugal force load case / selection #1)

		Bicycle Wheel - Rim Mass (kg)				
		i				
		1	2	3	4	5
b	1	49.9670				
	2	49.9674				
	3	49.9675	49.9523			
	4	49.9675	49.9584			
	5	49.9675	49.9615	49.9523		
	6	49.9675	49.9633	49.9563		
	7	49.9675	49.9644	49.9590	49.9525	
	8	49.9675	49.9651	49.9609	49.9554	
	9	49.9675	49.9656	49.9622	49.9576	49.9526
	10	49.9675	49.9660	49.9631	49.9593	49.9549

Table 2.29: Gradient table for the rim mass of the bicycle wheel (centrifugal force load case / selection #1)

		Bicycle Wheel - Rim Mass				
		i				
		1	2	3	4	5
b	1					
	2					
	3					
	4					
	5					
	6					
	7					
	8					
	9					
	10					

Table 2.30: Final mass of the strings for the bicycle wheel (centrifugal force load case / selection #1)

Bicycle Wheel - String Mass (kg)					
	i				
b	1	2	3	4	5
1	0.9934				
2	0.9922				
3	0.9919	1.0295			
4	0.9919	1.0145			
5	0.9918	1.0068	1.0270		
6	0.9918	1.0024	1.0178		
7	0.9918	0.9996	1.0117	1.0253	
8	0.9918	0.9978	1.0074	1.0188	
9	0.9918	0.9966	1.0043	1.0139	1.0243
10	0.9918	0.9957	1.0020	1.0102	1.0193

Table 2.31: Gradient table for the string mass of the bicycle wheel (centrifugal force load case / selection #1)

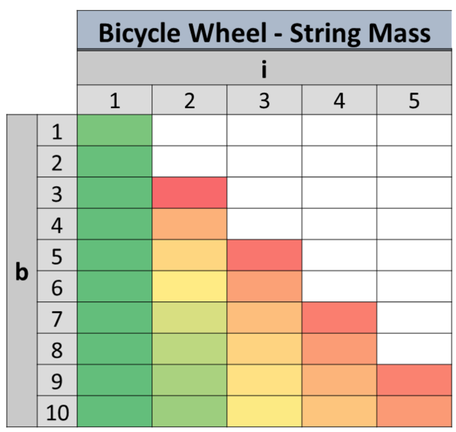

Table 2.32: Final total mass of the bicycle wheel (centrifugal force load case / selection #1)

Bicycle Wheel - Total Mass (kg)						
		i				
		1	2	3	4	5
b	1	50.9604				
	2	50.9596				
	3	50.9594	50.9818			
	4	50.9594	50.9729			
	5	50.9593	50.9683	50.9792		
	6	50.9593	50.9657	50.9741		
	7	50.9593	50.9640	50.9707	50.9777	
	8	50.9593	50.9629	50.9682	50.9743	
	9	50.9593	50.9622	50.9665	50.9716	50.9768
	10	50.9593	50.9616	50.9652	50.9695	50.9742

Table 2.33: Gradient table for the total mass of the bicycle wheel (centrifugal force load case / selection #1)

Bicycle Wheel - Total Mass						
		i				
		1	2	3	4	5
b	1					
	2					
	3					
	4					
	5					
	6					
	7					
	8					
	9					
	10					

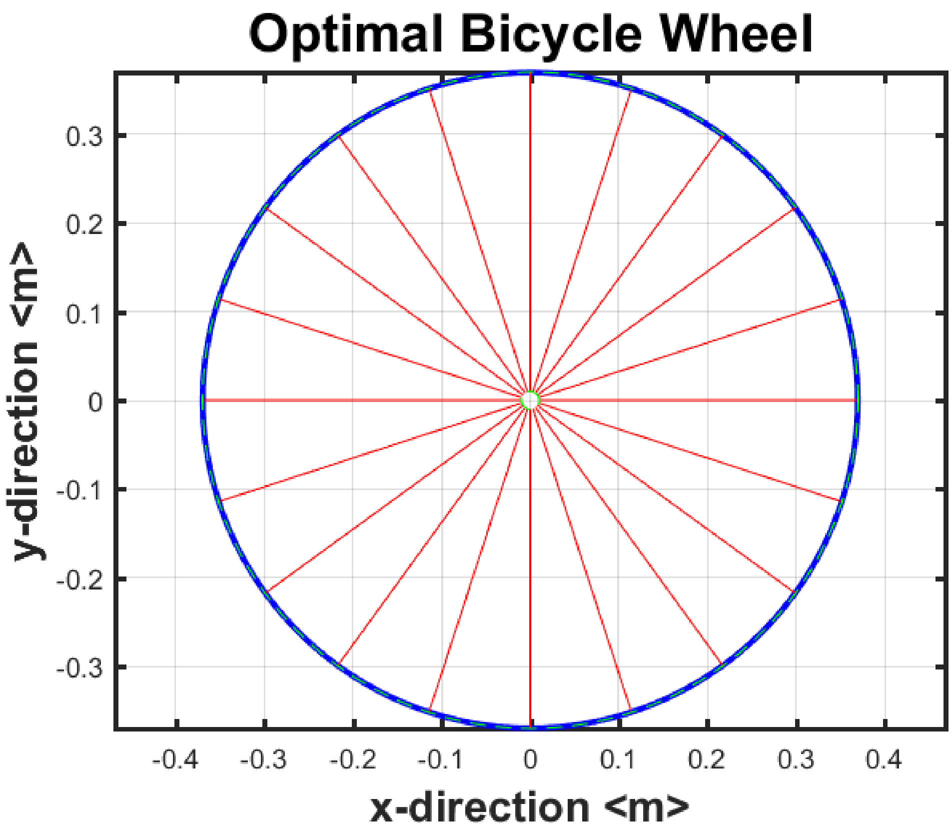

Figure 2.16: Optimal topology of the bicycle wheel (centrifugal force load case / selection #1)

2.4.2.2 *Centrifugal Force (Material Property Selection #2)*

Table 2.34: Final mass of the rim for the bicycle wheel (centrifugal force load case / selection #2)

		Bicycle Wheel - Rim Mass (kg)				
		i				
		1	2	3	4	5
b	1	43.5353				
	2	43.5404				
	3	43.5413	43.1758			
	4	43.5416	43.3232			
	5	43.5417	43.3981	43.1823		
	6	43.5418	43.4406	43.2774		
	7	43.5418	43.4668	43.3409	43.1898	
	8	43.5419	43.4841	43.3847	43.2591	
	9	43.5419	43.4961	43.4158	43.3111	43.1949
	10	43.5419	43.5047	43.4387	43.3506	43.2492

Table 2.35: Gradient table for the rim mass of the bicycle wheel (centrifugal force load case / selection #2)

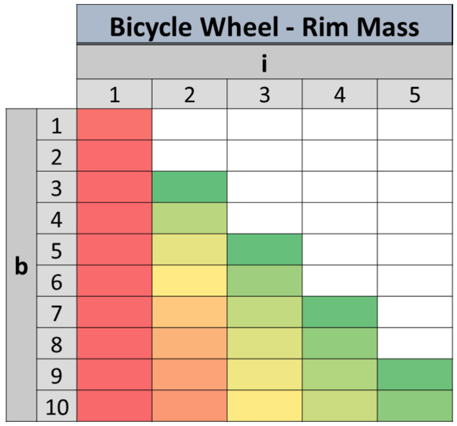

Table 2.36: Final mass of the strings for the bicycle wheel (centrifugal force load case / selection #2)

Bicycle Wheel - String Mass (kg)					
	i				
b	1	2	3	4	5
1	19.7673				
2	19.7525				
3	19.7499	20.6806			
4	19.7490	20.3083			
5	19.7486	20.1174	20.6105		
6	19.7483	20.0086	20.3859		
7	19.7482	19.9412	20.2345	20.5655	
8	19.7481	19.8968	20.1294	20.4079	
9	19.7481	19.8660	20.0543	20.2884	20.5379
10	19.7480	19.8439	19.9990	20.1970	20.4169

Table 2.37: Gradient table for the string mass of the bicycle wheel (centrifugal force load case / selection #2)

Bicycle Wheel - String Mass						
		i				
		1	2	3	4	5
b	1					
	2					
	3					
	4					
	5					
	6					
	7					
	8					
	9					
	10					

Table 2.38: Final total mass of the bicycle wheel (centrifugal force load case / selection #2)

Bicycle Wheel - Total Mass (kg)						
		i				
		1	2	3	4	5
b	1	63.3026				
	2	63.2929				
	3	63.2912	63.8564			
	4	63.2906	63.6315			
	5	63.2903	63.5154	63.7928		
	6	63.2901	63.4491	63.6634		
	7	63.2900	63.4080	63.5754	63.7553	
	8	63.2900	63.3809	63.5141	63.6670	
	9	63.2899	63.3621	63.4701	63.5995	63.7327
	10	63.2899	63.3486	63.4377	63.5476	63.6661

Table 2.39: Gradient table for the total mass of the bicycle wheel (centrifugal force load case / selection #2)

		Bicycle Wheel - Total Mass				
		i				
		1	2	3	4	5
b	1					
	2					
	3					
	4					
	5					
	6					
	7					
	8					
	9					
	10					

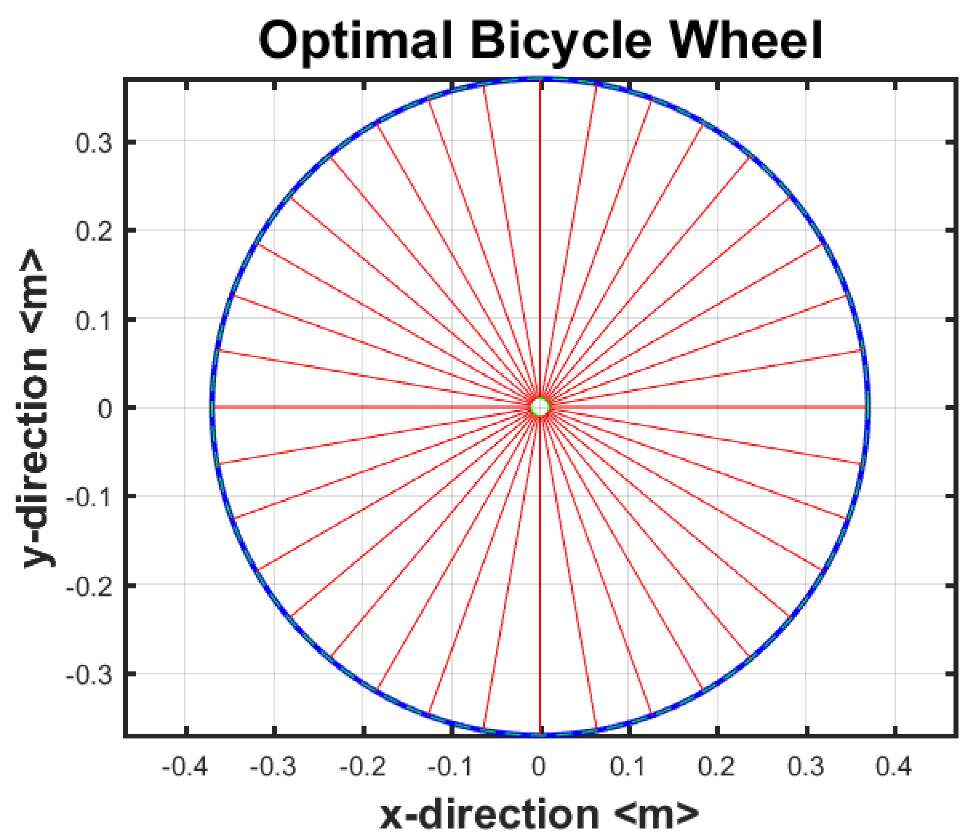

Figure 2.17: Optimal topology of the bicycle wheel (centrifugal force load case / selection #2)

2.4.2.3 Centrifugal Force And Torque (Material Property Selection #1)

Table 2.40: Final mass of the rim for the bicycle wheel (torque and centrifugal force load case / selection #1)

		Bicycle Wheel - Rim Mass (kg)				
		i				
		1	2	3	4	5
b	1	NS				
	2	NS				
	3	NS	50.0184			
	4	NS	50.0177			
	5	NS	50.0121	50.0178		
	6	NS	50.0095	50.0182		
	7	NS	50.0063	50.0153	50.0134	
	8	NS	50.0029	50.0148	50.0148	
	9	NS	49.9995	50.0139	50.0155	50.0131
	10	NS	49.9959	50.0128	50.0156	50.0144

Table 2.41: Gradient table for the rim mass of the bicycle wheel (torque and centrifugal force load case / selection #1)

		Bicycle Wheel - Rim Mass				
		i				
		1	2	3	4	5
b	1	NS				
	2	NS				
	3	NS				
	4	NS				
	5	NS				
	6	NS				
	7	NS				
	8	NS				
	9	NS				
	10	NS				

Table 2.42: Final mass of the strings for the bicycle wheel (torque and centrifugal force load case / selection #1)

		Bicycle Wheel - String Mass (kg)				
		i				
		1	2	3	4	5
b	1	NS				
	2	NS				
	3	NS	0.8378			
	4	NS	0.8421			
	5	NS	0.8596	0.8374		
	6	NS	0.8679	0.8383		
	7	NS	0.8774	0.8481	0.8492	
	8	NS	0.8875	0.8505	0.8470	
	9	NS	0.8978	0.8537	0.8463	0.8494
	10	NS	0.9083	0.8575	0.8467	0.8472

Table 2.43: Gradient table for the string mass of the bicycle wheel (torque and centrifugal force load case / selection #1)

		Bicycle Wheel - String Mass				
		i				
		1	2	3	4	5
b	1	NS				
	2	NS				
	3	NS				
	4	NS				
	5	NS				
	6	NS				
	7	NS				
	8	NS				
	9	NS				
	10	NS				

Table 2.44: Final total mass of the bicycle wheel (torque and centrifugal force load case / selection #1)

		Bicycle Wheel - Total Mass (kg)				
		i				
		1	2	3	4	5
b	1	NS				
	2	NS				
	3	NS	50.8562			
	4	NS	50.8598			
	5	NS	50.8716	50.8552		
	6	NS	50.8773	50.8565		
	7	NS	50.8837	50.8634	50.8626	
	8	NS	50.8905	50.8653	50.8618	
	9	NS	50.8973	50.8676	50.8617	50.8626
	10	NS	50.9043	50.8703	50.8624	50.8616

Table 2.45: Gradient table for the total mass of the bicycle wheel (torque and centrifugal force load case / selection #1)

		Bicycle Wheel - Total Mass				
		i				
		1	2	3	4	5
b	1	NS				
	2	NS				
	3	NS				
	4	NS				
	5	NS				
	6	NS				
	7	NS				
	8	NS				
	9	NS				
	10	NS				

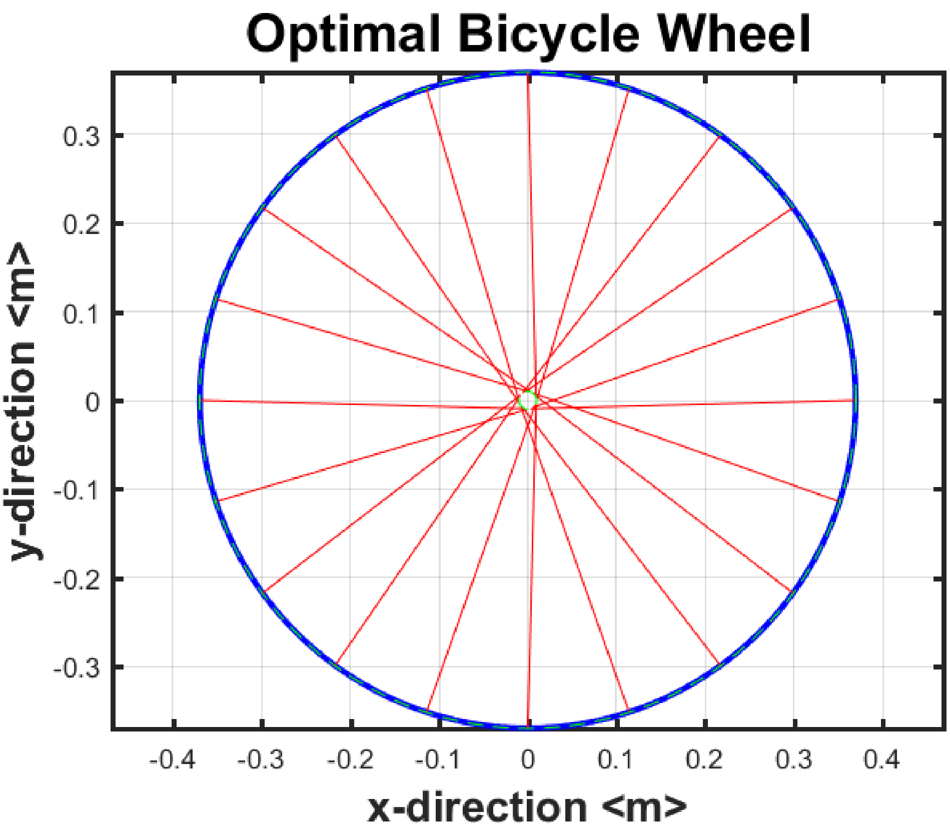

Figure 2.18: Optimal topology of the bicycle wheel (torque and centrifugal force load case / selection #1)

2.4.2.4 Centrifugal Force And Torque (Material Property Selection #2)

Table 2.46: Final mass of the rim for the bicycle wheel (torque and centrifugal force load case / selection #2)

		Bicycle Wheel - Rim Mass (kg)				
		i				
		1	2	3	4	5
b	1	NS				
	2	NS				
	3	NS	43.9252			
	4	NS	43.9845			
	5	NS	43.9250	43.9326		
	6	NS	43.8577	43.9787		
	7	NS	43.7479	43.9735	43.9243	
	8	NS	43.6823	43.9571	43.9500	
	9	NS	43.6147	43.8897	43.9014	43.8325
	10	NS	43.5471	43.8701	43.9115	43.9269

Table 2.47: Gradient table for the rim mass of the bicycle wheel (torque and centrifugal force load case / selection #2)

		Bicycle Wheel - Rim Mass				
		i				
		1	2	3	4	5
b	1	NS				
	2	NS				
	3	NS				
	4	NS				
	5	NS				
	6	NS				
	7	NS				
	8	NS				
	9	NS				
	10	NS				

Table 2.48: Final mass of the strings for the bicycle wheel (torque and centrifugal force load case / selection #2)

		Bicycle Wheel - String Mass (kg)				
		i				
		1	2	3	4	5
b	1	NS				
	2	NS				
	3	NS	18.5076			
	4	NS	18.3854			
	5	NS	18.5830	18.4401		
	6	NS	18.7931	18.3523		
	7	NS	19.1219	18.3970	18.4433	
	8	NS	19.3188	18.4649	18.4073	
	9	NS	19.5200	18.6753	18.5764	18.6967
	10	NS	19.7202	18.7430	18.5686	18.4564

Table 2.49: Gradient table for the string mass of the bicycle wheel (torque and centrifugal force load case / selection #2)

		Bicycle Wheel - String Mass				
		i				
		1	2	3	4	5
b	1	NS				
	2	NS				
	3	NS				
	4	NS				
	5	NS				
	6	NS				
	7	NS				
	8	NS				
	9	NS				
	10	NS				

Table 2.50: Final total mass of the bicycle wheel (torque and centrifugal force load case / selection #2)

		Bicycle Wheel - Total Mass (kg)				
		i				
		1	2	3	4	5
b	1	NS				
	2	NS				
	3	NS	62.4328			
	4	NS	62.3699			
	5	NS	62.5081	62.3727		
	6	NS	62.6508	62.3310		
	7	NS	62.8698	62.3706	62.3676	
	8	NS	63.0012	62.4220	62.3573	
	9	NS	63.1347	62.5650	62.4778	62.5292
	10	NS	63.2673	62.6131	62.4801	62.3834

Table 2.51: Gradient table for the total mass of the bicycle wheel (torque and centrifugal force load case / selection #2)

		Bicycle Wheel - Total Mass				
		i				
		1	2	3	4	5
b	1	NS				
	2	NS				
	3	NS				
	4	NS				
	5	NS				
	6	NS				
	7	NS				
	8	NS				
	9	NS				
	10	NS				

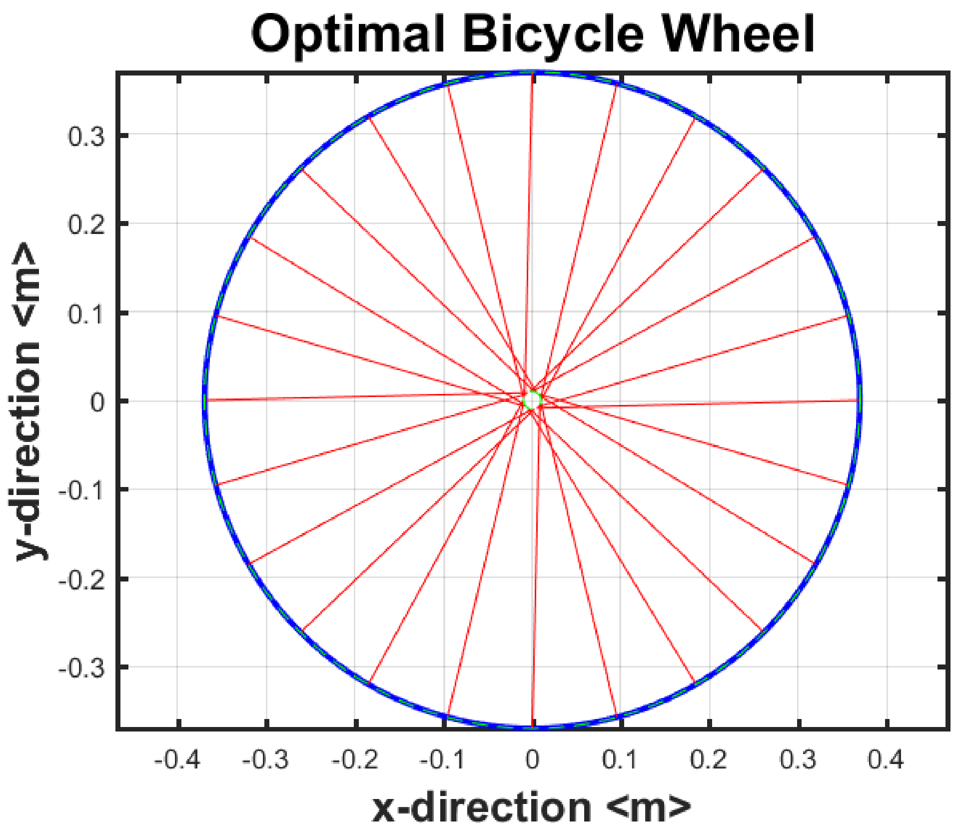

Figure 2.19: Optimal topology of the bicycle wheel (torque and centrifugal force load case / selection #2)

2.5 Joint Mass Penalty

Adding mass to the joints would increase the mass of each wheel. Enough mass would need to be used so that the joints are strong enough to endure the loads to manufacture the wheels. A joint mass penalty was not added to the results shown in the previous section. With that increase in mass the mass of either the rim or the strings or both would need to decrease so that the angular momentum of the wheel doesn't overshoot the requirement. This should result in a slight increase in the overall mass than what was presented in the previous section. Although the spiral wheel has more joints than the bicycle wheel the overall results on which wheel is more optimal should remain the same. The reasoning is the same as why the spiral wheel is mass optimal compared to the bicycle wheel when there is an angular momentum constraint. The mass increase due to the joints increases the inertia of the spiral wheel more so than the bicycle wheel.

2.6 Summary

The two-dimensional mass optimized design for a flywheel for use in a reaction wheel is performed in this chapter. First, two separate topologies were defined by deriving their connectivity matrices and nodal matrices. Two rim topologies were defined to combine with the spiral wheel and bicycle wheel topologies. Second, the two static load cases were defined for both the spiral and bicycle wheel topologies. The centrifugal force load case and the centrifugal force plus torque load case external force matrices were defined. Third, the algorithm created to minimize the mass of the wheel subject to an angular momentum constraint was outlined. Finally, the results from the algorithm were outlined for both topologies that influence the topology choices for the three-dimensional design of the wheel. The results show that for the two-dimensional wheel, the spiral tensegrity wheel is approximately 45-49% less massive compared to the flywheels used for the CMGs on the ISS for similar design constraints. The design of the wheel will be carried out in the next chapter to explore if the mass savings are still significant in three-dimensions.

3. THREE-DIMENSIONAL DESIGN

This chapter will characterize the nodal and connectivity matrices for a combination of the spiral wheel, bicycle wheel, and rim topologies discussed in Chapter 2. The load case utilizing the combination of the centrifugal forces and the forces due to an out of plane torque will be analyzed. The results in this chapter will show the combination of the spiral wheel and the bicycle wheel is a more optimal structure for minimal mass when compared to a solid wheel when a combination of centrifugal forces and torque are applied.

3.1 Topology

This section will describe one topology that will be used to design a minimal mass CMG in three-dimensions. The nodal matrix and the bar and string connectivity matrices will be defined for both the spiral wheel and the bicycle wheel. These topologies will be augmented with the rim topology from Chapter 2 utilizing the algorithm from Appendix B. The angle between nodes for the spiral wheel and the bicycle wheel will be set equal with one multiplied by a positive integer. The circumferential complexity of the spiral wheel will be equal to a coefficient multiplied by the complexity of the bicycle wheel. This eliminates one degree of freedom in the optimization process as well as keeps an even spacing between the nodes that lie on the rim of the wheel. This allows the rim topology to easily be augmented with the combination of the spiral wheel and bicycle wheel. Shown below in (3.1) is the angle between nodes for the spiral wheel, ϕ_S, set equal to the angle between nodes for the bicycle wheel, ϕ_B, multiplied by a positive integer, j. This integer allows freedom between the two complexities while keeping an equal spacing between the nodes that lie on the rim of the wheel.

$$j\phi_S = \phi_B \tag{3.1}$$

Substituting ϕ_S and ϕ_B with (2.6) and (2.20) respectively results in (3.2) shown below.

$$\frac{j\pi}{p} = \frac{\pi}{2b} \tag{3.2}$$

Solving for p results in (3.3).

$$p = 2jb \tag{3.3}$$

The angle between nodes will now lose the subscript for this chapter and will only be referred to as ϕ.

3.1.1 Spiral Wheel

The nodal and connectivity matrix for the spiral wheel will be the same as it was in the previous chapter. As seen in the results section from the previous chapter, the spiral wheel is more optimal than the bicycle wheel when only centrifugal forces are applied or when centrifugal forces plus a torque are applied for two-dimensions. For this reason the only strings in the x/y plane for this three-dimensional topology will be from the spiral wheel. For out of plane stiffness, the bicycle wheel topology will be used.

3.1.2 Bicycle Wheel

For out of plane stiffness, the three-dimensional bicycle wheel will be used. Figure 2.3 shows the numbering system for the nodes and strings for the bicycle wheel topology in three-dimensions. This image depicts a spoke arrangement with complexity three ($q = 3$) and a zero spoke angle, α, coming off the inner circle. Since the spiral wheel is more optimal for torques about the longitudinal axis of the wheel, the spoke angle will be set to zero in three-dimensions. Just like the bicycle wheel in two-dimensions, the inner ring of nodes are numbered so that the first half of those nodes would be on the top half of the axle. The second half of the inner ring of nodes will be on the bottom half of the axle. All of the inner node matrices and outer node matrices are different due to the axle having a non-zero length and the spoke angle being set to zero. The connectivity matrix will be exactly the same as it was in two-dimensions.

3.1.2.1 Nodal Matrix

The matrix describing the first set of inner nodes of the bicycle spokes is given below by (3.4), where L is the length of the axle.

$$\mathbf{N}_{I_1} = \begin{bmatrix} r\cos(0) & r\cos(2\phi) & \cdots & r\cos(2(q-1)\phi) \\ r\sin(0) & r\sin(2\phi) & \cdots & r\sin(2(q-1)\phi) \\ \frac{L}{2} & \frac{L}{2} & \cdots & \frac{L}{2} \end{bmatrix} \tag{3.4}$$

The matrix describing the second set of inner nodes of the bicycle spokes is given below by (3.5).

$$\mathbf{N}_{I_2} = \begin{bmatrix} r\cos(\phi) & r\cos(3\phi) & \cdots & r\cos((4q-1)\phi) \\ r\sin(\phi) & r\sin(3\phi) & \cdots & r\sin((4q-1)\phi) \\ -\frac{L}{2} & -\frac{L}{2} & \cdots & -\frac{L}{2} \end{bmatrix} \tag{3.5}$$

The matrices describing the outer nodes along the rim of the bicycle wheel are shown below in (3.6) and (3.7). These equations differ from the ones in Chapter 2 because the spoke angle index is set to zero.

$$\mathbf{N}_{O_1} = \begin{bmatrix} R\cos(0) & R\cos(2\phi) & \cdots & R\cos(2(q-1)\phi) \\ R\sin(0) & R\sin(2\phi) & \cdots & R\sin(2(q-1)\phi) \\ 0 & 0 & \cdots & 0 \end{bmatrix} \tag{3.6}$$

$$\mathbf{N}_{O_2} = \begin{bmatrix} R\cos(\phi) & R\cos(3\phi) & \cdots & R\cos((4q-1)\phi) \\ R\sin(\phi) & R\sin(3\phi) & \cdots & R\sin((4q-1)\phi) \\ 0 & 0 & \cdots & 0 \end{bmatrix} \tag{3.7}$$

3.2 Static Load Cases

This section will discuss the static load case that will be applied to the three-dimensional wheel discussed in the previous section. The load case will consist of centrifugal forces and an out of plane force perpendicular to the x/y plane due to changing the direction of the angular momentum vector. The mass of the rim (shown in blue in the images below) is evenly divided by the number of nodes that are coincident with the rim. Each of the string masses are divided by two and placed at each of the two nodes that defines each string. The external force matrix, **W**, will be shown below for each of the load cases for each of the wheels.

3.2.1 Centrifugal Force And Torque

The centrifugal force portion of the external force matrix for the three-dimensional wheel will be equal to the two-dimensional spiral wheel external force matrix other than adding the mass from the added bicycle strings into c_0 shown below in 3.8. The equations for c_1 through c_{q-1} remain unchanged as well as the external force matrix for the centrifugal forces, $\mathbf{W}_C$.

$$c_0 = \frac{r_0 \omega^2}{p} \left(m_r + \frac{m_{s_{total_1}} + m_{s_{bicycle}}}{2} \right) \tag{3.8}$$

The torque applied to the wheel is now applied out of the plane as if the wheel was being used as a CMG. The force on the nodes due to this torque is only applied to the nodes that lie on the outer rim of the wheel instead of to every node like in the two-dimensional case. This is due to the nodes of the spiral portion of the wheel being unable to be in equilibrium when a force perpendicular to the plane the wheel lies in is applied. In reality, the strings that make up the spiral portion of the wheel would have some bending stiffness that could accommodate these out of plane forces. The bending stiffness of the strings is not modeled, but these forces are much smaller than the centrifugal forces and even the out of plane forces applied to the nodes on the outer rim. It is assumed that the increase of mass of the wheel due to these out of plane forces is negligible.

The mass of the rim and the strings is distributed to the nodes of the wheel similarly as in Chapter 2 for the spiral wheel, but now with the addition of the mass of the bicycle strings. The force is now dependent on the perpendicular distance from the axis the wheel is being torqued about. For the equations to follow, it is assumed that axis is the y-axis of the wheel. The minimal mass results are independent of the choice of axis. The out of plane force for the nodes that lie on the circle that has a radius equal to r_0 is shown below in (3.9).

$$t_0 = \frac{\tau}{pI}\left(m_r + \frac{m_{s_{total_1}} + m_{s_{bicycle}}}{2}\right) \tag{3.9}$$

$$\mathbf{W}_T = \begin{bmatrix} 0 & t_0 & 0 \end{bmatrix}^T \begin{bmatrix} N_{11} & , & N_{12} & , & \cdots & , & N_{1p} & , & 0 \end{bmatrix} \tag{3.10}$$

3.3 Results

Using the algorithm developed in the previous chapter, the three-dimensional tensegrity wheel was optimized. The inputs into the algorithm were chosen to match the flywheel from the CMGs on the ISS from the introduction chapter as closely as possible. The table shown below lists the input parameters for the dimensions of the wheel, the angular momentum requirement, the angular rate of the wheel, and the torque that is applied to the wheel. The inner radius of the wheel was chosen to be as small as possible due to the mass optimal wheel having the smallest possible axis. The length of the axle was chosen arbitrarily, but intuitively the axle length would be as short as possible for minimal mass for this optimization process. Although this might not be the case when the dynamics of the wheel are considered since the out of plane stiffness would be a function of the axle length.

Table 3.1: Input parameters for the topology optimization

Parameters	**Values**
$\bar{\omega}$ (RPM)	6600
$\bar{h}$ (N*m*s)	4760
R (m)	0.37
r_q/r (m)	0.01
τ (N*m)	258

Two different material combinations between the rim and the strings were used. The first combination (Selection #1) uses Type 321 Stainless Steel for the rim and Spectra Fiber for the strings. The material properties for this selection is shown below in Table 3.2. The second combination (Selection #2) uses tungsten alloy K1850 for the rim and Ti-6Al-4V (Grade 5) titanium for the strings shown below in Table 3.3. The material selection not only results in a difference of mass for both topologies and both load cases, but also results in a difference in complexity for the optimal structure.

Table 3.2: Material combination selection #1

Parameters	**Values**
ρ_s	0.97e3 $\frac{kg}{m^3}$
σ_s	3000e6 Pa
ρ_b	8.00e3 $\frac{kg}{m^3}$
σ_b	415e6 Pa

Table 3.3: Material combination selection #2

Parameters	**Values**
ρ_s	4.43e3 $\frac{kg}{m^3}$
σ_s	880e6 Pa
ρ_b	18.50e3 $\frac{kg}{m^3}$
σ_b	655e6 Pa

The tables shown in the following subsections show the optimal complexity highlighted in green. For material property selection #2, the optimal complexity for the circumferential complexity is small. The algorithm only applies forces to the nodes on the rim that are connected to the strings. In reality, there would be forces applied to the rim in between these points. The bending moment due to these forces is not accounted for. The box highlighted yellow is a topology with slightly more mass, but with more points attached to the rim and would more closely match the assumption that a bending moment isn't applied to any of the members. The blank cells in the table correspond to complexity pairs that violate any of the geometric constraints presented earlier in the chapter. The cells filled with 'NS' or no solution are complexity pairs where the structure does not have a static equilibrium for that particular load case. The only table that has 'NS' in some cells is for the bicycle wheel when a torque is applied and the complexity pair is one in which the strings are oriented radially outwards from the spin axis.

3.3.0.1 Centrifugal Force And Torque (Material Property Selection #1)

Table 3.4: Final mass of the rim for the three-dimensional wheel (selection #1)

		Three-Dimensional Wheel - Rim Mass (kg)														
		q														
		1	2	3	4	5	6	7	8	9	10	11	12	13	14	15
p	3	50.2308	50.2011	50.2018												
	4	50.2313	50.1935	50.2028	50.1937											
	5	50.2317	50.1902	50.1847	50.1929	50.1980										
	6	50.2319	50.1882	50.1926	50.2021	50.1924	50.1960									
	7	50.2320	50.1869	50.1823	50.1926	50.1756	50.2029	50.1975								
	8	50.2320	50.1864	50.1561	50.1938	50.1887	50.1832	50.1960	50.1979							
	9	50.2321	50.1858	50.1566	50.1924	50.1940	50.1786	50.2000	50.1946	50.1946						
	10	50.2321	50.1515	50.1605	50.1910	50.1700	50.1910	50.1784	50.2013	50.1985	50.1971					
	11	50.2321	50.1850	50.1723	50.1776	50.1994	50.1912	50.1788	50.1826	50.2019	50.2004	50.1971				
	12	50.2321	50.1846	50.1858	50.1831	50.1821	50.1841	50.1890	50.1820	50.1959	50.1975	50.1951	50.1966			
	13	50.2322	50.1844	50.1854	50.1851	50.1705	50.1930	50.1944	50.1811	50.1867	50.1989	50.2003	50.1975	50.1965		
	14	50.2322	50.1843	50.1713	50.1673	50.1782	50.1832	50.1742	50.1953	50.1869	50.1885	50.2036	50.1981	50.1992	50.1967	
	15	50.2322	50.1842	50.1876	50.1879	50.1887	50.1828	50.1831	50.1888	50.1883	50.1854	50.1862	50.1893	50.1954	50.1990	50.1952

Table 3.5: Gradient table for the rim mass of the three-dimensional wheel (selection #1)

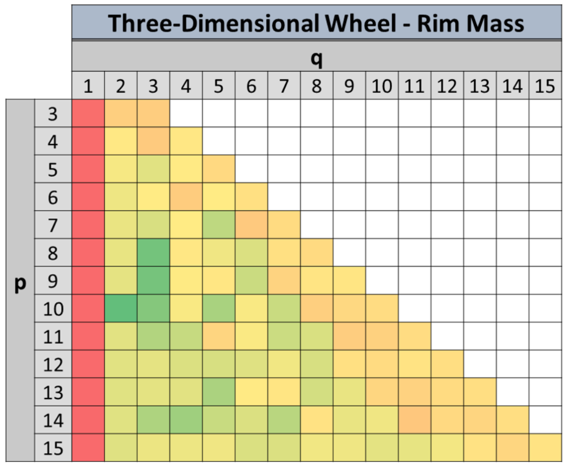

Table 3.6: Final mass of the strings for the three-dimensional wheel (selection #1)

Three-Dimensional Wheel - String Mass (kg)																
		q														
		1	2	3	4	5	6	7	8	9	10	11	12	13	14	15
p	3	0.2206	0.2730	0.2329												
	4	0.2196	0.3024	0.2582	0.2489											
	5	0.2188	0.3150	0.3175	0.2753	0.2379										
	6	0.2183	0.3221	0.3064	0.2666	0.2730	0.2430									
	7	0.2183	0.3266	0.3359	0.2999	0.3271	0.2429	0.2381								
	8	0.2183	0.3289	0.4053	0.2991	0.3018	0.3055	0.2574	0.2370							
	9	0.2180	0.3309	0.4059	0.3063	0.2969	0.3248	0.2569	0.2585	0.2454						
	10	0.2179	0.4015	0.3808	0.3145	0.3611	0.3009	0.3192	0.2528	0.2462	0.2386					
	11	0.2179	0.3335	0.3691	0.3420	0.2903	0.3023	0.3215	0.3039	0.2484	0.2413	0.2387				
	12	0.2180	0.3348	0.3364	0.3379	0.3360	0.3268	0.3028	0.3170	0.2684	0.2555	0.2522	0.2400			
	13	0.2179	0.3353	0.3375	0.3378	0.3667	0.3036	0.2939	0.3201	0.2990	0.2616	0.2479	0.2467	0.2382		
	14	0.2178	0.3357	0.3722	0.3768	0.3488	0.3285	0.3464	0.2886	0.3045	0.2930	0.2482	0.2523	0.2419	0.2389	
	15	0.2178	0.3362	0.3318	0.3285	0.3235	0.3317	0.3268	0.3110	0.3057	0.3019	0.2951	0.2782	0.2565	0.2423	0.2407

Table 3.7: Gradient table for the string mass of the three-dimensional wheel (selection #1)

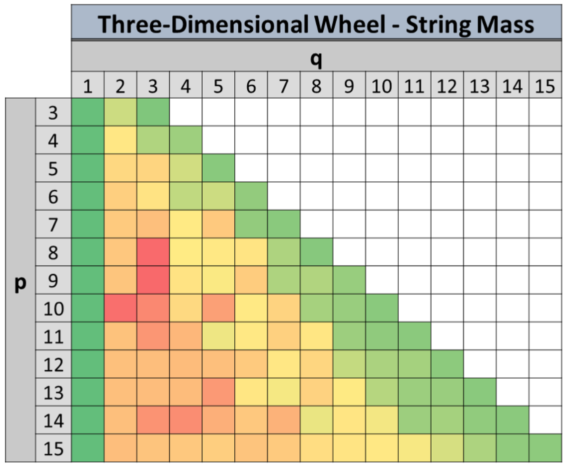

Table 3.8: Final total mass of the three-dimensional wheel (selection #1)

Three-Dimensional Wheel - Total Mass (kg)															
p \ q	1	2	3	4	5	6	7	8	9	10	11	12	13	14	15
3	50.9540	50.9768	50.9374												
4	50.9536	50.9986	50.9636	50.9453											
5	50.9531	51.0078	51.0048	50.9708	50.9386										
6	50.9529	51.0130	51.0016	50.9714	50.9681	50.9417									
7	50.9529	51.0162	51.0209	50.9952	51.0054	50.9485	50.9383								
8	50.9529	51.0180	51.0641	50.9956	50.9932	50.9913	50.9560	50.9375							
9	50.9528	51.0194	51.0652	51.0014	50.9936	51.0060	50.9596	50.9558	50.9427						
10	50.9527	51.0556	51.0439	51.0081	51.0338	50.9946	51.0003	50.9567	50.9474	50.9383					
11	50.9527	51.0212	51.0440	51.0222	50.9924	50.9961	51.0030	50.9892	50.9529	50.9443	50.9384				
12	50.9528	51.0220	51.0248	51.0237	51.0208	51.0135	50.9944	51.0016	50.9670	50.9557	50.9499	50.9393			
13	50.9527	51.0224	51.0255	51.0255	51.0399	50.9993	50.9910	51.0038	50.9884	50.9631	50.9508	50.9468	50.9373		
14	50.9526	51.0227	51.0462	51.0468	51.0296	51.0144	51.0233	50.9866	50.9940	50.9842	50.9544	50.9530	50.9437	50.9382	
15	50.9527	51.0230	51.0221	51.0191	51.0149	51.0172	51.0126	51.0024	50.9966	50.9900	50.9839	50.9702	50.9545	50.9440	50.9385

Table 3.9: Gradient table for the total mass of the three-dimensional wheel (selection #1)

Three-Dimensional Wheel - Total Mass																
		q														
		1	2	3	4	5	6	7	8	9	10	11	12	13	14	15
p	3															
	4															
	5															
	6															
	7															
	8															
	9															
	10															
	11															
	12															
	13															
	14															
	15															

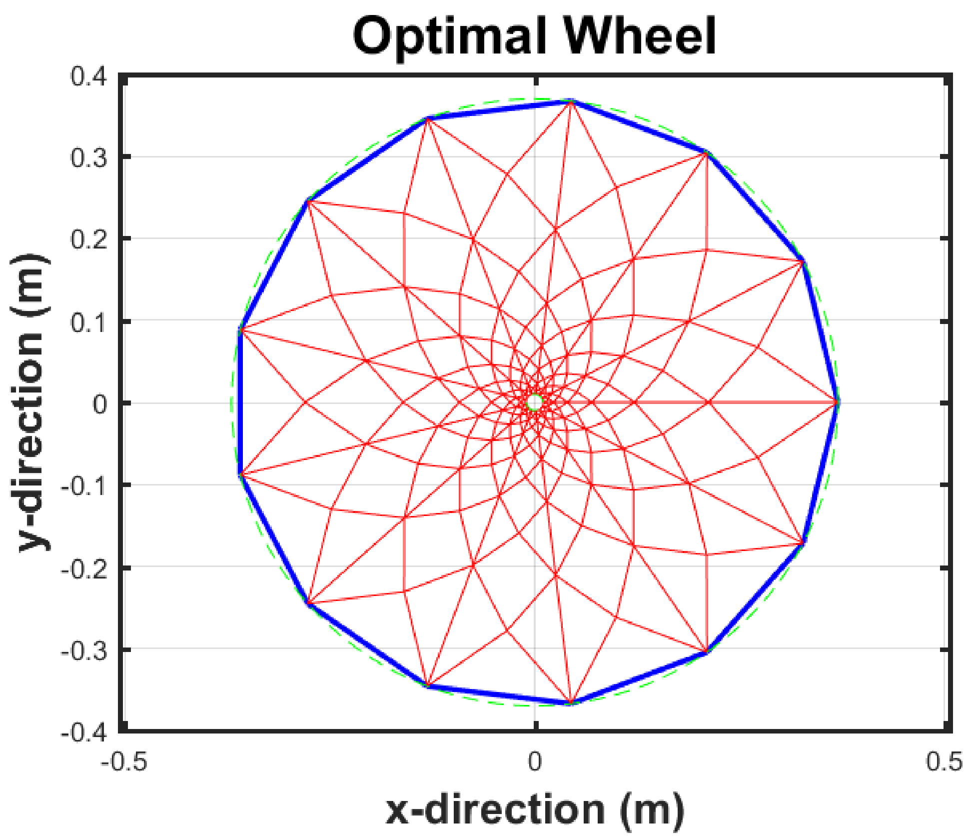

Figure 3.1: Optimal topology of the three-dimensional wheel (top view / selection #1)

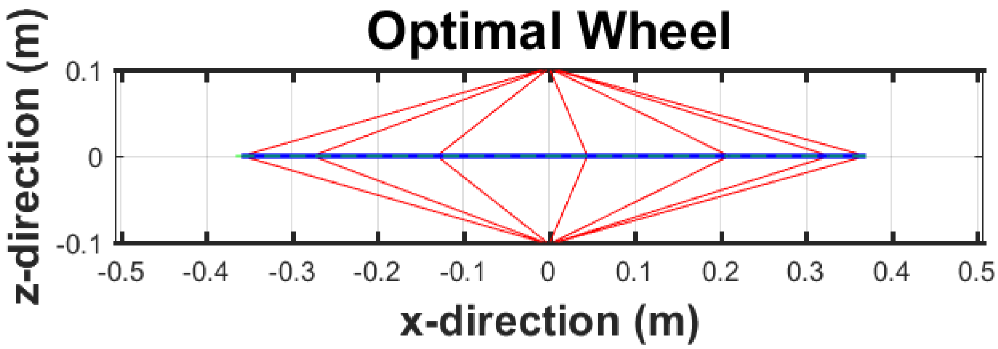

Figure 3.2: Optimal topology of the three-dimensional wheel (side view / selection #1)

3.3.0.2 Centrifugal Force And Torque (Material Property Selection #2)

Table 3.10: Final mass of the rim for the three-dimensional wheel (selection #2)

Three-Dimensional Wheel - Rim Mass (kg)

p \ q	1	2	3	4	5	6	7	8	9	10	11	12	13	14	15	16	17	18	19	20
3	47.4020	46.4917	46.4221																	
4	47.4264	46.3536	46.5571	46.2110																
5	47.4404	46.3118	46.5840	46.5924	46.3859															
6	47.4484	47.3868	46.4323	46.6498	46.6122	46.4033														
7	47.4518	46.2350	46.5822	46.6553	46.6299	46.5043	46.4022													
8	47.4540	46.2226	46.5809	46.6692	46.2688	46.3062	46.6025	46.4562												
9	47.4566	46.2131	46.5793	46.6342	46.6884	46.4170	46.5736	46.5283	46.4081											
10	47.4585	47.4824	46.3889	46.6495	46.7485	46.7211	46.2713	46.6541	46.5490	46.4303										
11	47.4590	47.4901	46.5737	46.3954	46.5979	46.7176	46.1882	46.5864	46.6456	46.4303	46.3795									
12	47.4593	47.4960	46.5669	46.6127	46.0612	46.6247	46.5099	46.3072	46.6672	46.4603	46.5451	46.4390								
13	47.4604	47.5454	46.3342	46.4138	46.7723	46.7009	46.7395	46.7200	46.7375	46.4427	46.5805	46.5454	46.4353							
14	47.4612	47.5495	46.5397	46.2930	46.4976	46.5255	46.6707	46.4758	46.7127	46.6725	46.6363	46.5795	46.4939	46.4639						
15	47.4612	47.5521	46.5711	46.6464	46.4578	46.7197	46.7802	46.5631	46.3916	46.4370	46.2381	46.5277	46.5723	46.4799	46.4334					
16	47.4612	47.5543	46.3302	46.2881	46.2533	46.5362	46.6716	46.6986	46.5506	46.4325	46.3271	46.5529	46.5892	46.4736	46.5316	46.4230				
17	47.4618	47.5567	46.5657	46.6937	46.3442	46.5442	46.5905	46.5558	46.5544	46.5638	46.4771	46.4237	46.4081	46.3606	46.6481	46.5291	46.4366			
18	47.4623	47.5587	46.5673	46.3990	46.4647	46.7456	46.6845	46.7694	46.7023	46.5583	46.4546	46.6496	46.2528	46.6268	46.6101	46.5768	46.4724	46.4050		
19	47.4622	47.5599	46.5650	46.6439	46.4122	46.4948	46.4731	46.4479	46.7019	46.6732	46.4510	46.3826	46.7743	46.4630	46.6035	46.4134	46.5523	46.5199	46.4344	
20	47.4621	47.5609	46.5642	46.6412	46.7502	46.2151	46.7170	46.6539	46.5867	46.7710	46.4930	46.6728	46.7157	46.4200	46.3756	46.7140	46.5806	46.5950	46.5028	46.4377

Table 3.11: Gradient table for the rim mass of the three-dimensional wheel (selection #2)

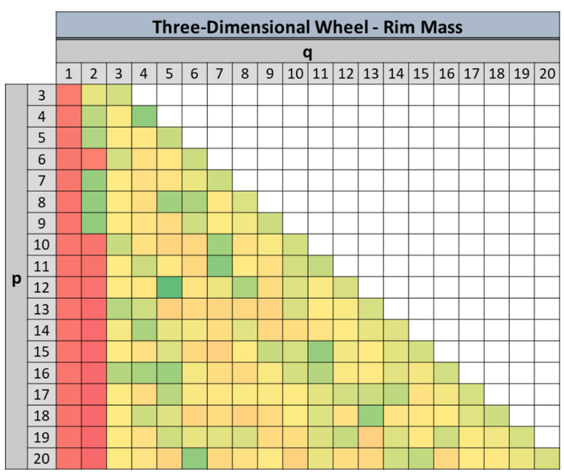

Table 3.12: Final mass of the strings for the three-dimensional wheel (selection #2)

Three-Dimensional Wheel - String Mass (kg)																				
	q																			
p	1	2	3	4	5	6	7	8	9	10	11	12	13	14	15	16	17	18	19	20
3	8.4157	10.0172	8.7060																	
4	8.3674	10.8179	9.4385	9.2151																
5	8.3378	11.1159	9.9021	9.1781	8.7908															
6	8.3209	8.2606	10.6374	9.5851	8.9964	8.7929														
7	8.3146	11.4838	10.3654	9.9151	9.3478	9.2089	8.7855													
8	8.3109	11.5557	10.4804	10.1043	10.7715	10.1254	8.8671	8.7007												
9	8.3049	11.6058	10.6696	10.2668	9.9126	10.0609	9.3212	8.9357	8.7851											
10	8.3006	8.1635	11.1661	10.4178	9.8831	9.6477	10.5012	9.0789	8.9296	8.7930										
11	8.3001	8.1589	10.7816	11.0746	10.3831	9.8282	11.0645	9.5203	9.0249	9.0975	8.8593									
12	8.2998	8.1554	10.8291	10.6599	11.8889	10.2391	10.1995	10.4163	9.1701	9.3044	8.8740	8.7803								
13	8.2973	8.0189	11.4129	11.1512	9.9298	10.0598	9.8500	9.4093	9.2135	9.7291	8.9618	8.8389	8.7814							
14	8.2952	8.0150	10.8290	11.4826	10.8746	10.7611	10.0706	10.4297	9.5248	9.3001	9.1498	8.9183	8.9064	8.7218						
15	8.2955	8.0139	10.7539	10.6803	11.0750	10.2545	9.8470	10.2633	10.5949	10.1047	10.3289	9.3718	9.0266	8.9586	8.7852					
16	8.2959	8.0130	11.4646	11.5405	11.5238	10.6287	10.1783	10.0217	10.2010	10.1875	10.3228	9.4354	9.1118	9.1781	8.8360	8.7544				
17	8.2944	8.0104	10.9163	10.5809	11.3133	10.7506	10.5400	10.3611	10.2751	9.9622	9.9836	9.9604	9.7300	9.6274	8.7962	8.8204	8.7789			
18	8.2931	8.0082	10.7930	11.3691	11.1051	10.2625	10.2266	9.8947	10.0023	10.1286	10.1885	9.5178	10.3376	9.2388	9.0648	8.8897	8.9211	8.7886		
19	8.2936	8.0080	10.9347	10.7510	11.2497	11.0156	10.8668	10.7389	9.9747	9.8923	10.2902	10.2982	9.0844	9.6559	9.2132	9.4359	8.8861	8.8101	8.7988	
20	8.2941	8.0078	10.9424	10.7577	10.4085	11.7375	10.4029	10.4582	10.4618	9.8043	10.4136	9.7033	9.5287	10.0067	9.8927	8.9596	9.0690	8.8252	8.8227	8.7903

Table 3.13: Gradient table for the string mass of the three-dimensional wheel (selection #2)

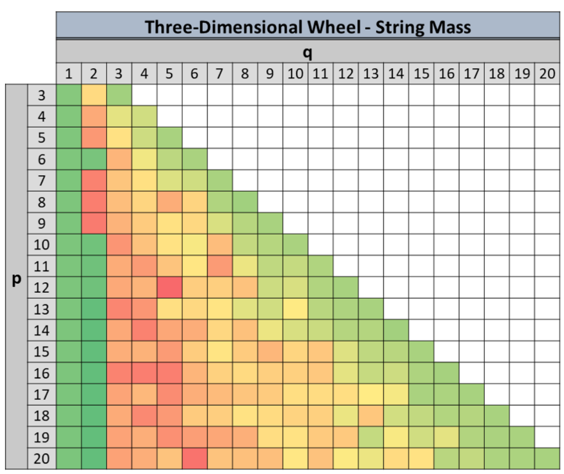

Table 3.14: Final total mass of the three-dimensional wheel (selection #2)

		Three-Dimensional Wheel - Total Mass (kg)																			
		q																			
		1	2	3	4	5	6	7	8	9	10	11	12	13	14	15	16	17	18	19	20
p	3	56.9801	57.6713	56.2904																	
p	4	56.9562	58.3339	57.1579	56.5885																
p	5	56.9406	58.5901	57.6485	56.9328	56.3391															
p	6	56.9317	56.8098	58.2321	57.3972	56.7710	56.3586														
p	7	56.9288	58.8812	58.1100	57.7328	57.1402	56.8756	56.3501													
p	8	56.9272	58.9407	58.2237	57.9359	58.2027	57.5940	56.6319	56.3193												
p	9	56.9239	58.9812	58.4112	58.0633	57.7634	57.6404	57.0572	56.6264	56.3556											
p	10	56.9215	56.8084	58.7174	58.2297	57.7940	57.5313	57.9350	56.8955	56.6409	56.3856										
p	11	56.9215	56.8114	58.5177	58.6323	58.1434	57.7082	58.4151	57.2691	56.8328	56.6901	56.4012									
p	12	56.9215	56.8138	58.5584	58.4350	59.1125	58.0261	57.8718	57.8859	56.9997	56.9271	56.5815	56.3816								
p	13	56.9200	56.7267	58.9094	58.7274	57.8645	57.9231	57.7519	57.2917	57.1134	57.3342	56.7047	56.5467	56.3791							
p	14	56.9188	56.7269	58.5310	58.9380	58.5346	58.4490	57.9037	58.0678	57.3999	57.1350	56.9485	56.6601	56.5627	56.3480						
p	15	56.9192	56.7284	58.4874	58.4891	58.6952	58.1366	57.7895	57.9888	58.1489	57.7041	57.7293	57.0620	56.7614	56.6009	56.3809					
p	16	56.9195	56.7297	58.9571	58.9910	58.9394	58.3273	58.0124	57.8827	57.9140	57.7824	57.8124	57.1507	56.8633	56.8141	56.5299	56.3398				
p	17	56.9186	56.7295	58.6444	58.4371	58.8198	58.4572	58.2929	58.0793	57.9919	57.6884	57.6231	57.5465	57.3005	57.1504	56.6068	56.5119	56.3780			
p	18	56.9178	56.7293	58.5226	58.9305	58.7322	58.1705	58.0735	57.8265	57.8670	57.8493	57.8055	57.3297	57.7528	57.0280	56.8372	56.6289	56.5559	56.3559		
p	19	56.9182	56.7303	58.6621	58.5572	58.8243	58.6728	58.5023	58.3492	57.8389	57.7279	57.9036	57.8431	57.0210	57.2814	56.9792	57.0117	56.6008	56.4924	56.3956	
p	20	56.9186	56.7311	58.6690	58.5612	58.3211	59.1149	58.2823	58.2745	58.2109	57.7377	58.0690	57.5385	57.4068	57.5892	57.4307	56.8360	56.8120	56.5825	56.4879	56.3905

Table 3.15: Gradient table for the total mass of the three-dimensional wheel (selection #2)

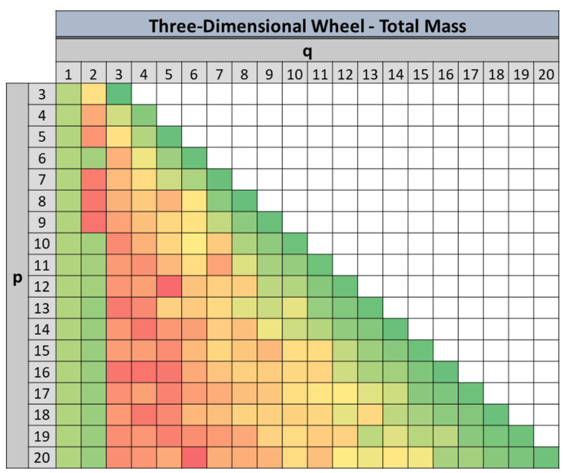

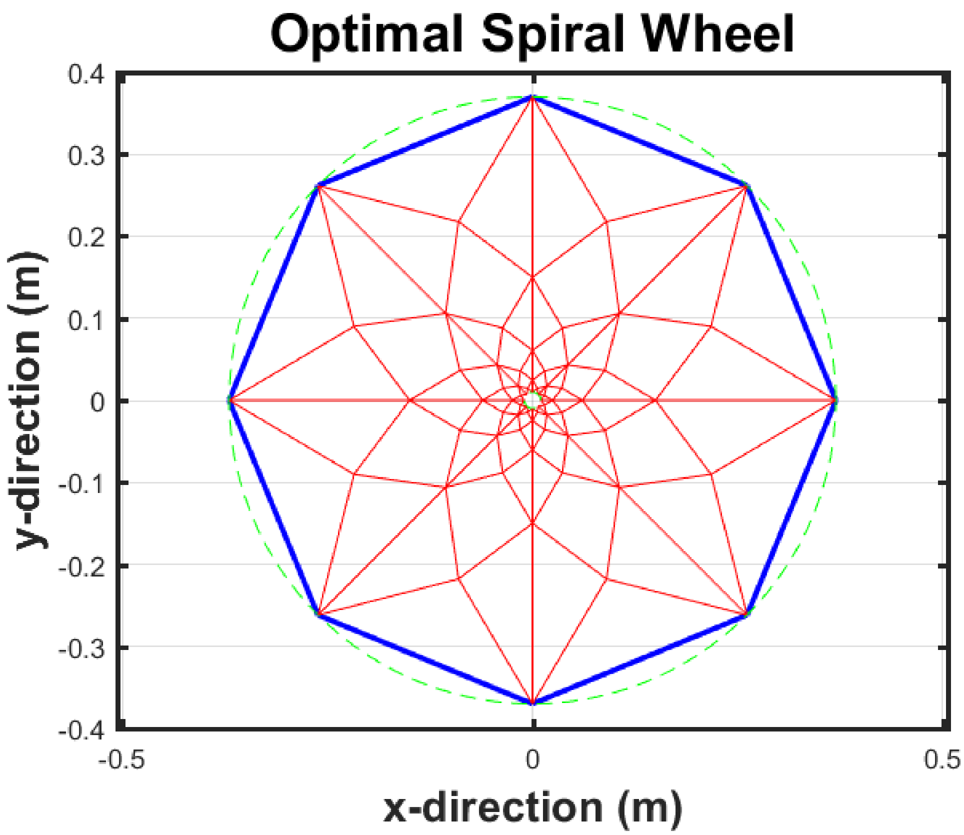

Figure 3.3: Optimal topology of the three-dimensional wheel (top view / selection #2)

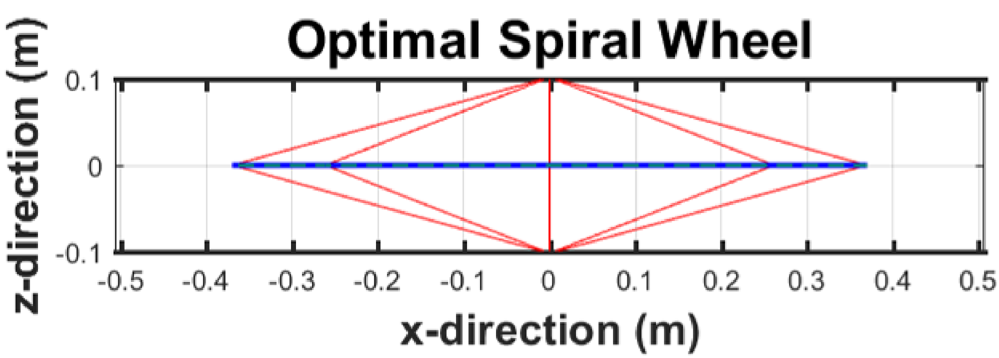

Figure 3.4: Optimal topology of the three-dimensional wheel (side view / selection #2)

3.4 Prestress Considerations

So far prestress has not been considered for the strings. Like a bicycle wheel, the strings could be prestressed before any loads are applied. This would increase the stiffness of the wheel, but also increase the mass. The bicycle wheel strings could be prestressed independently of the spiral wheel strings to increase the out of plane stiffness for example. In the future, when the stiffness of the wheel is considered, the amount of prestress will be an important variable to consider.

3.5 Volume Comparison

Assuming the flyhweel on the ISS is flat and made of stainless steel with the same density as the stainless steel chosen for the tensegrity wheel, the thickness of the ISS flywheel should be approximately 0.03 meters. The axle length chosen for the tensegrity wheel is 0.2 meters. The mass of the tensegrity wheel decreases as the axle length is decreased, but the out of plane stiffness would also decrease. At the moment the ISS flywheel takes up less volume than the tensegrity flywheel, but when the stiffness of the tensegrity flywheel is considered the actual needed axle length will be found. At this time it is difficult to make an accurate volume comparison between the two wheels.

3.6 Summary

The three-dimensional mass optimized design for a flywheel for use in a CMG is performed in this chapter. One topology was defined by combining the spiral and bicycle wheel topologies from the previous chapter using their connectivity matrices and nodal matrices. The first rim topology from the previous chapter was re-used for the three-dimensional wheel. Second, the static load cases were defined. A combination of centrifugal force and an out of plane torque was applied to the wheel. Finally, the results from the algorithm were outlined. The results show that for the three-dimensional wheel, the tensegrity wheel is approximately 45-49% less massive compared to the flywheels used for the CMGs on the ISS for similar design constraints.

4. CONCLUSION

The goal of designing a flywheel for a reaction wheel or a CMG that can produce equivalent levels of angular momentum and torque while reducing the mass was achieved. The connectivity matrices and the nodal matrix were derived for the bicycle wheel, spiral wheel, and rim. After the topologies were defined, the force matrices were defined for two different loading conditions for each of the different wheel designs. An algorithm to minimize the mass of the topologies subject to the loading conditions that were defined was created. Finally, the algorithm was used for several complexity combinations and the minimal mass results were presented. More steps need to be taken in the future to bring this design from the mass optimized structure presented to a physical flywheel that can be used with as much confidence as the current solid flywheel designs. The flexible body dynamics of the mass optimized structures should be examined. It should be expected that the mass values presented will increase due to the dynamic loads, but there is significant flexibility in the choice of complexities for the topologies. If the optimal topology from the quasi-static loads has natural frequencies that are near the frequency of the forcing functions that the flywheel will experience, there are other topology options that do not substantially increase the optimal mass. The next step would be to build and test the final topology design. This step would be needed to verify the accuracy of the analysis and as a proof of concept that a tensegrity flywheel is capable of producing outputs that match those of the solid flywheel with significant mass savings.

REFERENCES

[1] Kenji Nagase, R. E. Skelton, "Minimal mass design of tensegrity structures", Proc. SPIE 9061, Sensors and Smart Structures Technologies for Civil, Mechanical, and Aerospace Systems 2014, 90610W (8 March 2014).

[2] Maxwell J. On reciprocal figures, frames and diagrams of force. The scientific papers of James Clerk Maxwell, 2:161207, 1872. doi:http://dx.doi.org/10. 1017/CBO9780511710377.014.

[3] Michell A. The limit of economy of material in frame structures. Phil.Mag. Series VI, 8, nov 1904.

[4] Skelton, Robert E., and Maurício C. de Oliveira. "Optimal tensegrity structures in bending: the discrete Michell truss." Journal of the Franklin Institute 347.1 (2010): 257-283.

[5] Jacot, Benjamin Benjamin Paul Emmanuel. A strain tensor method for three-dimensional optimal Michell structures. Diss. Massachusetts Institute of Technology, 2016.

[6] Gavin, Henri P. "Bicycle-wheel spoke patterns and spoke fatigue." Journal of engineering mechanics 122.8 (1996): 736-742.

[7] Huang, Jinhua, and Georges M. Fadel. "Heterogeneous flywheel modeling and optimization." Materials & Design 21.2 (2000): 111-125.

[8] Stodola, A., Steam and Gas Turbines, Vol. 1, McGraw-Hill, New York, 1927, pp. 372-400.

[9] Sandgren, E., and K. M. Ragsdell. "Optimal flywheel design with a general thickness form representation." Journal of Mechanisms, Transmissions, and Automation in Design 105.3 (1983): 425-433.

[10] Burgoyne, C. I., and Dilmaghanian, R. (1993). "Bicycle wheel as prestressed structure." J. Engrg. Mech., 119(3),439-455.

[11] Burt, Richard R., and Richard W. Loffi. "Failure analysis of international space station control moment gyro." 10th European Space Mechanisms and Tribology Symposium. Vol. 524. 2003.

APPENDIX A

TENSEGRITY TOPOLOGY REPRESENTATION

Tensegrity topologies are defined by a nodal matrix, bar connectivity matrix, and string connectivity matrix. The figure below shows an arbitrary tensegrity system. The red lines represent strings or members that can only take tension and the blue lines represent bars or members that can take tension or compression. Let the i^{th} column of the matrix $\boldsymbol{N}$ be the three-dimensional vector $\boldsymbol{n}_i$ corresponding to the i^{th} node in the network. Each of the n_b bars will have an assigned vector name ($\boldsymbol{b}_i$, $i = 1$, $\cdots$, n_b). The same is done for each of the n_s strings ($\boldsymbol{s}_i$, $i = 1$, $\cdots$, n_s). Let the i^{th} column of the bar matrix $\boldsymbol{B}$ be the bar vector $\boldsymbol{b}_i$ that lies along the length of the i^{th} bar. Similarly, the i^{th} column of the string matrix $\boldsymbol{S}$ be the string vector $\boldsymbol{s}_i$ that lies along the length of the i^{th} string. The connectivity matrices are defined as follows, define the elements of the bar connectivity matrix $\boldsymbol{C}_B$ to be $[\boldsymbol{C}_B]_{ij} = -1$ if the bar vector $\boldsymbol{b}_i$ is directed away from the node $\boldsymbol{n}_j$, $[\boldsymbol{C}_B]_{ij} = 1$ if the bar vector $\boldsymbol{b}_i$ is directed towards the node $\boldsymbol{n}_j$, and $[\boldsymbol{C}_B]_{ij} = 0$ if the bar vector $\boldsymbol{b}_i$ is not connected to the node $\boldsymbol{n}_j$. The string connectivity matrix $\boldsymbol{C}_S$ is constructed the same way using the string vectors $\boldsymbol{s}_i$.

An example of how to construct the nodal matrix and connectivity matrices for a specific tensegrity system will be shown below. First, a choice on how to number the nodes of the system is required. The numbering can be arbitrary, but there is usually a good choice for the numbering to allow for connectivity matrices that are structured in a more aesthetically pleasing way. For this example, the nodes are numbered as shown in the figure below. The bar vectors and string vector's directions need to be specified and the directions for this example are shown below in the figure.

To create the nodal matrix $\boldsymbol{N}$, the node vectors are placed in numbered order in each column and is shown below. Each nodal vector is a 3×1 vector.

$$\boldsymbol{N} = \begin{bmatrix} \boldsymbol{n}_1 & \boldsymbol{n}_2 & \boldsymbol{n}_3 & \boldsymbol{n}_4 \end{bmatrix} \tag{A.1}$$

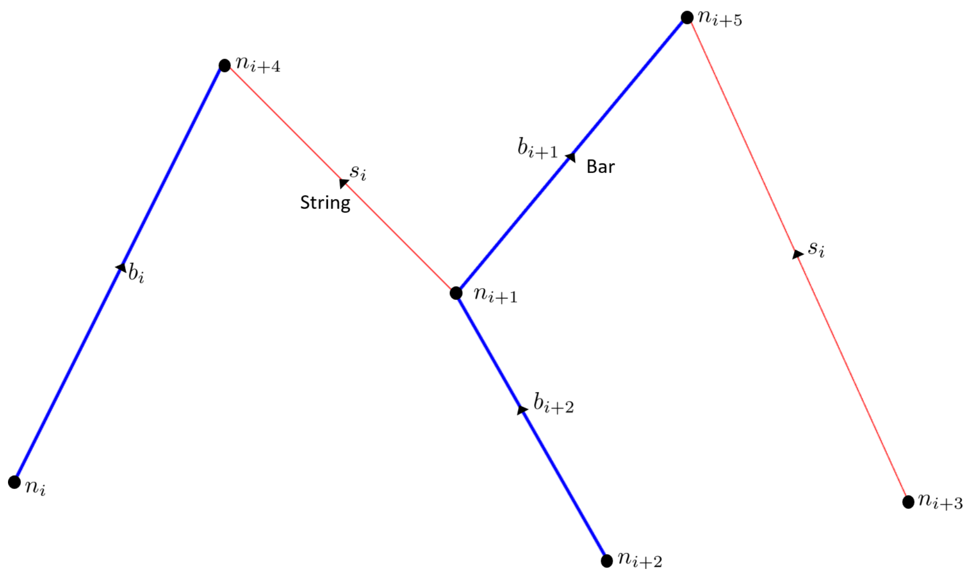

Figure A.1: Tensegrity System.

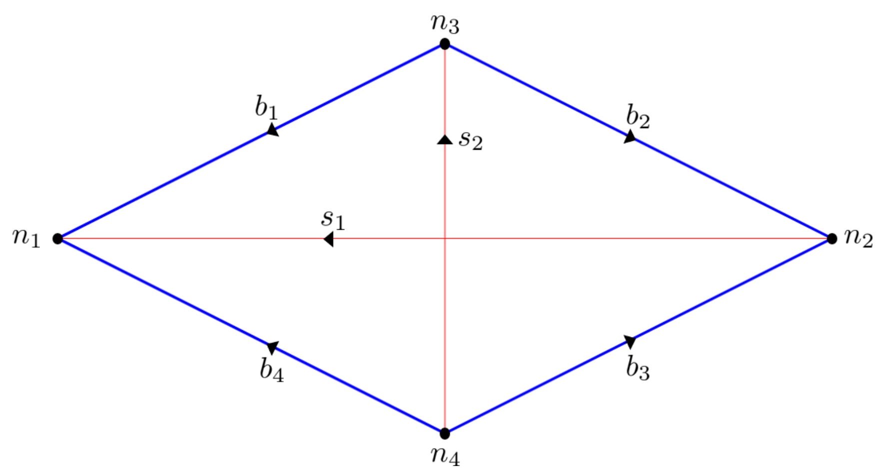

Figure A.2: Tensegrity System Example.

The rows of the bar connectivity matrix $\boldsymbol{C}_B^T$ represent the nodes of the system and the columns represent the directions of the bar vectors. For $\boldsymbol{b}_1$ you would place a 1 in the first row and the first column since the tip of that vector is connected to the first node and you would put a -1 in the third row and first column because the tail is connected to the third node and you would put zeros in the rest of the rows of the first column. Then you would start with $\boldsymbol{b}_2$ in the second column and so on. Using the system shown in the figure above the corresponding bar connectivity is shown in

(A.2).

$$C_B^T = \begin{bmatrix} 1 & 0 & 0 & 1 \\ 0 & 1 & 1 & 0 \\ -1 & -1 & 0 & 0 \\ 0 & 0 & -1 & -1 \end{bmatrix} \tag{A.2}$$

The same process is used to create the string connectivity matrix C_S^T and the resulting matrix is shown in A.3.

$$C_S^T = \begin{bmatrix} 1 & 0 \\ -1 & 0 \\ 0 & 1 \\ 0 & -1 \end{bmatrix} \tag{A.3}$$

APPENDIX B

ALGORITHM FOR COMBINING TENSEGRITY TOPOLOGIES

An algorithm for combining the structures of two different tensegrity topologies will be presented in this section. The usefulness of this algorithm will be shown in an example and will also be used for the bicycle topology to combine the structure of the spokes with the structure of the rim. The inputs to this algorithm will be the nodal matrix, bar connectivity, and string connectivity of the first and second structure. The outputs will be a single nodal matrix, bar connectivity, and string connectivity that were created by augmenting the inputs in a specified way dictated by this algorithm.

The first step of this algorithm is to augment the nodal matrices of the first structure and the second structure $\boldsymbol{N}_1$ and $\boldsymbol{N}_2$ respectively. This is done by searching for common nodes between the two structures. Let $\boldsymbol{N}_1 = [\boldsymbol{n}_1, \boldsymbol{n}_2, \cdots, \boldsymbol{n}_k]$ and let $\boldsymbol{N}_2 = [\boldsymbol{n}_1^{'}, \boldsymbol{n}_2^{'}, \cdots, \boldsymbol{n}_m^{'}]$ where k and m are the number of nodes in $\boldsymbol{N}_1$ and $\boldsymbol{N}_2$ respectively. The duplicate nodes are deleted from $\boldsymbol{N}_2$, so after the search for the matching nodes say that $\boldsymbol{n}_1 = \boldsymbol{n}_3^{'}$ and $\boldsymbol{n}_3 = \boldsymbol{n}_1^{'}$, this would mean that $\boldsymbol{n}_1^{'}$ and $\boldsymbol{n}_3^{'}$ are deleted from the nodal matrix of the second structure and is now $\boldsymbol{N}_2 = [\boldsymbol{n}_2^{'}, \boldsymbol{n}_4^{'}, \cdots, \boldsymbol{n}_{m-n_d}^{'}]$ where n_d is the number of deleted nodes. The nodes in $\boldsymbol{N}_2$ are then renumbered starting after the last index of $\boldsymbol{N}_1$, so $\boldsymbol{N}_2 = [\boldsymbol{n}_{k+1}, \boldsymbol{n}_{k+2}, \cdots, \boldsymbol{n}_{k+m-n_d}]$. Now the two nodal matrices are augmented together to form one nodal matrix for the structure $\boldsymbol{N} = [\boldsymbol{n}_1, \boldsymbol{n}_2, \cdots, \boldsymbol{n}_{k+m-n_d}]$.

The second step is to augment the bar and string connectivity matrices together with the new nodal structure. The $\bullet$ in each entry in the connectivity matrices can be a 1, -1, or 0. The two connectivity matrices shown below in B.1 and B.2 correspond to the fist structure and the second structure that will be combined.

$$
\boldsymbol{C}_{B_1}^{T} = \begin{array}{c} \\ n_1 \\ n_2 \\ n_3 \\ \vdots \\ n_k \end{array} \begin{array}{c} \begin{array}{ccccc} b_1 & b_2 & b_3 & \cdots & b_{n_b} \end{array} \\ \left[\begin{array}{ccccc} \bullet & \bullet & \bullet & \cdots & \bullet \\ \bullet & \bullet & \bullet & \cdots & \bullet \\ \bullet & \bullet & \bullet & \cdots & \bullet \\ \vdots & \vdots & \vdots & \vdots & \vdots \\ \bullet & \bullet & \bullet & \cdots & \bullet \end{array} \right] \end{array} \tag{B.1}
$$

$$
\boldsymbol{C}_{B_2}^{T} = \begin{array}{c} \\ n_1' \\ n_2' \\ n_3' \\ \vdots \\ n_m' \end{array} \begin{array}{c} \begin{array}{ccccc} b_1' & b_2' & b_3' & \cdots & b_{n_b'}' \end{array} \\ \left[\begin{array}{ccccc} \bullet & \bullet & \bullet & \cdots & \bullet \\ \bullet & \bullet & \bullet & \cdots & \bullet \\ \bullet & \bullet & \bullet & \cdots & \bullet \\ \vdots & \vdots & \vdots & \vdots & \vdots \\ \bullet & \bullet & \bullet & \cdots & \bullet \end{array} \right] \end{array} \tag{B.2}
$$

Now you would pick out the rows of the second connectivity matrix that correspond with matching nodes from the first structure. The same nodes will be kept as the matching nodes from the previous paragraph, so that $\boldsymbol{n}_1 = \boldsymbol{n}_3'$ and $\boldsymbol{n}_3 = \boldsymbol{n}_1'$. These rows are highlighted red and shown below in B.3.

$$
\boldsymbol{C}_{B_2}^{T} = \begin{array}{c} \\ n_1' \\ n_2' \\ n_3' \\ \vdots \\ n_m' \end{array} \begin{array}{c} \begin{array}{ccccc} b_1' & b_2' & b_3' & \cdots & b_{n_b'}' \end{array} \\ \left[\begin{array}{ccccc} \color{red}\bullet & \color{red}\bullet & \color{red}\bullet & \cdots & \color{red}\bullet \\ \bullet & \bullet & \bullet & \vdots & \bullet \\ \color{red}\bullet & \color{red}\bullet & \color{red}\bullet & \vdots & \color{red}\bullet \\ \vdots & \vdots & \vdots & \vdots & \vdots \\ \bullet & \bullet & \bullet & \cdots & \bullet \end{array} \right] \end{array} \tag{B.3}
$$

Now the rows that correspond to the matching nodes are removed from the bar connectivity of the second structure and augmented into the bar connectivity for the first structure by placing them into the rows that represent the matching nodes and are added as new columns representing new bars. The rows that do not correspond to a matching node are filled in with zeros in the added columns. This is shown below in B.4. The rest of the rows that were not removed from the second connectivity matrix are shown below in blue in B.5.

$$\boldsymbol{C}_{B_1}^T = \begin{array}{c} \\ n_1 \\ n_2 \\ n_3 \\ \vdots \\ n_k \end{array} \begin{array}{c} \begin{array}{cccccccccc} b_1 & b_2 & b_3 & \cdots & b_{n_b} & b_{n_b+1} & b_{n_b+2} & b_{n_b+3} & \cdots & b_{n_b+n_b'} \end{array} \\ \begin{bmatrix} \bullet & \bullet & \bullet & \cdots & \bullet & \color{red}{\bullet} & \color{red}{\bullet} & \color{red}{\bullet} & \cdots & \color{red}{\bullet} \\ \bullet & \bullet & \bullet & \cdots & \bullet & 0 & 0 & 0 & \cdots & 0 \\ \bullet & \bullet & \bullet & \cdots & \bullet & \color{red}{\bullet} & \color{red}{\bullet} & \color{red}{\bullet} & \cdots & \color{red}{\bullet} \\ \vdots & \vdots & \vdots & \vdots & \vdots & 0 & 0 & 0 & \cdots & 0 \\ \bullet & \bullet & \bullet & \cdots & \bullet & 0 & 0 & 0 & \cdots & 0 \end{bmatrix} \end{array} \tag{B.4}$$

$$\boldsymbol{C}_{B_2}^T = \begin{array}{c} \\ n_2' \\ n_4' \\ n_5' \\ \vdots \\ n_{m-n_d}' \end{array} \begin{array}{c} \begin{array}{ccccc} b_1' & b_2' & b_3' & \cdots & b_{n_b'}' \end{array} \\ \begin{bmatrix} \color{blue}{\bullet} & \color{blue}{\bullet} & \color{blue}{\bullet} & \cdots & \color{blue}{\bullet} \\ \color{blue}{\bullet} & \color{blue}{\bullet} & \color{blue}{\bullet} & \cdots & \color{blue}{\bullet} \\ \color{blue}{\bullet} & \color{blue}{\bullet} & \color{blue}{\bullet} & \cdots & \color{blue}{\bullet} \\ \vdots & \vdots & \vdots & \vdots & \vdots \\ \color{blue}{\bullet} & \color{blue}{\bullet} & \color{blue}{\bullet} & \cdots & \color{blue}{\bullet} \end{bmatrix} \end{array} \tag{B.5}$$

The blue rows from B.5 are then augmented into the first bar connectivity matrix by placing them in the newly created columns below the last row of the original first bar connectivity matrix. The indexes corresponding to the old columns and the new rows are filled in with zeros. The news rows start their indexing after the last index from the original rows. This is shown below in B.6

$$
\boldsymbol{C}_{B_1}^T = \begin{array}{c} \\ n_1 \\ n_2 \\ n_3 \\ \vdots \\ n_k \\ n_{k+1} \\ n_{k+2} \\ n_{k+3} \\ \vdots \\ n_{k+m-n_d} \end{array}
\begin{array}{c} \begin{array}{cccccccccc} b_1 & b_2 & b_3 & \cdots & b_{n_b} & b_{n_b+1} & b_{n_b+2} & b_{n_b+3} & \cdots & b_{n_b+n_b'} \end{array} \\
\begin{bmatrix}
\bullet & \bullet & \bullet & \cdots & \bullet & \color{red}{\bullet} & \color{red}{\bullet} & \color{red}{\bullet} & \cdots & \color{red}{\bullet} \\
\bullet & \bullet & \bullet & \cdots & \bullet & 0 & 0 & 0 & \cdots & 0 \\
\bullet & \bullet & \bullet & \cdots & \bullet & \color{red}{\bullet} & \color{red}{\bullet} & \color{red}{\bullet} & \cdots & \color{red}{\bullet} \\
\vdots & \vdots & \vdots & \vdots & \vdots & 0 & 0 & 0 & \cdots & 0 \\
\bullet & \bullet & \bullet & \cdots & \bullet & 0 & 0 & 0 & \cdots & 0 \\
0 & 0 & 0 & \cdots & 0 & \color{blue}{\bullet} & \color{blue}{\bullet} & \color{blue}{\bullet} & \cdots & \color{blue}{\bullet} \\
0 & 0 & 0 & \cdots & 0 & \color{blue}{\bullet} & \color{blue}{\bullet} & \color{blue}{\bullet} & \cdots & \color{blue}{\bullet} \\
0 & 0 & 0 & \cdots & 0 & \color{blue}{\bullet} & \color{blue}{\bullet} & \color{blue}{\bullet} & \cdots & \color{blue}{\bullet} \\
\vdots & \vdots & \vdots & \vdots & \vdots & \vdots & \vdots & \vdots & \vdots & \vdots \\
0 & 0 & 0 & \cdots & 0 & \color{blue}{\bullet} & \color{blue}{\bullet} & \color{blue}{\bullet} & \cdots & \color{blue}{\bullet}
\end{bmatrix} \end{array}
\tag{B.6}
$$

This final bar connectivity matrix will represent the combined topology of the first and second structures. This will now be simply referred to as $\boldsymbol{C}_B^T$. The final step is to search for columns in $\boldsymbol{C}_B^T$ that have non-zero values in the same rows. The duplicate columns are deleted so that there are not duplicate bars in the same locations. The number of the duplicate bars that are deleted start at the largest number, so if $\boldsymbol{b}_2$ and $\boldsymbol{b}_7$ are duplicate than $\boldsymbol{b}_7$ is the one deleted. The augmentation process for the string connectivity matrices is performed in the same manner as for the bar connectivity matrices. The algorithm presented in this section is summarized below and will be referred to as Algorithm 1.

Algorithm 1 Inputs: $\boldsymbol{N}_1, \boldsymbol{C}_{B_1}^T, \boldsymbol{C}_{S_1}^T, \boldsymbol{N}_2, \boldsymbol{C}_{B_2}^T, \boldsymbol{C}_{S_2}^T$ Outputs: $\boldsymbol{N}, \boldsymbol{C}_B^T, \boldsymbol{C}_S^T$.

Search for common nodes between the two structures.
Delete common nodes from $\boldsymbol{N}_2$.
Rename nodes in $\boldsymbol{N}_2$ and augment $\boldsymbol{N}_1$ with $\boldsymbol{N}_2$ to create $\boldsymbol{N}$.
Augment $\boldsymbol{C}_{B_1}^T$ with $\boldsymbol{C}_{B_2}^T$ to create $\boldsymbol{C}_B^T$.
Augment $\boldsymbol{C}_{S_1}^T$ with $\boldsymbol{C}_{S_2}^T$ to create $\boldsymbol{C}_S^T$.
Delete common columns from $\mid \boldsymbol{C}_B^T \mid$.
Delete common columns from $\mid \boldsymbol{C}_S^T \mid$.

B.1 Example

An example will be shown to demonstrate the algorithm for combining topologies. Shown below are two separate tensegrity structures that will be combined. The numbering of the nodes, bars, and strings is arbitrary.

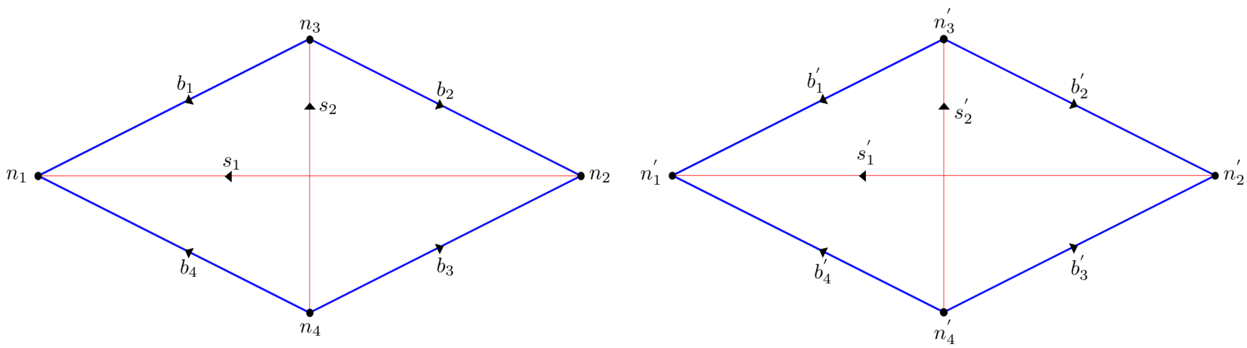

Figure B.1: Two tensegrity structures with numbering shown.

Now taking the two tensegrity structures shown above, lets look at an example demonstrating the algorithm. Now the nodal matrix and the connectivity matrices need to be augmented so that the structures are combined into one. The first step is to search for common nodes between the two structures. Looking at the figure below, it is easy to see that $\boldsymbol{n}_2 = \boldsymbol{n}_3'$ and $\boldsymbol{n}_4 = \boldsymbol{n}_1'$.

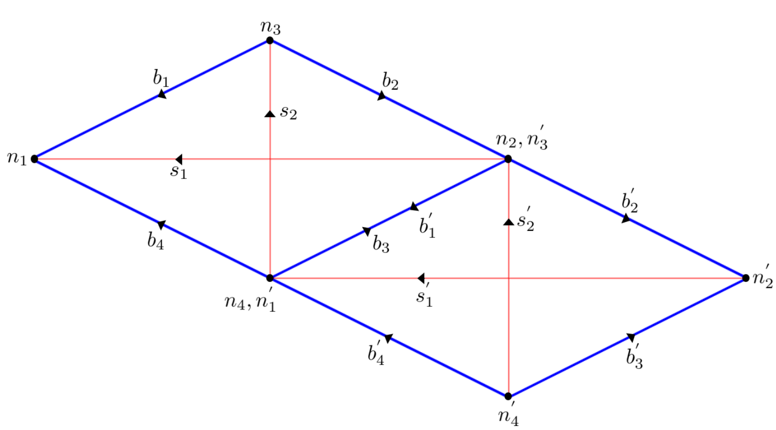

Figure B.2: Two tensegrity structures that share a two common nodes.

For this example, the inputs for Algorithm 1 are:

$$\boldsymbol{N}_1 = [\boldsymbol{n}_1, \boldsymbol{n}_2, \boldsymbol{n}_3, \boldsymbol{n}_4] \tag{B.7}$$

$$\boldsymbol{C}_{B_1}^T = \begin{bmatrix} 1 & 0 & 0 & 1 \\ 0 & 1 & 1 & 0 \\ -1 & -1 & 0 & 0 \\ 0 & 0 & -1 & -1 \end{bmatrix} \tag{B.8}$$

$$\boldsymbol{C}_{S_1}^T = \begin{bmatrix} 1 & 0 \\ -1 & 0 \\ 0 & 1 \\ 0 & -1 \end{bmatrix} \tag{B.9}$$

$$\boldsymbol{N}_2 = [\boldsymbol{n}_1^{'}, \boldsymbol{n}_2^{'}, \boldsymbol{n}_3^{'}, \boldsymbol{n}_4^{'}] \tag{B.10}$$

$$\boldsymbol{C}_{B_2}^T = \begin{bmatrix} 1 & 0 & 0 & 1 \\ 0 & 1 & 1 & 0 \\ -1 & -1 & 0 & 0 \\ 0 & 0 & -1 & -1 \end{bmatrix} \tag{B.11}$$

$$\boldsymbol{C}_{S_2}^T = \begin{bmatrix} 1 & 0 \\ -1 & 0 \\ 0 & 1 \\ 0 & -1 \end{bmatrix} \tag{B.12}$$

The outputs for Algorithm 1 are:

$$\boldsymbol{N} = [\boldsymbol{n}_1, \boldsymbol{n}_2, \boldsymbol{n}_3, \boldsymbol{n}_4, \boldsymbol{n}_5, \boldsymbol{n}_6] \tag{B.13}$$

$$\boldsymbol{C}_B^T = \begin{bmatrix} 1 & 0 & 0 & 1 & 0 & 0 & 0 \\ 0 & 1 & 1 & 0 & -1 & 0 & 0 \\ -1 & -1 & 0 & 0 & 0 & 0 & 0 \\ 0 & 0 & -1 & -1 & 0 & 0 & 1 \\ 0 & 0 & 0 & 0 & 1 & 1 & 0 \\ 0 & 0 & 0 & 0 & 0 & -1 & -1 \end{bmatrix} \tag{B.14}$$

$$\boldsymbol{C}_S^T = \begin{bmatrix} 1 & 0 & 0 & 0 \\ -1 & 0 & 0 & 1 \\ 0 & 1 & 0 & 0 \\ 0 & -1 & 1 & 0 \\ 0 & 0 & -1 & 0 \\ 0 & 0 & 0 & -1 \end{bmatrix} \tag{B.15}$$

The final structure is shown below in Figure B.3 with the new numbering for the nodes, bars, and strings.

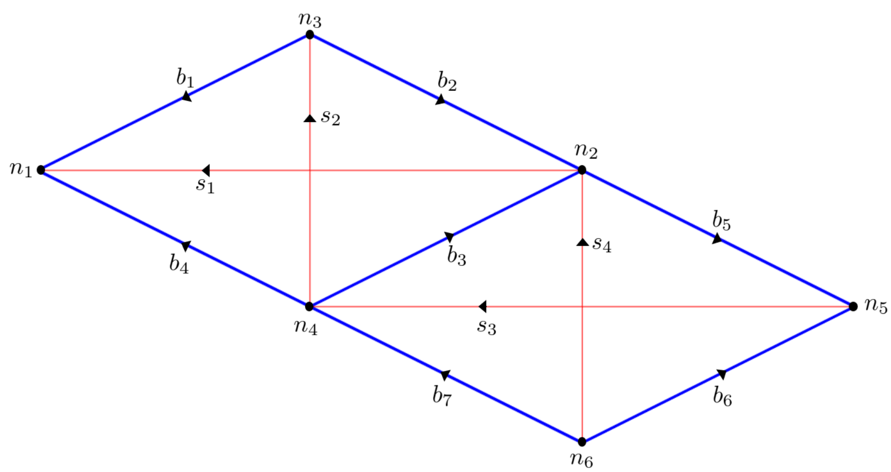

Figure B.3: One tensegrity structure with new numbering for nodes, bars, and strings.